University of Nevada, Reno

Development and Validation of MM5 MOS-Based Forecast Equations for Mixing Height

A thesis submitted in partial fulfillment of the
requirements for the degree of Master of Science in
Atmospheric Science

by

Douglas J. Pibal

Dr. Timothy J. Brown/Thesis Advisor

August, 2007

THE GRADUATE SCHOOL

We recommend that the thesis
prepared under our supervision by

DOUGLAS J. PIBAL

Entitled

Development And Validation Of MM5 MOS-Based Forecast Equations For Mixing Height

be accepted in partial fulfillment of the
requirements for the degree of

MASTER OF SCIENCE

Timothy J. Brown, Ph. D., Advisor

Beth Hall, Ph. D., Committee Member

Fred Harris, Ph. D., Graduate School Representative

Marsha H. Read, Ph. D., Associate Dean, Graduate School

August, 2007

Abstract

To address the problem of forecasting mixing height, especially to aid those who make pollution advisories or plan prescribed burns, model output statistics (MOS) was used to develop forecast equations from MM5 model output and observed mixing heights. Two hundred forecast equations were developed, corresponding to each combination of five sounding locations in California and Nevada, two times of day (00 and 12UTC), four seasons and five forecast lead-times. Validation methods included scatterplots of observed versus forecasted mixing heights, boxplots showing the magnitude and spread of individual forecast errors, and calculation of R-squared and bias statistics. The results suggest that the MM5 MOS-based forecast equations, using a parcel method to determine the observed mixing heights from standard National Weather Service (NWS) soundings, produce reasonable results for summer at all five stations and fall at Nevada stations for forecasts leading up to 00UTC (afternoon).

Acknowledgements

I would like to thank Beth Hall and Tim Brown for their assistance, CEFA (Climate, Ecosystem, and Fire Applications) for its support and CANSAC (California and Nevada Smoke and Air Committee) for its MM5 data.

Table of Contents

Tables

Figures

CHAPTER 1

INTRODUCTION

Mixing height is the height of the atmospheric layer adjacent to the ground in which the air is well mixed due to convection or mechanical turbulence (Seibert *et al.* 1997). It determines the extent to which pollutants can become diluted, and whether conditions are favorable for prescribed burning. Knowledge of mixing height affects forecasts of ozone concentration and assessment of emission control strategies. Mixing height is also used as a parameter in dispersion and air pollution models.

Many atmospheric variables can relate to or affect mixing height. Atmospheric mixing is caused by convection and turbulence. Convection occurs due to changes in the buoyancy of air caused by changes in temperature and moisture. Temperature is incorporated into variables such as air temperature, ground temperature, soil temperature, heat flux and radiation tendency. Turbulence is affected by wind speed and surface friction.

Problem Definition

This study was concerned with the problem of forecasting mixing height, especially to aid those who make pollution advisories or plan prescribed burns. As human populations grow and cities expand, air quality determinants such as mixing height will become increasingly important. To address this problem, model output statistics (MOS) derived from a mesoscale model and observations was used to develop mixing height forecast equations. The MOS approach incorporates forecasted atmospheric variables from a numerical weather prediction model, along with a predictand, in this case mixing height, into regression equations. The resulting equations contain those variables that are most significant for making the prediction.

The model output statistics (MOS) approach is advantageous because there are important differences between the real world and the representation from an atmospheric model. Local weather can be affected by topography or small bodies of water that are not accounted for in the model. Statistical relationships between model output and the observed values can help to reduce differences (Wilks 2006). A disadvantage of MOS is that numerical weather prediction models are changed and updated occasionally. This means that the model's output variables will not have been determined using a consistent method over time.

The potential value of developing and validating these equations includes the following:

- The equations can be used operationally to produce mixing height forecasts for 00 and 12UTC near the five station locations included in the study.
- Mixing height is difficult to forecast because it is dependent on interacting physical processes. The MOS approach determines which among many variables are statistically most significant for determining mixing height. Validation of these equations addresses the feasibility of applying MOS to mixing height.
- The results of the study can provide insight useful for those interested in developing MOS equations for mixing height over a broader region or at a

finer scale. The validation allows comparison of the differences in seasons, forecast lead-times and coastal versus inland locations.

Research Objectives

The objectives of this study were to develop MOS-based forecast equations from MM5 model output and observed mixing heights determined from standard NWS soundings, and to validate these equations against corresponding data. The results of the development and validation of these equations can be used for each potential value described in the previous section. Additionally, it is anticipated that these equations will be utilized operationally in a mesoscale modeling forecast system for California and Nevada, operated under the California and Nevada Smoke and Air Committee (CANSAC).

Two hundred forecast equations were developed, corresponding to each combination of five sounding locations in California and Nevada, two times per day (00UTC and 12UTC), four seasons of the year, and five forecast lead-times (0, 12, 24, 36, and 48 hour). In addition to the many MM5 model output variables, 24-hour persistence determined from the soundings was also included as a predictor variable. Mixing heights were determined from the soundings by application of Stull's (1991) parcel method. Figure 1 shows a flowchart of the MOS and validation process used in this study.

Validation methods included scatterplots of observed versus forecasted mixing heights, boxplots showing the magnitude and spread of individual forecast errors, and calculation of R-squared and bias statistics. Other trends or characteristics were also examined, such as similarities or differences in seasons or forecast lead-times.

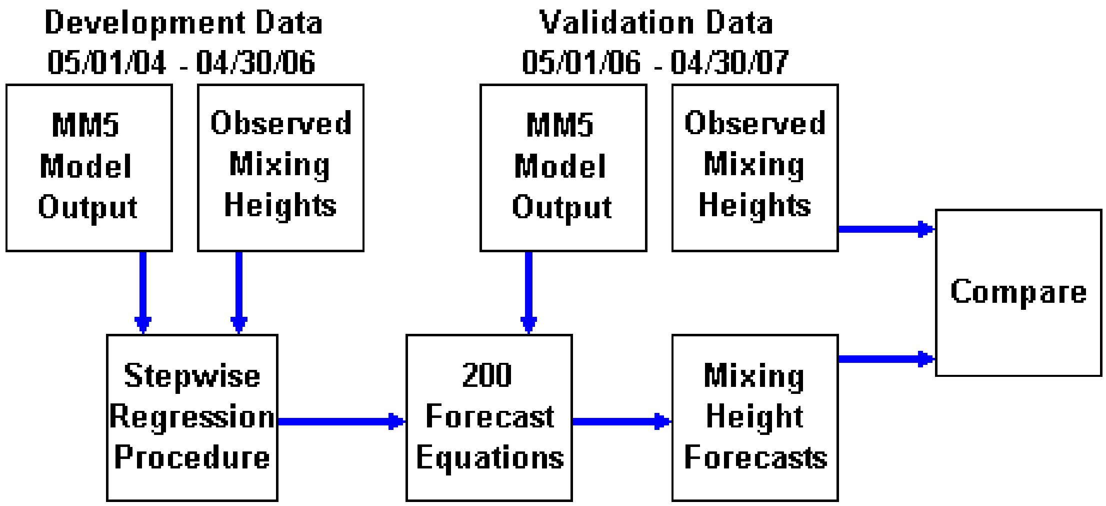

Figure 1-1 Flowchart of the MOS and validation process.

CHAPTER 2

BACKGROUND

Applications of Mixing Height

Mixing height and wind speed determine the extent to which ground-level air pollutants can become diluted, so mixing height is important for those who would make predictions of pollution concentrations or issue air pollution advisories (Miller 1967; Russell and Uthe 1974; Piringer *et al.* 1998). The Clean Air Act requires a minimum mixing height of 500 m for prescribed burning (NWS 2006) and knowledge of mixing height is useful for those concerned with smoke dispersion from wildland fires (Fearon 2000). Mixing height is an essential parameter for dispersion and air pollution models (Van Pul *et al.* 1994; Seibert *et al.* 1997; 2000). Many model parameterizations are calculated as a function of mixing height (Marsik *et al.* 1995), and these parameterizations can be used to represent boundary layer processes in global circulation models (Hanna and Yang 1985). Measurement of pollution concentrations for the purpose of assessing emission control strategies requires knowledge of mixing height (Berman *et al.* 1999). Forecasts of ozone concentration are extremely sensitive to mixing height uncertainties (Fay *et al*. 1997; Berman *et al*. 1999). Mixing heights are linked to precipitation anomaly when there is greater convection caused by the urban heat island (Russell *et al*. 1974).

Boundary Layer Structure and Evolution

During convective conditions, the boundary layer can be described in terms of three sublayers. The surface layer, covering the bottom 5 to 10% of a convective boundary layer, has a superadiabatic lapse rate, decreasing humidity with height and a sharp vertical wind shear due to ground friction. In the mixed layer, covering the middle 50 to 80% of a convective boundary layer, variables such as potential temperature, humidity, aerosol concentration, and wind speed and direction are roughly constant with height due to strong vertical mixing. The entrainment layer at the top of the boundary layer marks the transition from the mixed layer to the stable, relatively nonturbulent free atmosphere above. The entire convective boundary layer is often simply referred to as the mixed layer (Stull 1988; Seibert *et al.* 1997).

During the daytime, the mixed layer is generated from a combination of solar radiation being absorbed by the ground and heat conducted to the adjacent air, resulting in greater buoyancy and convection (Holzworth 1964). Since convection is driven by ground heating, the mixing height has a diurnal and seasonal cycle with higher mixing heights associated with warmer ground temperatures. The convective structures (thermal plumes) mix atmospheric properties due to the exchange of energy and matter (Seibert *et al.* 1997), and this turbulent mixing results in an adiabatic lapse rate (Leahey and Friend 1971).

Synoptic conditions can also have a strong influence on the mixed layer as vertical motion can either be enhanced or suppressed depending upon synoptic-scale factors (Crespi *et al.* 1995). When convection leads to clouds and rain showers, the mixed layer will be modified in a random fashion (Martin *et al.* 1988). In fact, if the mixing height reaches the condensation level, the cloud base height often coincides with the mixing height during the afternoon (Coulter and Holdridge 1998). During and after precipitation, the mixed layer structure can become very ill-defined (Coulter and Holdridge 1998).

The evolution of the boundary layer on a typical sunny day can be described by four stages. First, the morning's sunlight generates shallow convection that slowly grows, eroding the previous night's surface inversion at the rate of 10 to 100 m/hr. Second, during late morning when the mixed layer height reaches the residual layer from the previous day, there is rapid growth at the rate of 100 to 1000 m/hr until the capping inversion is reached. Third, the mixing height remains relatively constant during the afternoon, with further growth mainly caused by entrainment at the top. Fourth, the sun sets and the ground cools, creating a surface inversion which prevents further mixing from the ground while leaving the higher mixed layer as the residual layer (Martin *et al.* 1988; Stull 1988; Seibert *et al.* 1997).

Under convective conditions, entrainment leads to growth of the mixed layer. Rising buoyant thermals gain momentum and penetrate into the stable air at the top of the mixed layer. The negatively-buoyant thermal then sinks back to the mixed layer. However, during the overshoot, the warmer air from the free atmosphere above is pushed downward into the mixed layer where it is quickly mixed so that it loses its buoyancy. The mixing height increases as free atmosphere air is entrained into the mixed layer due to the overshooting thermals (Stull 1988).

A stable boundary layer forms, instead of a mixed layer, during the night as the ground cools, or any time the surface is cooler than the air above, such as may occur during warm advection (Van Pul *et al.* 1994). Because the mixing is primarily mechanically generated by wind, the stable boundary layer is more difficult to describe and model (Stull 1988). Mechanical (wind shear or convergence) and thermal (buoyant) turbulence are the two mechanisms that cause mixing (Crespi *et al.* 1995). Buoyancy tends to mix more uniformly because convection favors vertical motion whereas wind shear favors horizontal motion (Stull 1988). The diurnal variability in mixing height due to wind shear has been found to be substantially smaller than the variability due to buoyancy (Crespi *et al.* 1995). However, on days with overcast skies and at least moderate wind speeds, wind shear can control the mixing (Van Pul *et al.* 1994). Any mechanical mixing within a nighttime surface inversion will produce mixing heights that are likely to be less than 100 m, which is much less than those due to buoyancy (Marsik *et al.* 1995).

The characteristics of the ground itself affect the mixing height. Topographic barriers can cause mechanical mixing. The heat capacity of water causes major differences in mixing height between land and sea (Hsu 1979). The mixing height over a coastal area is affected by the temperature of the nearby waters and its effect on warm or cold air advection (McElroy and Smith 1991). The mixing height in May can be greater than in the summer because the soil is bare after the snow melts and grass has not yet grown (Lokoshchenko 2002). The urban heat-island effect can also raise the mixing height (Cheng *et al.* 2002).

Measurement of Mixing Height

There are different methods of measurement or calculation of mixing height. Measurement devices include radiosondes, lidars, sodar and wind profilers (Hanna *et al.*

1985). Even when a single measurement device is used, there are different techniques that can be used to determine the mixing height from the data. Remote operating systems, such as lidar, sodar and wind profilers, have the advantage of continuous operation, and do not interact with the air for which the characteristics are being measured (Seibert *et al.* 2000).

The nighttime mixing height is less defined than during the day. It has been defined as the height where turbulence becomes zero, the height of the low-level jet, the top of the surface inversion, or the height where the Richardson number exceeds 0.25 (Hanna *et al.* 1985). Mixing heights governed by wind shear instead of buoyancy are much harder to determine (Seibert *et al.* 2000). When a surface inversion is present, some models set the mixing height equal to zero (Russell and Uthe 1978).

Radiosondes routinely measure the atmospheric temperature profile, and are thus the most common source for operational determination of mixing height (Seibert *et al.* 2000). National Weather Service (NWS) radiosondes are released only twice daily, at 00 and 12UTC, so they are not sufficient for studying the evolution of mixing height. The mixing height can change by more than one kilometer in as short as one hour (White and Senff 1999). Since radiosondes are point measurements, there is also the possibility of passing within an exceptionally strong thermal, or through a cloud, both of which would give misleading results (Marsik *et al.* 1995). Mixing heights determined from standard radiosondes sometimes result in high uncertainty, especially at night (Seibert *et al.* 2000). An uncertainty of 50 m is expected under the best of conditions (Hanna *et al.* 1985).

The idea of the parcel method for determining mixing height is to follow the surface temperature upward dry adiabatically, as if it were a buoyant parcel of air, until it intersects the environmental temperature profile. The point of intersection is the estimated mixing height. Parcel methods are only suitable for unstable, convective conditions (Seibert *et al.* 2000). Unfortunately, lack of fully developed convection can be common (Piringer *et al.* 1998). Moisture in the air increases its buoyancy, leading to a higher mixing height (Berman *et al.* 1999). Therefore, the parcel method should be based on the virtual potential temperature (Seibert *et al.* 1997).

Stull's (1991) parcel method displaces parcels of virtual potential temperature upward from a sounding's relative maxima and downward from its minima. Parcels are tracked until they intersect the environmental profile or the ground. Overlapping movement regions are considered as a single unstable region. The mixing height is determined as the height of a surface-based unstable region.

There are several other methods for estimating the mixing height from sounding data. Some methods attempt to include the effects of temperature advection or subsidence, which are ignored in the simple parcel method (Seibert *et al.* 2000). The mixing height may be associated with a "critical inversion" for which the lapse rate exceeds 5 K/km, and the temperature difference between inversion base and top exceeds 2 K (Piringer *et al.* 1998). Parcel methods can be adjusted simply by adding an equation-based excess temperature at the surface (Seibert *et al.* 2000). The mixing height may be estimated as the inversion base height plus half of the depth of the inversion layer (Seibert *et al.* 2000). Other methods based on the bulk Richardson number take wind shear into account (Seibert *et al.* 2000).

Lidar (light detection and ranging) can be used to determine mixing height remotely and continuously. Transmitted laser light scatters off of particles in the atmosphere, and the lidar detects the backscattered energy. The mixing height is determined as the height at which the amount of scattering drops off (White and Senff 1999). Because lidar is directly measuring particle concentrations, it is sometimes considered a “true” measure of the mixing height (Coulter 1979; Hanna *et al.* 1985). However, there are some problems. A detected drop in particle concentration may actually correspond to the top of the residual layer from the previous day (White and Senff 1999; Seibert *et al.* 2000). Advective transport of particles can lead to misleading results (Seibert *et al.* 2000). One study found that there was no distinct dropoff of the return signal in a large number of cases (Steyn *et al.* 1999). It is also impossible for lidar to measure above clouds (Marsik *et al.* 1995).

Sodars (sound detection and ranging), or acoustic sounders, are another remote measuring device. Sodars send out a sound and detect a return signal that is sensitive to temperature fluctuations between the mixed layer and the warmer capping inversion (Russell and Uthe 1978; Coulter 1979; Stull 1988). Sodar estimates are based on volume averages rather than point measurements and may therefore yield more accurate results, particularly in complex terrain (Melas 1990). A significant drawback of sodars is their limited range. The maximum range is about 1 km, and the lowest range is about 40 m (Hanna *et al.* 1985; Seibert *et al.* 2000). Therefore, sodar is only appropriate during the night or early morning (Stull 1988), and even at those times will not be able to detect a strong surface inversion (Lokoshchenko 2002).

Another remote measuring device is the radar wind profiler. The wind profiler sends out an electromagnetic signal, and the return signal depends on temperature and especially moisture fluctuations associated with the inversion capping the convective mixed layer (Marsik *et al.* 1995; Coulter and Holdridge 1998; Seibert *et al.* 2000). Caution should be used when interpreting the return signal due to additional scattering from clouds, precipitation (Marsik *et al.* 1995), buildings or insects (Fearon 2000).

Modeling Mixing Height

Equations and models are also used to determine mixing height, or to model temperature profiles on which to apply a parcel method. Approximately 50 different equations are used to parameterize mixing height in different dispersion models (White and Senff 1999). Models may include the effects of advection and subsidence (Steyn and Oke 1982; Fearon 2000). Mixing height formulas can be functions of friction velocity, Monin-Obukhov length, Coriolis parameter (Hanna *et al.* 1985; Piringer *et al.* 1998), soil moisture (Seibert *et al.* 2000), stability, temperature and wind velocity (Cheng *et al.* 2002). Models also derive mixing height using an analysis of the bulk Richardson number (Seibert *et al.* 2000).

Most of the existing studies involving mixing height (but not MOS equations) compare the mixing heights measured by different methods (such as lidar and radiosonde). Studies involving discrete measurements usually have less than 100 data points, and continuous measurements tend to span a few weeks. There seems to be agreement that mixing heights during the night are much more complicated than convective mixing heights during the day. Hanna *et al.* (1985) found uncertainties of 10% during the daytime and 25 to 100% during the night. Hanna and Yang (2001) found that 60% of model simulations of daytime mixing height were within 20% of observations, but for low observed values such as 300 m, the error was a factor of 2 to 4. Cheng *et al.* (2002) found that the parcel method, with errors of 15%, did better compared to an equation-based method. Berman *et al.* (1999) found mixing heights based on their MM5 output to be 10 to 20% too low at coastal sites, and within 25% at inland sites.

Crespi *et al.*'s (1995) study provides the closest comparison to this study, but it was focused on mixing height evolution under different synoptic conditions. Observed mixing heights were determined by application of a simple parcel method applied to temperature profile data, and complemented by winds and relative humidity. Profile data was obtained using free and tethered balloon sounding systems at one location throughout the day for a few days during each of 15 months. In Crespi's study, nonlinear regression equations were developed for mixing height as a function of time of day. Stepwise regression equations were also developed that related mixing height to other observed variables. The possible predictors included direct and diffuse solar radiation, mean horizontal wind speed, surface air temperature and time of day. These are "perfect prog" (perfect prognosis) equations that use other observed variables as predictors as opposed to MOS equations that use forecasted predictor variables from a numerical model (Wilks 2006). Operationally, both methods substitute forecasted values into the equations. Under clear skies mixing height equations included direct and diffuse sunlight as predictors. Under cloudy conditions diffuse sunlight and V-wind were included.

CHAPTER 3

DATA

Sounding Data

Standard 00 and 12UTC soundings taken by the NWS were obtained for the three-year period from May 1, 2004 through April 30, 2007 from the University of Wyoming Department of Atmospheric Science website (http://weather.uwyo.edu/upperair/sounding.html). Figure 3-1 shows a portion of the table format of the sounding data. Only the height (HGHT) and virtual potential temperature (THTV) columns were needed.

72493 OAK Oakland Int Observations at 00Z 01 Jul 2006

PRES hPa	HGHT m	TEMP C	DWPT C	RELH %	MIXR g/kg	DRCT deg	SKNT knot	THTA K	THTE K	THTV K
1017.0	3	19.2	12.2	64	8.85	260	8	290.9	316.2	292.5
1000.0	149	15.6	9.6	67	7.55	265	7	288.8	310.3	290.1
981.7	305	14.6	9.8	73	7.81	270	5	289.2	311.5	290.6
958.0	512	13.2	10.1	81	8.16	263	6	289.9	313.2	291.3
947.0	610	14.8	8.5	66	7.39	260	7	292.4	313.8	293.7
941.0	663	15.6	7.6	59	7.00	263	8	293.8	314.3	295.1
938.0	691	16.4	2.4	39	4.87	264	8	294.9	309.4	295.8
925.0	810	20.0	3.0	32	5.16	270	9	299.8	315.4	300.7
914.0	914	22.3	2.7	28	5.13	270	10	303.2	319.0	304.1
908.0	971	23.6	2.6	25	5.11	274	10	305.1	320.9	306.0
886.0	1184	23.8	2.8	25	5.31	288	11	307.4	324.0	308.4

Figure 3-1 Example sounding output data for Oakland, CA.

Figure 3-2 shows a map of and Table 3-1 provides information about the sounding locations. On the west coast, 00UTC occurs at 4:00 or 5:00 PM local time depending on daylight savings time, and 12UTC occurs at 4:00 or 5:00 AM. This study refers to 00UTC as "afternoon" and 12UTC as "early morning". The parcel methods of determining mixing height are really only designed for the convective conditions of afternoon, and not for nighttime. However, this study applies the same method to the early morning soundings for comparison with the afternoon. Table 3-2 lists the number of missing data points for both the soundings and the MM5 model output. There were a significant number of missing soundings at the DRA station.

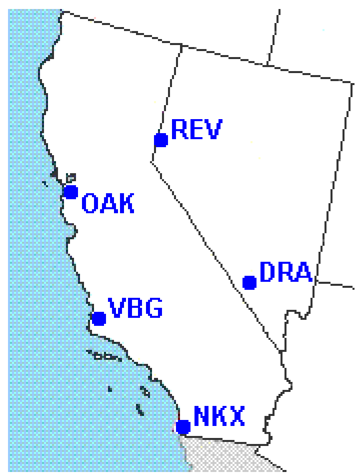

Figure 3-2 Geographical locations of the sounding data used in the study.

Table 3-1 Brief description of the NWS sounding stations.

Station	Latitude	Longitude	Elev. (m)	Name	Location
DRA	36.62 N	116.02 W	1006	Desert Rock Airport	Mercury, NV
NKX	32.83 N	117.12 W	134	Miramar Marine Corps Air Station	San Diego, CA
OAK	37.75 N	122.22 W	6	Oakland Metro International Airport	Oakland, CA
REV	39.57 N	119.78 W	1516	Reno NWS Forecast Office	Reno, NV
VBG	34.75 N	120.57 W	121	Vandenberg Air Force Base	Lompoc, CA

Table 3-2 Number of missing sounding and MM5 model data. Each data point represents one day. Possible days in spring is 92, summer is 92, fall is 91 and winter is 90. Values for MM5 model are the same for all stations and forecast lead-times.

			00UTC						12UTC					
			MM5 Model	Soundings DRA	NKX	OAK	REV	VBG	MM5 Model	Soundings DRA	NKX	OAK	REV	VBG
Development	May 2004 - April 2005	Spring	5	28	3	7	6	4	4	20	2	6	2	2
		Summer	8	0	1	0	1	3	13	1	1	1	1	4
		Fall	0	12	7	9	14	9	3	14	8	11	18	7
		Winter	4	15	2	3	2	1	2	10	2	4	3	2
	May 2005 - April 2006	Spring	1	42	2	2	2	22	3	29	3	1	3	22
		Summer	1	41	1	5	0	1	0	28	0	2	0	1
		Fall	0	45	0	5	0	1	2	32	0	5	0	0
		Winter	2	43	0	3	1	28	2	31	2	5	3	31
Validation	May 2006 - April 2007	Spring	6	51	3	4	5	3	7	41	5	6	7	5
		Summer	0	42	1	1	14	22	0	29	1	1	11	24
		Fall	6	45	5	5	6	7	6	33	5	5	4	5
		Winter	3	43	0	2	1	3	2	31	1	6	1	4

MM5 Model Output

MM5 model output was obtained from CANSAC (California and Nevada Smoke and Air Committee, http://cefa.dri.edu/COFF/cofframe.php) for the three-year period from May 1, 2004 through April 30, 2007. Table 3-2 lists the number of missing data points. The model output data used in this study was from the innermost domain (D3) as shown in Figure 3-2. This domain has a 4-km grid resolution and 31 vertical levels. More specific model setup and scheme information can be found on the CANSAC website. Observed sounding mixing heights were associated with MM5 output data at the closest model gridpoints. With a 4-km grid resolution, the maximum offset between gridpoint and sounding location was a few kilometers. Horizontal wind variables are located at grid corners while all other variables are at grid centers.

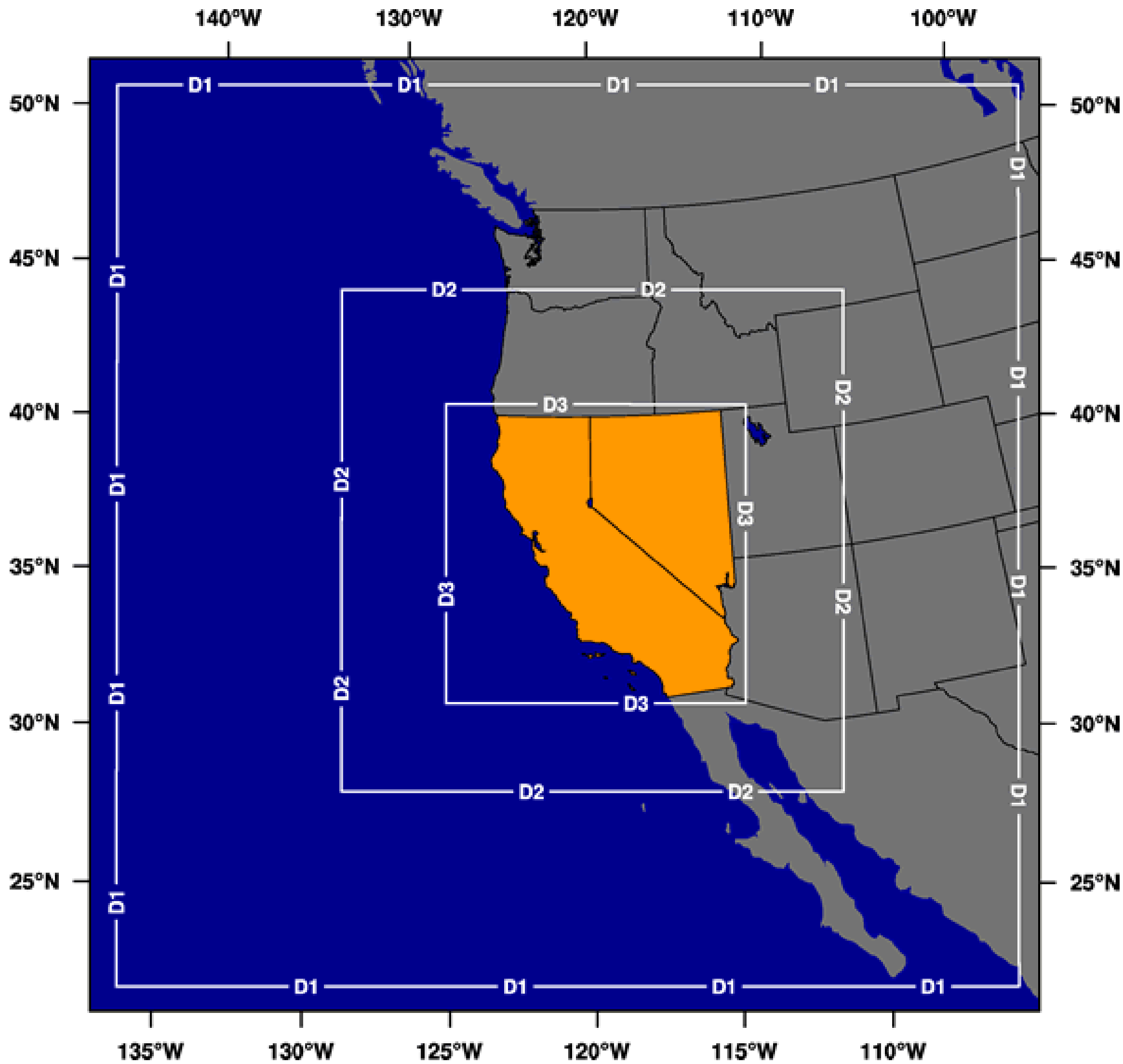

Figure 3-3 Map showing the CANSAC - MM5 model output domain.

Output was obtained for model runs at 00 and 12UTC, and for each of 0, 12, 24, 36, and 48 hour forecasts. Forecasts leading up to 00UTC (afternoon) included 00Z F00, 12Z F12, 00Z F24, 12Z F36, and 00Z F48, where 00Z and 12Z indicate the model run time and "F" precedes the forecast lead-time. Forecasts leading up to 12UTC (early morning) included 12Z F00, 00Z F12, 12Z F24, 00Z F36, and 12Z F48. Table 3-3 lists the MM5 output variables used in this study. Any output that was constant, such as terrain height, was not used.

Table 3-3 The 269 MM5 output variables used as predictors in this study. The variable numbers refer to the model vertical level. One non-MM5 variable, 24-hour persistence (24PER), was also used.

Abbrev.	Predictor Variables	Units
GRNDT	Ground temperature	K
PBLHT	PBL height	m
REGIM	PBL regime (category, 1-4)	
SHFLX	Surface sensible heat flux	W/m^2
LHFLX	Surface latent heat flux	W/m^2
UST	Frictional velocity	m/s
SWDWN	Surface downward shortwave radiation	W/m^2
LWDWN	Surface downward longwave radiation	W/m^2
SWOUT	Top outgoing shortwave radiation	W/m^2
LWOUT	Top outgoing longwave radiation	W/m^2
SOIT 1-6	Soil temperature in a few layers	K
T2	Temperature at 2 m	K
Q2	Mixing ratio at 2 m	kg/kg
U10	U-wind at 10 m	m/s
V10	V-wind at 10 m	m/s
TK (1-31)	Turbulent kinetic energy	J/kg
RT (1-31)	Atmospheric radiation tendency	K/DAY
T (1-31)	Temperature	K
Q (1-31)	Water vapor mixing ratio	kg/kg
PP (1-31)	Perturbation pressure	Pa
U (1-31)	U-wind	m/s
V (1-31)	V-wind	m/s
W (1-32)	Vertical velocity	m/s

The vertical levels 1-31 are half-sigma levels numbered from the ground up. The *W* variable, with vertical levels 1-32, uses full-sigma levels. The values of sigma for these levels can be found on the CANSAC website. For the half-sigma levels, vertical level 1 (nearest to the ground) has sigma equal to 0.998505, and vertical level 31 has sigma equal to 0.014075. For the full-sigma levels, vertical level 1 has sigma equal to 1, and vertical level 32 has sigma equal to 0. The atmospheric pressure at these vertical levels can be calculated from

$$pressure(i,j,k) = sigma(k) * pstar(i,j) + ptop + PP(i,j,k), \quad \text{(Equation 3-1)}$$

where the sigma coordinate is constant for a given vertical level, *pstar* is constant for a given station location, and *ptop* is constant within the model. *Ptop* is reference pressure at the model top, and is set at a constant 10000 Pa. *Pstar* is equal to the reference surface pressure minus *ptop*, and is constant for each station as follows: DRA=75644 Pa, NKX=87524 Pa, OAK=89448 Pa, REV=73728 Pa, and VBG=88524 Pa. This leaves the pressure at each vertical level as only a function of the pressure perturbation *PP*. Once the pressure is known, the altitude *Z* can be calculated from the hydrostatic equation,

$$\Delta P = -\rho g \Delta Z, \quad \text{(Equation 3-2)}$$

where ΔP is the change in pressure, ρ is density, g is gravity, and ΔZ is the change in altitude. The hypsometric equation could also be used, given in one form as

$$Z_2 - Z_1 = 29.3\, T_v \ln(P_1/P_2), \quad \text{(Equation 3-3)}$$

where Z is altitude, P is pressure and T_v is the mean virtual temperature within the layer.

The main moisture variable in the MM5 output is the water vapor mixing ratio Q. The mixing ratio is the ratio of the mass of water vapor to the mass of dry air, and is given in units of kg/kg. The saturation mixing ratio varies with temperature and pressure. Higher temperatures and lower pressures have higher values of saturation mixing ratio. Relative humidity, a more familiar water vapor variable, is equal to the mixing ratio divided by the saturation mixing ratio.

One additional variable used in this study, which was not produced as MM5 output, was 24-hour persistence (24PER). This was the value of the sounding-determined mixing height 24 hours prior to the time of the model or equation forecast. During the two years of data used for equation development, 24PER was directly obtainable from the soundings. During the third year used for validation, 24PER could be directly obtained from the sounding 24 hours prior to the 0, 12, and 24-hour forecasts only. For the 36 and 48-hour forecasts, 24PER was taken as the result of the 12 and 24-hour MOS equation mixing height forecast.

CHAPTER 4

METHODS

Stull Mixing Height Procedure

Stull's (1991) procedure for determining stability was used as a parcel method for determining mixing height from the virtual potential temperature profiles within the sounding data. Virtual potential temperature takes the buoyant effects of water vapor into account. The procedure is applied by displacing air parcels upward from every relative maxima, and downward from every relative minima within the profile. This represents the buoyant motions of air parcels with different densities. The air parcels move dry adiabatically (straight up or down since potential temperature is conserved) until intersecting either the profile or the ground. Regions of parcel ascent or descent are unstable, and overlapping unstable regions blend into one. The mixing height is the height of the unstable region (if any) which is connected to the ground. Figure 4-1 shows several examples of determining mixing height by application of Stull's method to a virtual potential temperature profile.

Potential temperature is the temperature that an air parcel would have if it moved up or down dry adiabatically to a standard pressure (usually 1000 hPa). Figure 3-1 reveals that the sounding data used in this study lists potential temperatures with reference to 1000 hPa. The 1000 hPa vertical level has equal values for temperature (15.6 C) and potential temperature (288.8 K) since 15.6 C + 273.15 = 288.8 K. Potential temperature is related to height by

$$\theta(z) = T(z) + \Gamma_d * z, \qquad \text{(Equation 4-1)}$$

where θ is potential temperature, T is temperature, Γ_d is the dry adiabatic lapse rate (a constant 9.8 K/km) and z is the vertical coordinate.

Mixing heights in this study are defined in terms of meters above ground level, not in reference to 1000 hPa. The potential temperatures in the sounding data could all be adjusted so that they are in reference to the ground, but since this would simply adjust them all by a constant amount, the intersection points of the air parcels with the profile would be exactly the same as if the data were not adjusted. For example, in Figure 3-1 the difference between z-coordinate 149 m at 1000 hPa and ground-level z-coordinate 3 m at 1017 hPa is 146 m. To change all potential temperatures so that they are in reference to the ground, add $\Gamma_d * z$ = 0.0098 K/m * 146 m = 1.4 K to every potential temperature. However, this linear alteration is unnecessary since raising the ground-level parcel would intersect the potential temperature profile at exactly the same height. The same applies to higher elevation stations like REV for which the ground level pressure is always less than the 1000 hPa reference pressure.

In this study, the method was applied to each sounding by examining the virtual potential temperatures sequentially by vertical level from the ground up. The algorithm proceeds as follows: (1) Save the ground temperature. (2) Find the first intersection (possibly at height zero) of the ground temperature with an increasing profile. (3) Step upward from there, keeping track of the maximum temperature. (4) If the profile temperature ever drops below the ground temperature, then raise the maximum temperature up to an intersection with the (increasing) profile, and return to step 3. The mixing height is the highest intersection found during this procedure.

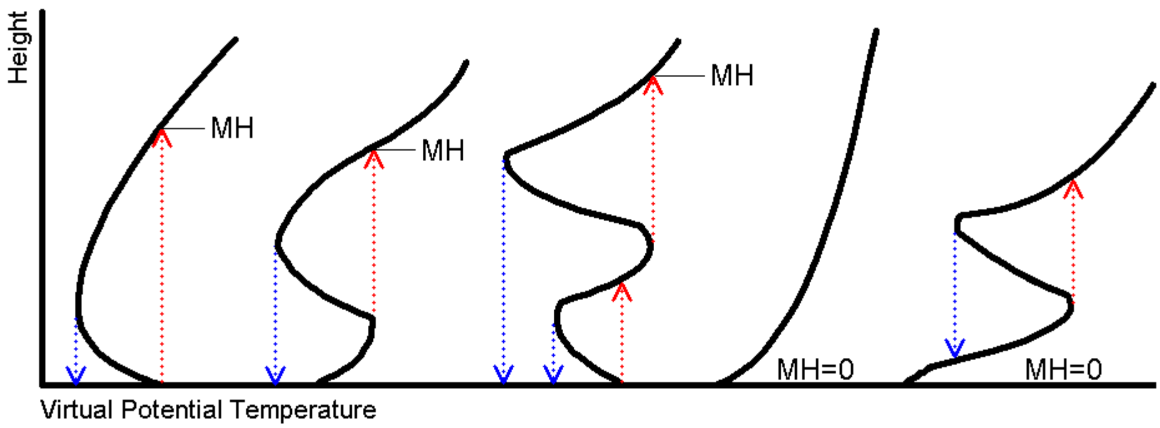

Figure 4-1 Five examples of determining mixing height using Stull's method on virtual potential temperature profiles. Red arrows represent ascending air parcels. Blue arrows represent descending air parcels. Virtual potential temperature increases to the right. Height increases upward.

Forecast Equation Development

Two hundred forecast equations were developed, representing each combination of 00UTC (afternoon) and 12UTC (early morning), five stations (DRA, NKX, OAK, REV and VBG), four seasons (spring, summer, fall, winter), and five forecast lead-times (F00, F12, F24, F36 and F48). Spring data included the months of March, April and May; summer included June, July and August; fall included September, October and November; winter included December, January and February. The MM5 data and sounding mixing heights within the two-year period from May 1, 2004 through April 30, 2006 were used for equation development. The MM5 data within the one-year period from May 1, 2006 through April 30, 2007 were used in the resulting equations to obtain mixing height forecasts, and these were compared with the sounding mixing heights during this period.

In addition to the 269 MM5 output variables, 24-hour persistence was used as a predictor variable. This is the value of the sounding mixing height 24 hours prior to the forecast time. For F00, F12 and F24, both the development and validation data can obtain a value for 24-hour persistence from actual sounding mixing heights. For F36 and F48, the development data can use sounding mixing heights, but the validation data cannot. Instead, 24-hour persistence for F36 and F48 was taken as the mixing heights generated from the corresponding F12 and F24 forecast equations.

All of the predictor variables in both the development and validation data were standardized by subtracting the mean, then dividing by the standard deviation of each variable within its data category. (A data category consists of a station, season and forecast lead-time, leading up to either 00 or 12UTC.) Standardization allows variables with different scales and units to be compared, giving them all a constant variance (standard deviations equal to one). The sounding mixing heights in the development data were also standardized. The mean and standard deviation for the original soundings were saved so that they could be applied to the result obtained from plugging the standardized validation variables into the forecast equations, undoing the standardization of the result to obtain a meaningful mixing height forecast.

Any variable which had all zeros (or constant) within its category caused a problem because the standard deviation was zero, and standardizing then divided by zero. In these cases the variables were omitted from equation development. At the model initialization (0-hour forecast), the following variables were not output and therefore excluded: PBLHT, REGIM, SHFLX, LHFLX, UST, SWDWN, LWDWN, SWOUT, LWOUT, T2, Q2, U10, V10, TK (1-31), RT (1-31), and W (32). Any forecasts for night excluded SWDWN and SWOUT since there was no sunlight at that time. A few forecasts for night, particularly during cold months, excluded 24-hour persistence because the sounding mixing heights were all zero. In nine out of the 200 equations, all forecasting for nighttime (12UTC), the development sounding mixing heights were all zero. Unlike individual predictor variables, the predictand cannot be excluded from equation development. To address this issue, the standard deviation was set to 0.01 (1 cm) which is well within the margin of error since all sounding mixing heights were rounded to the nearest meter. However, this adjustment did not matter because regression equations failed to develop when the predictand was all zeros. (In order to predict a result which is always zero, coefficients should all be zero.)

The "stepwisefit" function from MATLAB's Statistics Toolbox was used to produce the 200 forecast equations. This function performs forward stepwise regression, adding the most statistically significant term (lowest p-value) at each step until a stopping criterion is met. The default maximum p-value for adding a predictor is 0.05 and the minimum for removing a predictor is 0.10. The resulting variables and coefficients included in the mixing height forecast equations are listed in Appendix A.

Goodness of fit measures were calculated as the regression equations were developed. These included the F-ratio, root-mean squared error (RMSE) and adjusted R-squared value. The F-ratio is a qualitative measure of the strength of a regression, with a higher value meaning a stronger relationship between x and y (Wilks 2006). The RMSE gives the typical error magnitude of the forecast variable. The R-squared statistic, or coefficient of determination, can be interpreted as the proportion of the forecast variable that is accounted for by the regression (Wilks 2006). Adjusted R-squared is the R-squared statistic that has been adjusted for the residual degrees of freedom.

The MM5 output variables (and 24-hour persistence) from the validation data are put into the equations to produce mixing height forecasts. A mixing height developed from a forecast equation is still in scaled form, so the mean and standard deviation of the sounding mixing height from the development data are used to undo the scaling. Tables 4-1 and 4-2 list the mean and standard deviation used for each of the 200 equations. In this study, mixing heights were rounded to the nearest meter and negative forecasts were set to zero.

Table 4-1 Mean and standard deviation of observed mixing heights in the development data. Forecast hours (e.g., F12) lead up to 00UTC (afternoon).

		DRA		NKX		OAK		REV		VBG	
		Mean (m agl)	Std. (m)	Mean (m agl)	Std. (m)	Mean (m agl)	Std. (m)	Mean (m agl)	Std. (m)	Mean (m agl)	Std. (m)
Spring	00Z F00	2399	813	760	424	694	483	1316	1091	447	344
	12Z F12	2425	835	746	414	671	477	1355	1091	436	343
	00Z F24	2427	833	752	420	668	474	1364	1093	432	340
	12Z F36	2465	836	751	421	671	474	1417	1119	427	339
	00Z F48	2460	829	754	418	658	468	1411	1112	429	340
Summer	00Z F00	3357	1099	479	220	384	279	2630	1365	318	162
	12Z F12	3317	1087	474	224	381	279	2612	1370	320	164
	00Z F24	3362	1091	479	220	376	274	2622	1367	322	162
	12Z F36	3372	1071	468	220	380	279	2628	1347	322	161
	00Z F48	3378	1106	473	220	383	281	2618	1363	326	161
Fall	00Z F00	1916	1206	466	355	380	373	1361	1278	292	239
	12Z F12	1865	1159	455	352	364	354	1336	1277	294	240
	00Z F24	1871	1186	466	355	378	374	1339	1273	291	239
	12Z F36	1818	1139	464	358	372	377	1328	1266	284	242
	00Z F48	1799	1154	461	358	375	375	1309	1260	287	242
Winter	00Z F00	829	774	453	470	318	394	398	590	293	341
	12Z F12	831	773	472	481	332	415	383	584	303	350
	00Z F24	817	763	461	474	338	423	380	579	303	353
	12Z F36	838	771	466	473	348	431	378	574	313	354
	00Z F48	821	761	467	474	334	411	364	569	307	354

Table 4-2 Mean and standard deviation of observed mixing heights in the development data. Forecast hours (e.g., F12) lead up to 12UTC (early morning).

		DRA		NKX		OAK		REV		VBG	
		Mean (m agl)	Std. (m)	Mean (m agl)	Std. (m)	Mean (m agl)	Std. (m)	Mean (m agl)	Std. (m)	Mean (m agl)	Std. (m)
Spring	12Z F00	0	5	45	160	28	120	3	34	11	88
	00Z F12	0	5	41	155	28	120	3	34	11	88
	12Z F24	0	5	43	158	29	122	3	34	11	88
	00Z F36	0	5	39	149	30	122	3	34	11	88
	12Z F48	0	5	49	165	30	122	3	34	12	88
Summer	12Z F00	0	4	83	184	48	96	6	75	13	44
	00Z F12	0	4	80	182	48	96	6	74	13	44
	12Z F24	0	4	83	183	45	90	6	75	13	44
	00Z F36	0	4	81	182	45	94	6	74	13	44
	12Z F48	0	0	76	174	47	96	6	75	13	44
Fall	12Z F00	3	29	57	164	13	55	18	202	35	342
	00Z F12	3	29	56	162	12	54	18	200	34	337
	12Z F24	3	29	55	162	14	57	19	204	35	344
	00Z F36	3	29	53	160	13	56	18	201	34	339
	12Z F48	3	29	53	161	12	53	19	204	35	345
Winter	12Z F00	0	0	15	65	1	15	12	72	14	132
	00Z F12	0	0	15	65	1	15	13	72	14	133
	12Z F24	0	0	15	65	0	0	12	72	14	132
	00Z F36	0	0	15	66	0	0	10	62	14	134
	12Z F48	0	0	15	65	0	0	12	71	14	132

Validation Methods

Within each of the 200 categories (00 and 12UTC, five stations, four seasons and five forecast lead-times), the MOS mixing height forecasts were validated against the sounding mixing heights using several methods.

First, scatterplots were produced showing the observed values from the soundings versus the forecasted values from the MOS equations. The "$y = x$" line was drawn for comparison to show the location of a perfect forecast. For convenient comparison, the scatterplots of different seasons are horizontally adjacent and the scatterplots of different forecast lead-times leading up to the same sounding mixing heights are vertically adjacent. The scatterplots provide the quickest impression of the results of this study. They show how well the forecast and observed mixing heights correlate along the $y = x$ line, and allow a visual estimation of the extent (in meters) and frequency of error.

Second, the value of adjusted R-squared was computed from the linear correlation between the observed and forecasted mixing heights. R-squared, the coefficient of determination, is the proportion of the variation that can be accounted for by the regression (Wilks 2006). Adjusted R-squared is the R-squared statistic that has been adjusted for the residual degrees of freedom. Higher R-squared values are sometimes interpreted to mean higher forecast skill. However, this statistic must be interpreted with caution because it is insensitive to scale (Murphy 1995). Two different scatterplots laid out in the same pattern, but with one having a variability of 10 meters and the other 500 meters around the $y = x$ line, would have the same value for R-squared even though one situation shows much greater forecast skill than the other.

The third validation method was to compute the bias statistic. Bias, or mean error, is equal to the mean forecast minus the mean observation. A positive bias indicates that forecasts are too high on average, and negative bias indicates that forecasts are too low. Unlike the R-squared statistic, bias indicates the scale of forecast error. However, it is limited because it only uses the average forecast and observation.

The fourth method was to graph boxplots which describe the spread and magnitude of individual forecast errors. The box in the center of each boxplot represents the middle 50% of the forecast errors. The "whiskers" extending from the box represent the top and bottom 25% of forecast errors, minus outliers which are indicated with red plus signs. Some of the outliers in the boxplots are not shown because the scale was cut off to provide the best graphic display overall, but the scatterplots show all data points. Outliers were determined by the 1.5 times interquartile range criterion for maximum whisker length.

CHAPTER 5

RESULTS

Listings of the predictor variables included in the forecast equations are located in Appendix A. The tables in Appendix B provide the number of occurrences of each predictor variable. All stations and forecast lead-times are grouped together so that each count refers to 25 equations. The following observations can be made regarding the inclusion of MM5 variables in the MOS forecast equations:

- Pressure perturbation (PP) is rarely included.
- The three wind components U, V and W are included in roughly equal measure.
- Temperature (T) and soil temperature (SOIT1-6) are noticeably more common for forecasts leading up to 00UTC (afternoon) compared to 12UTC (early morning).
- Two-meter mixing ratio (Q2) is also noticeably more common for 00UTC.
- Radiation tendency (RT) has a relatively strong showing in the equations.
- 24-hour persistence (24PER) is by far the most common predictor variable for forecasts leading up to 00UTC (afternoon), except for during the spring. For forecasts leading up to 12UTC (early morning), 24PER is more common in the spring.
- Latent heat flux (LHFLX) makes a strong showing in winter and spring for forecasts leading up to 00UTC.

- The only variables that are never included are two-meter temperature (T2) and pressure perturbation (PP) at 12 of the vertical levels.

Goodness of fit measures were calculated as the regression equations were developed. Table 5-1 shows the F-ratio for the 200 forecast equations. The F-ratio is a qualitative measure of the strength of a regression, with a higher value meaning a stronger relationship between *x* and *y* (Wilks 2006). The values in the table generally indicate better, more stable results for forecasts leading up to 00UTC (afternoon) compared to 12UTC (early morning). Considering only the 00UTC cases, the following observations for F-ratio can be made:

- “OAK summer” has the best F-ratios, with “DRA fall” placing second.
- The Nevada stations DRA and REV have their highest F-ratios during the fall, but the coastal stations NKX, OAK and VBG have their lowest F-ratios during the fall.
- “DRA spring” and “OAK summer” show a decrease in F-ratio with increasing forecast lead time, but the other 18 cases leading up to 00UTC do not.

Those cases leading up to 12UTC in which the regression included no coefficients are indicated with an F-ratio of “NaN” (not-a-number). Nine of the 12UTC equations, mostly during the winter, could not be developed because the predictand mixing heights were all zero. These are indicated in Table 5-1 with “No eq.” (no equation). The DRA Spring 00Z F12 case is a strange one where the TK(22) predictor variable was always 0.2 except for a higher value on one date, and the sounding mixing heights were all zero except for a higher value on exactly the same date. Therefore, the TK(22) variable correlated extremely well with the sounding and the results of the regression indicate that the variable is a perfect predictor, but this can be interpreted as a fluke since the variable counts in Appendix B show no particular emphasis for this variable.

Table 5-1 F-Ratio for each of 200 equations. Forecast hours (e.g., F12) lead up to 00UTC (afternoon) or 12UTC (early morning).

		Forecasts leading up to 00UTC (afternoon)						Forecasts leading up to 12UTC (early morning)				
		DRA	NKX	OAK	REV	VBG		DRA	NKX	OAK	REV	VBG
Spring	00Z F00	34	27	29	15	24	12Z F00	13	19	7	NaN	6
	12Z F12	23	22	16	10	20	00Z F12	9e15	24	7	5	47
	00Z F24	21	20	21	11	20	12Z F24	44	10	12	6	29
	12Z F36	19	22	20	11	24	00Z F36	40	7	9	5	28
	00Z F48	16	16	20	14	23	12Z F48	25	12	6	NaN	61
Summer	00Z F00	49	33	66	53	35	12Z F00	4	8	10	6	5
	12Z F12	20	22	46	10	23	00Z F12	5	10	7	6	40
	00Z F24	19	20	45	11	23	12Z F24	NaN	6	7	NaN	10
	12Z F36	12	21	43	11	24	00Z F36	7	9	9	NaN	6
	00Z F48	20	16	41	10	27	12Z F48	No eq.	7	14	NaN	6
Fall	00Z F00	55	20	22	34	15	12Z F00	12	14	10	51	NaN
	12Z F12	33	19	16	30	13	00Z F12	32	16	9	10	NaN
	00Z F24	32	19	17	25	14	12Z F24	44	11	9	6	52
	12Z F36	34	13	19	28	14	00Z F36	118	12	13	12	44
	00Z F48	33	15	14	34	14	12Z F48	16	11	10	7	5
Winter	00Z F00	50	22	20	26	23	12Z F00	No eq.	9	8	11	5
	12Z F12	27	15	25	23	26	00Z F12	No eq.	19	19	8	22
	00Z F24	23	22	15	17	23	12Z F24	No eq.	14	No eq.	16	62
	12Z F36	23	20	20	26	18	00Z F36	No eq.	32	No eq.	6	81
	00Z F48	22	18	17	19	26	12Z F48	No eq.	13	No eq.	11	45

Table 5-2 shows the root-mean squared error (RMSE) for the 200 forecast equations. The RMSE gives the typical error magnitude of the forecast variable. Since the development variables were all standardized, the error magnitudes listed in the table can be interpreted as the number of standard deviations. The RMSE for forecasts leading up to 00UTC (afternoon) are lower than those leading up to 12UTC (early morning) in most cases. The 12UTC cases displaying a RMSE equal to one are the equations that did not include any variables. "No eq." (no equation) means that the predictand values were all zeros so no equation could be developed.

Considering only the 00UTC cases, the following observations for RMSE can be made:

- "OAK summer" and "DRA fall" have the lowest RMSE values.
- The Nevada stations DRA and REV have their lowest RMSE during the fall, but the RMSE of the coastal stations NKX, OAK and VBG are among their highest during the fall.
- There is no clear association between an increasing forecast lead-time and an increasing RMSE.

Table 5-2 RMSE for each of 200 equations. Forecast hours (e.g., F12) lead up to 00UTC (afternoon) or 12UTC (early morning).

		Forecasts leading up to 00UTC (afternoon)						Forecasts leading up to 12UTC (early morning)				
		DRA	NKX	OAK	REV	VBG		DRA	NKX	OAK	REV	VBG
Spring	00Z F00	0.58	0.69	0.73	0.71	0.69	12Z F00	0.69	0.80	0.98	1.00	0.93
	12Z F12	0.44	0.59	0.64	0.88	0.57	00Z F12	0.00	0.80	0.95	0.97	0.36
	00Z F24	0.59	0.64	0.60	0.88	0.62	12Z F24	0.37	0.87	0.84	0.95	0.92
	12Z F36	0.58	0.67	0.64	0.90	0.52	00Z F36	0.53	0.82	0.92	0.97	0.92
	00Z F48	0.58	0.66	0.72	0.93	0.70	12Z F48	0.38	0.87	0.94	1.00	0.67
Summer	00Z F00	0.44	0.61	0.55	0.57	0.64	12Z F00	0.99	0.85	0.85	0.95	0.99
	12Z F12	0.51	0.71	0.45	0.80	0.62	00Z F12	0.95	0.86	0.84	0.97	0.54
	00Z F24	0.65	0.62	0.47	0.86	0.64	12Z F24	1.00	0.93	0.89	1.00	0.95
	12Z F36	0.73	0.66	0.45	0.84	0.69	00Z F36	0.91	0.86	0.78	1.00	0.93
	00Z F48	0.57	0.68	0.52	0.80	0.69	12Z F48	No eq.	0.84	0.78	1.00	0.96
Fall	00Z F00	0.47	0.71	0.66	0.62	0.81	12Z F00	0.83	0.87	0.92	0.58	1.00
	12Z F12	0.44	0.62	0.73	0.64	0.69	00Z F12	0.42	0.72	0.91	0.97	1.00
	00Z F24	0.43	0.61	0.67	0.63	0.75	12Z F24	0.34	0.86	0.89	0.98	0.37
	12Z F36	0.53	0.78	0.59	0.61	0.72	00Z F36	0.21	0.80	0.90	0.97	0.48
	00Z F48	0.52	0.71	0.71	0.64	0.81	12Z F48	0.63	0.83	0.92	0.98	0.98
Winter	00Z F00	0.54	0.65	0.74	0.73	0.69	12Z F00	No eq.	0.88	0.98	0.90	0.97
	12Z F12	0.53	0.67	0.68	0.75	0.64	00Z F12	No eq.	0.83	0.80	0.94	0.83
	00Z F24	0.52	0.71	0.71	0.72	0.57	12Z F24	No eq.	0.77	No eq.	0.80	0.73
	12Z F36	0.51	0.76	0.66	0.76	0.62	00Z F36	No eq.	0.65	No eq.	0.93	0.50
	00Z F48	0.66	0.72	0.74	0.73	0.72	12Z F48	No eq.	0.75	No eq.	0.78	0.42

Table 5-3 lists the adjusted R-squared statistic for the development of the 200 forecast equations. For forecasts leading up to 12UTC (early morning), the equations which included no variables show an adjusted R-squared value of zero, and the cases in which no equation could be developed because all of the predictand values were zero are indicated as “No eq.” (no equation). The adjusted R-squared values for 12UTC are generally lower than those for 00UTC. In addition, the 12UTC values seem somewhat unstable. Consider the 12UTC “VBG spring” case that with increasing forecast lead-time jumps from values of 0.13 to 0.87, then back to 0.15. This suggests that the 12UTC (early morning) forecast equations may be untrustworthy.

Considering only the 00UTC (afternoon) cases, the following observations for adjusted R-squared for equation development can be made:

- The Nevada stations DRA and REV have their highest values during the fall.
- There is no clear association between an increasing forecast lead-time and a decreasing R-squared.
- “OAK summer” and “DRA fall” have the highest values overall, but other cases are nearly as high.
- “REV spring,” and “REV summer” to a lesser extent, show noticeably lower R-squared values after the 0-hour forecast.

Table 5-3 Adjusted R-Squared for each of 200 equations. Forecast hours (e.g., F12) lead up to 00UTC (afternoon) or 12UTC (early morning).

		Forecasts leading up to 00UTC (afternoon)						Forecasts leading up to 12UTC (early morning)				
		DRA	NKX	OAK	REV	VBG		DRA	NKX	OAK	REV	VBG
Spring	00Z F00	0.66	0.52	0.47	0.49	0.52	12Z F00	0.52	0.35	0.03	0.00	0.13
	12Z F12	0.81	0.65	0.59	0.22	0.67	00Z F12	1.00	0.35	0.09	0.06	0.87
	00Z F24	0.65	0.59	0.63	0.22	0.61	12Z F24	0.86	0.24	0.29	0.10	0.15
	12Z F36	0.66	0.55	0.58	0.19	0.73	00Z F36	0.72	0.33	0.16	0.05	0.15
	00Z F48	0.66	0.56	0.48	0.13	0.51	12Z F48	0.85	0.24	0.11	0.00	0.55
Summer	00Z F00	0.80	0.63	0.70	0.68	0.59	12Z F00	0.02	0.28	0.27	0.10	0.02
	12Z F12	0.74	0.49	0.80	0.35	0.62	00Z F12	0.09	0.26	0.29	0.05	0.70
	00Z F24	0.57	0.61	0.78	0.26	0.59	12Z F24	0.00	0.13	0.19	0.00	0.10
	12Z F36	0.47	0.57	0.79	0.29	0.52	00Z F36	0.17	0.25	0.39	0.00	0.12
	00Z F48	0.67	0.53	0.73	0.35	0.52	12Z F48	No eq.	0.29	0.38	0.00	0.07
Fall	00Z F00	0.78	0.50	0.56	0.61	0.33	12Z F00	0.31	0.24	0.15	0.66	0.00
	12Z F12	0.80	0.61	0.47	0.59	0.52	00Z F12	0.82	0.47	0.16	0.05	0.00
	00Z F24	0.81	0.62	0.55	0.59	0.43	12Z F24	0.88	0.26	0.21	0.03	0.86
	12Z F36	0.71	0.39	0.66	0.62	0.47	00Z F36	0.96	0.36	0.18	0.06	0.77
	00Z F48	0.72	0.49	0.50	0.58	0.34	12Z F48	0.59	0.30	0.15	0.03	0.04
Winter	00Z F00	0.71	0.58	0.44	0.47	0.53	12Z F00	No eq.	0.22	0.04	0.19	0.05
	12Z F12	0.72	0.55	0.54	0.43	0.59	00Z F12	No eq.	0.30	0.36	0.11	0.31
	00Z F24	0.73	0.50	0.49	0.48	0.67	12Z F24	No eq.	0.41	No eq.	0.35	0.46
	12Z F36	0.74	0.43	0.57	0.42	0.61	00Z F36	No eq.	0.57	No eq.	0.12	0.75
	00Z F48	0.57	0.48	0.45	0.46	0.47	12Z F48	No eq.	0.43	No eq.	0.39	0.82

Forecasts Leading up to 00UTC (Afternoon)

Table 5-4 lists the adjusted R-squared statistic for the validation year. The adjusted R-squared, adjusted for the residual degrees of freedom, is somewhat lower than the regular R-squared statistic. R-squared is non-negative, but adjusted R-squared can end up negative. R-squared can be affected by outliers. Compare the similarity, except for outliers, between the scattersplots “DRA Summer F00” and “DRA Summer F24” in Figure 5-1. The F00 adjusted R-squared value is 0.72, whereas the F24 adjusted R-squared value is -0.01 due to the outliers. In Table 5-4, “No eq.” (no equation) indicates equations which could not be developed because all predictands were zero, “NaN” (not-a-number) indicates equations which did not have any predictors included, and “horiz.”

indicates where an R-squared value was not defined because the data plotted as a horizontal line (all validation observed mixing heights were zero). All adjusted R-squared values for forecasts leading up to 12UTC were either undefined or very low.

Considering only the 00UTC (afternoon) cases, the following observations for adjusted R-squared for the validation data can be made:

- Nevada stations DRA and REV have their highest values during the fall.
- Except for the REV station, 00UTC winter values are fairly high and do not at all resemble the 12UTC (early morning) results.
- The 0-hour forecast often has a higher R-squared value than the other forecast lead-times. This is because the 0-hour forecast corresponds to the model's initialization, which is based on observed data.
- Other than a few cases such as "REV Fall" or "OAK Spring", there is no clear association between an increasing forecast lead-time and a decreasing R-squared.
- During the summer, Nevada stations DRA and REV have sharp reductions of adjusted R-squared after the 0-hour forecast, but the coastal stations NKX, OAK and VBG remain fairly consistent for all the forecast lead times.

Table 5-4 Adjusted R-squared for the validation year. Forecast hours (e.g., F12) lead up to 00UTC (afternoon) or 12UTC (early morning).

		Forecasts leading up to 00UTC (afternoon)						Forecasts leading up to 12UTC (early morning)				
		DRA	NKX	OAK	REV	VBG		DRA	NKX	OAK	REV	VBG
Spring	00Z F00	0.00	0.51	0.58	0.37	0.29	12Z F00	horiz	-0.03	0.04	NaN	-0.03
	12Z F12	0.14	0.16	0.39	0.05	0.34	00Z F12	horiz	-0.02	-0.03	-0.02	-0.03
	00Z F24	0.19	0.29	0.37	0.07	0.15	12Z F24	horiz	-0.01	-0.02	-0.02	-0.03
	12Z F36	0.07	0.27	0.36	0.02	0.11	00Z F36	horiz	-0.02	-0.03	-0.02	-0.03
	00Z F48	-0.05	-0.03	0.18	-0.03	0.20	12Z F48	horiz	-0.03	-0.03	NaN	-0.03
Summer	00Z F00	0.72	0.52	0.52	0.68	0.47	12Z F00	horiz	0.24	-0.01	-0.01	-0.03
	12Z F12	0.06	0.26	0.54	0.13	0.46	00Z F12	horiz	0.00	-0.02	-0.03	-0.03
	00Z F24	-0.01	0.25	0.37	0.15	0.36	12Z F24	NaN	-0.02	0.00	NaN	-0.03
	12Z F36	-0.05	0.13	0.21	0.02	0.40	00Z F36	horiz	-0.02	-0.02	NaN	-0.03
	00Z F48	0.14	0.08	0.30	0.11	0.37	12Z F48	No eq.	-0.02	0.01	NaN	0.01
Fall	00Z F00	0.74	0.27	0.31	0.67	0.27	12Z F00	horiz	0.01	-0.02	-0.03	NaN
	12Z F12	0.41	0.33	0.19	0.63	0.07	00Z F12	horiz	0.11	-0.03	-0.02	NaN
	00Z F24	0.48	0.16	0.14	0.60	0.21	12Z F24	horiz	-0.02	-0.03	-0.02	-0.03
	12Z F36	0.40	0.10	0.09	0.47	0.04	00Z F36	horiz	-0.03	-0.03	-0.02	-0.02
	00Z F48	0.50	0.17	0.16	0.48	0.08	12Z F48	horiz	-0.02	-0.02	-0.03	-0.02
Winter	00Z F00	0.33	0.51	0.33	0.21	0.27	12Z F00	No eq.	-0.01	0.01	-0.01	0.00
	12Z F12	0.53	0.39	0.36	0.07	0.32	00Z F12	No eq.	-0.02	-0.03	-0.01	0.44
	00Z F24	0.26	0.38	0.29	0.16	0.15	12Z F24	No eq.	-0.02	No eq.	-0.02	-0.02
	12Z F36	0.37	0.48	0.29	0.11	0.28	00Z F36	No eq.	0.00	No eq.	-0.02	-0.03
	00Z F48	0.56	0.28	0.31	0.10	0.18	12Z F48	No eq.	-0.01	No eq.	-0.02	-0.03

Table 5-5 lists the bias for forecasts leading up to 00UTC (afternoon) and the corresponding mean observation for comparison. Different forecast lead-times leading up to the same set of observed mixing heights show a slight variation in mean value due to a small number of missing data points. The following observations can be made regarding bias for forecasts leading up to 00UTC:

- While the Nevada stations DRA and REV show the usual trend of higher mixing heights during the warmer times of year, the California coastal stations NKX, OAK and VBG show lower mean observed mixing heights during the summer.

- The bias shows that summer, fall and winter forecasts at stations OAK and VBG are very good.
- Summer forecasts in general are very good, especially when considering the bias as a percentage of mean observed value.
- There is a noticeable tendency to underforecast, shown as negative bias, especially for the Nevada stations DRA and REV.

Table 5-5 Bias and mean observation of validation data. Forecast hours (e.g., F12) lead up to 00UTC (afternoon).

		DRA		NKX		OAK		REV		VBG	
		Mean Obs. (m agl)	Bias (m)	Mean Obs. (m agl)	Bias (m)	Mean Obs. (m agl)	Bias (m)	Mean Obs. (m agl)	Bias (m)	Mean Obs. (m agl)	Bias (m)
Spring	00Z F00	2834	-435	710	52	555	144	2022	-700	362	89
	12Z F12	2867	-443	663	151	545	190	1981	-610	343	96
	00Z F24	2838	-411	670	-51	537	264	2012	-647	340	112
	12Z F36	2768	-302	647	106	545	135	1942	-525	334	121
	00Z F48	2708	-248	656	98	532	133	1979	-568	343	89
Summer	00Z F00	3258	99	562	-82	309	82	2966	-318	327	-9
	12Z F12	3288	-128	554	-80	309	80	3006	-393	327	-7
	00Z F24	3255	119	567	-89	313	-21	2982	-353	325	-4
	12Z F36	3072	300	555	-87	304	83	3001	-373	314	9
	00Z F48	2988	747	563	-90	310	76	2999	-382	319	7
Fall	00Z F00	2091	-175	679	-212	344	68	1625	-221	335	-43
	12Z F12	1979	-109	682	-214	351	16	1640	-286	337	-39
	00Z F24	1979	-108	673	-191	341	46	1608	-245	333	-40
	12Z F36	1798	50	675	-270	328	90	1605	-245	339	-43
	00Z F48	1798	161	673	-209	328	64	1569	-261	337	-47
Winter	00Z F00	978	-125	938	-478	353	-21	722	-308	356	-51
	12Z F12	1054	-189	936	-446	378	-25	725	-321	363	-48
	00Z F24	1054	-209	931	-462	375	-17	733	-321	356	-41
	12Z F36	1094	-303	939	-465	378	56	727	-333	355	-53
	00Z F48	1094	-224	926	-450	372	-28	711	-325	344	-24

Figures 5-1 through 5-5 are scatterplots of observed versus forecasted mixing heights leading up to 00UTC (afternoon). The scatterplots give an immediate impression of the quality of the forecasts. Perfect forecasts lie on the line $y = x$. The vertical and horizontal scales match for every scatterplot. Note that the scales vary for different stations and seasons. The following observations can be made regarding the scatterplots for forecasts leading up to 00UTC (afternoon):

- In Figure 5-1, the DRA scatterplots contain less data points than those for the other stations due to missing soundings. The best forecasts appear to be made by the MOS equations during the summer and fall.
- In Figure 5-2, the NKX mixing height forecasts look best during the spring and summer.
- In Figure 5-3, the OAK forecasts look best during the summer. During the summer, fall and winter, there is a noticeable horizontal cluster of points along the x-axis, corresponding to forecasts paired with observations of zero. This phenomenon happens to a much greater extent in nearly every scatterplot for forecasts leading up to 12UTC (early morning).
- In Figure 5-4, the REV forecasts look best during the fall.
- In Figure 5-5, the VBG forecasts appear to be of fairly consistent quality across all seasons.

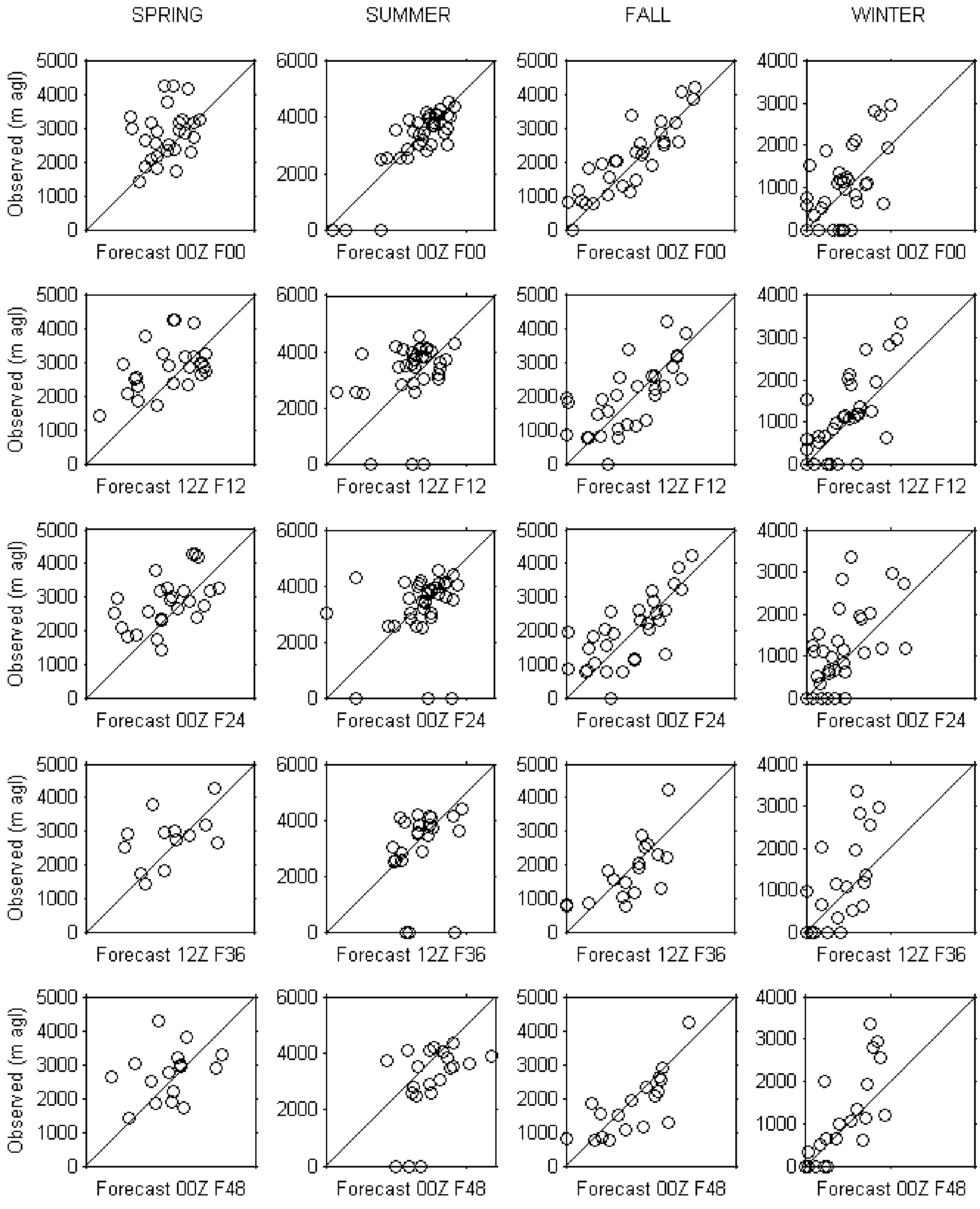

Figure 5-1 Scatterplots of forecasts leading up to 00UTC (afternoon) for DRA.

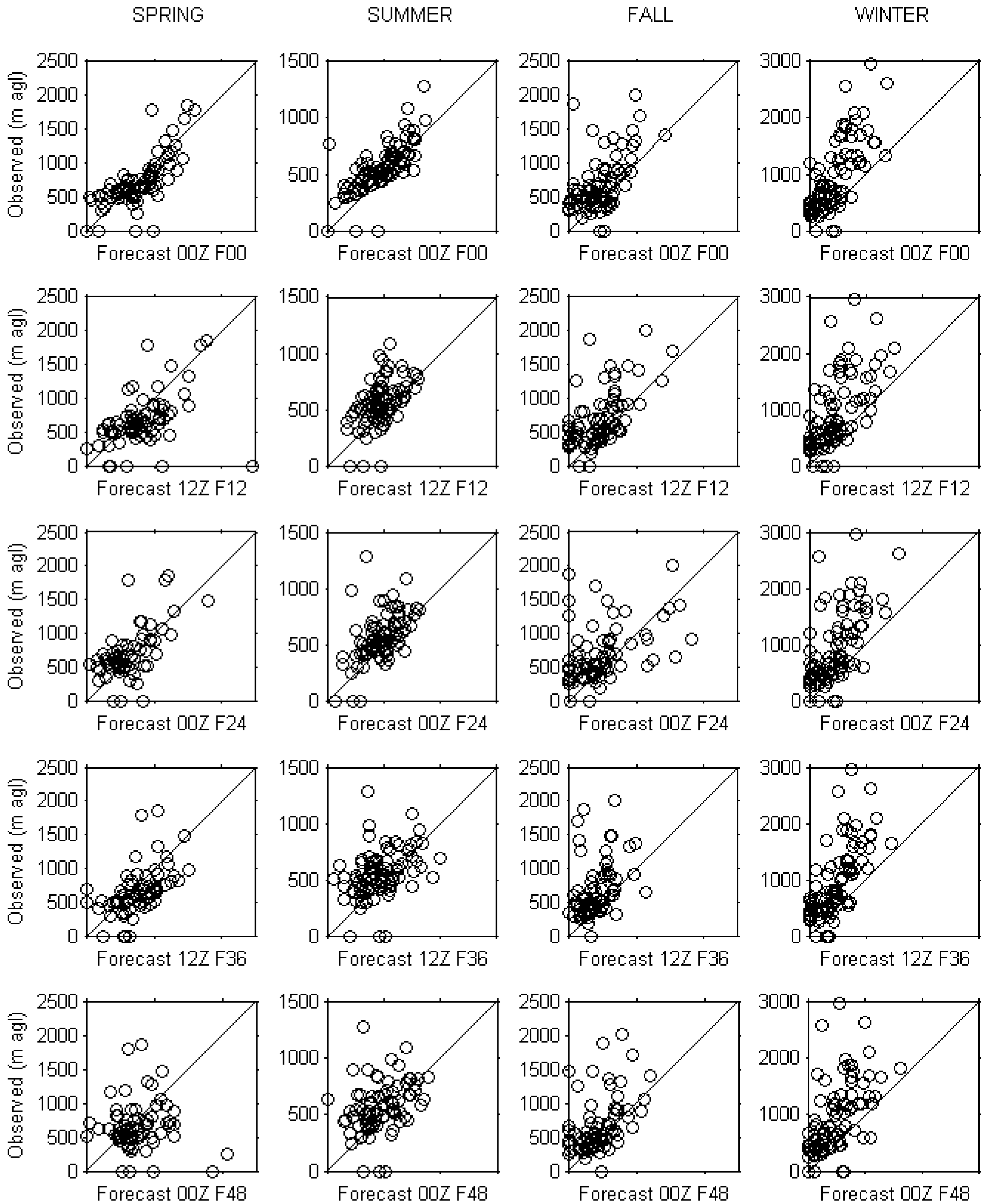

Figure 5-2 Scatterplots of forecasts leading up to 00UTC (afternoon) for NKX.

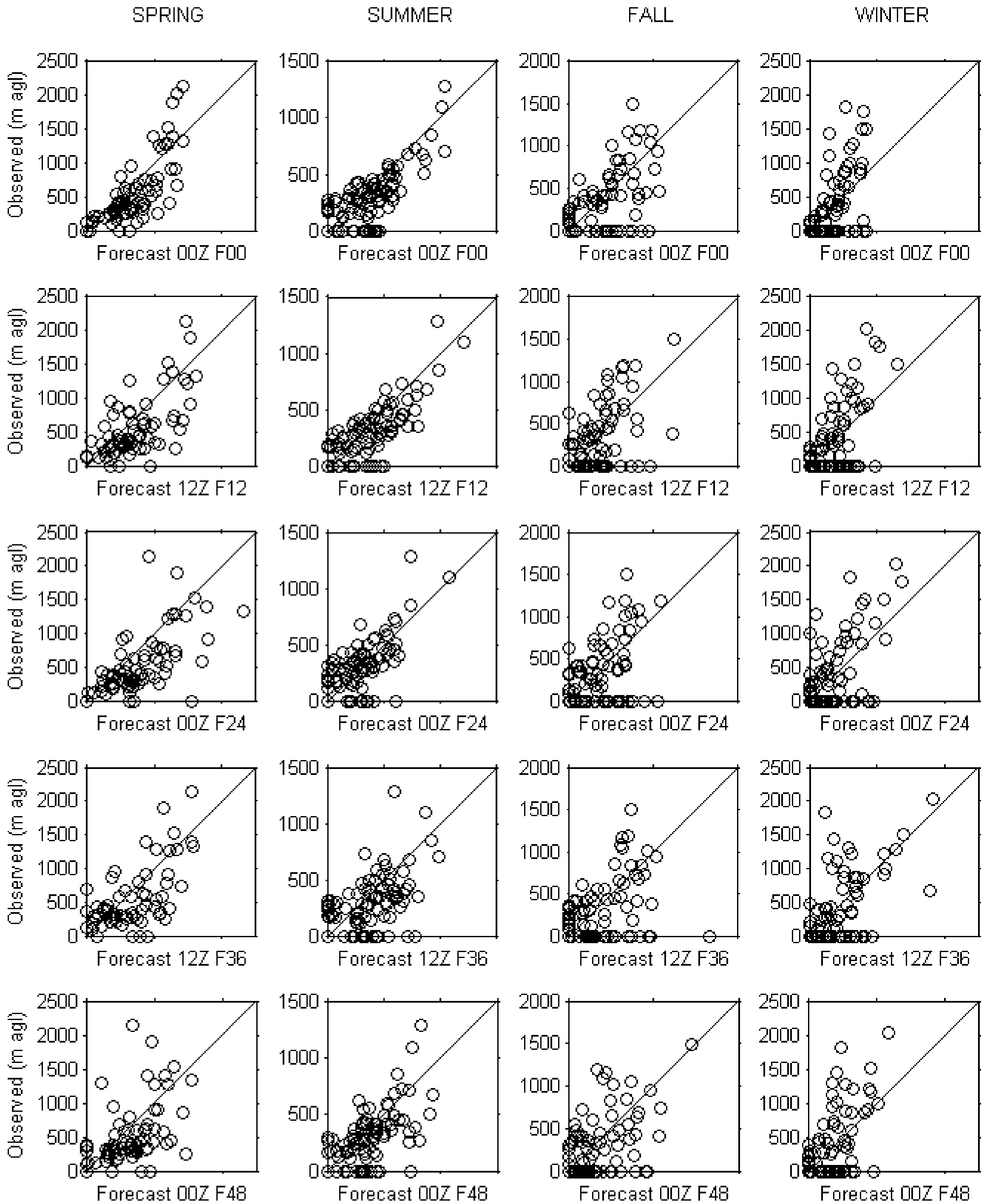

Figure 5-3 Scatterplots of forecasts leading up to 00UTC (afternoon) for OAK.

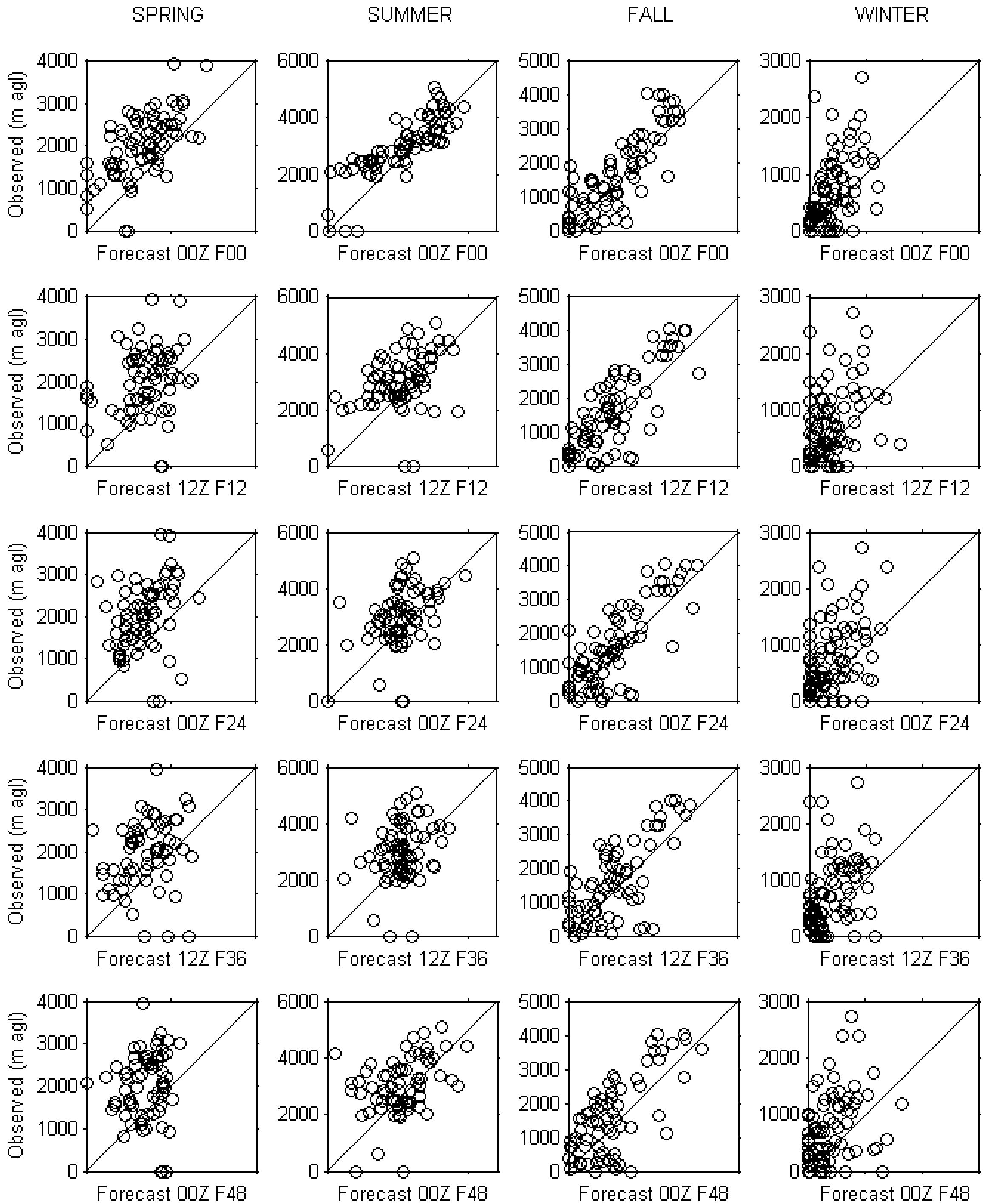

Figure 5-4 Scatterplots of forecasts leading up to 00UTC (afternoon) for REV.

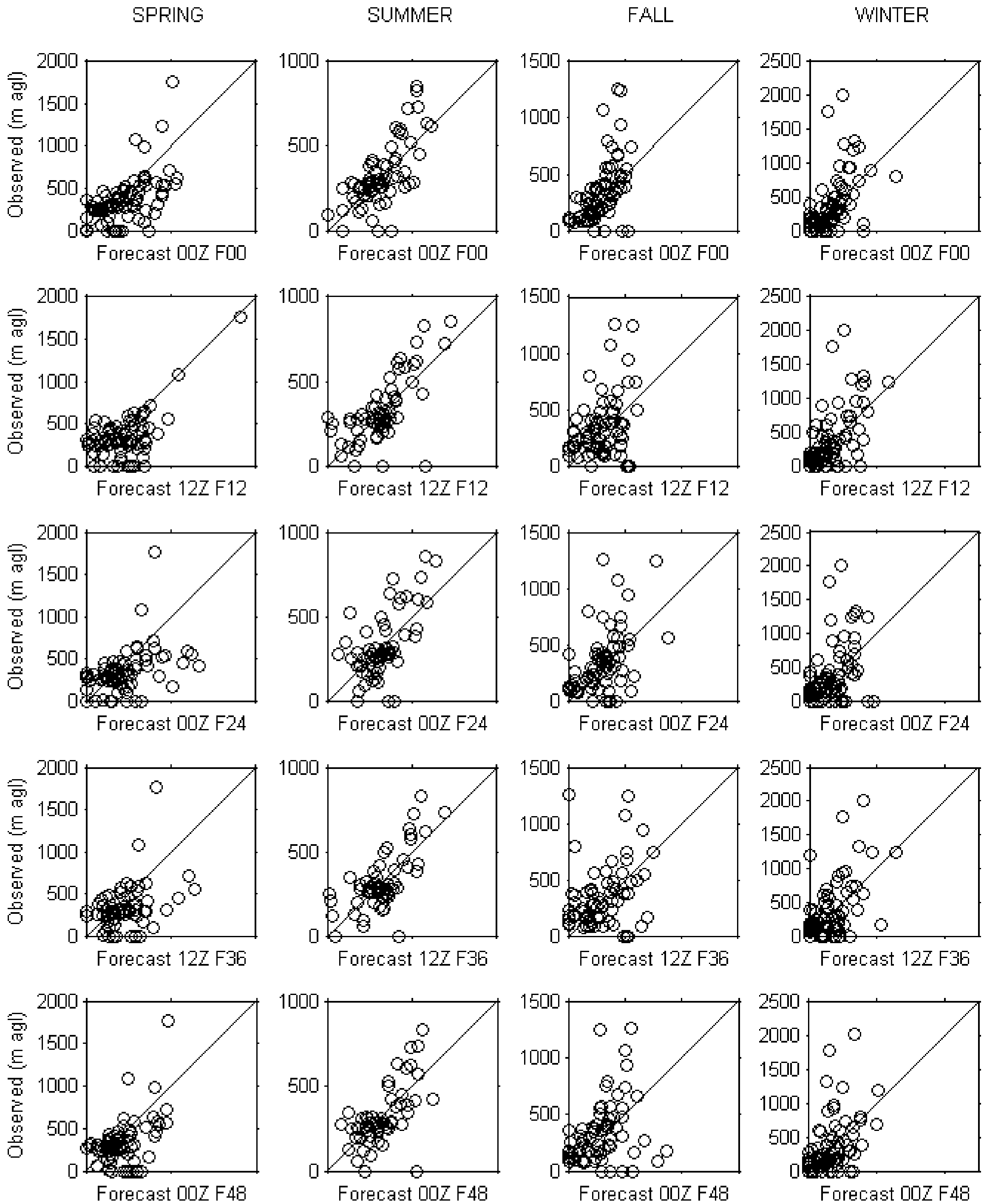

Figure 5-5 Scatterplots of forecasts leading up to 00UTC (afternoon) for VBG.

Figures 5-6 through 5-10 are boxplots showing the magnitude (in meters) and spread of individual forecast errors for forecasts leading up to 00UTC (afternoon). The median forecast error is at the line within the box, and 50% of forecast errors lie within the box. The following observations can be made for the boxplots of forecast errors for forecasts leading up to 00UTC (afternoon):

- At DRA (Figure 5-6), there is a tendency for the equations to underforecast in the spring, but the median error is usually closer to zero during the other seasons. The spread of the errors is fairly constant across all seasons.
- At NKX (Figure 5-7), the median error is close to zero in the spring while the equations underforecast during the other seasons, especially the winter. The smallest spread in the summer indicates good results, while the largest spread during the winter indicates a greater frequency of poor results.
- At OAK (Figure 5-8), there is a slight overforecast during the spring, but the median error is extremely close to zero during the summer, fall and winter. The smallest spread occurs during summer, and there is a fairly consistent larger spread during the other seasons.
- At REV (Figure 5-9), there is a tendency to underforecast in all seasons, especially during the spring. There is a smaller spread during the winter, but the mean mixing height is also less than during the other seasons.

- At VBG (Figure 5-10), there is a slight overforecast during spring, but the median error is very near zero during the other seasons. The reduced spread indicates good results during summer.

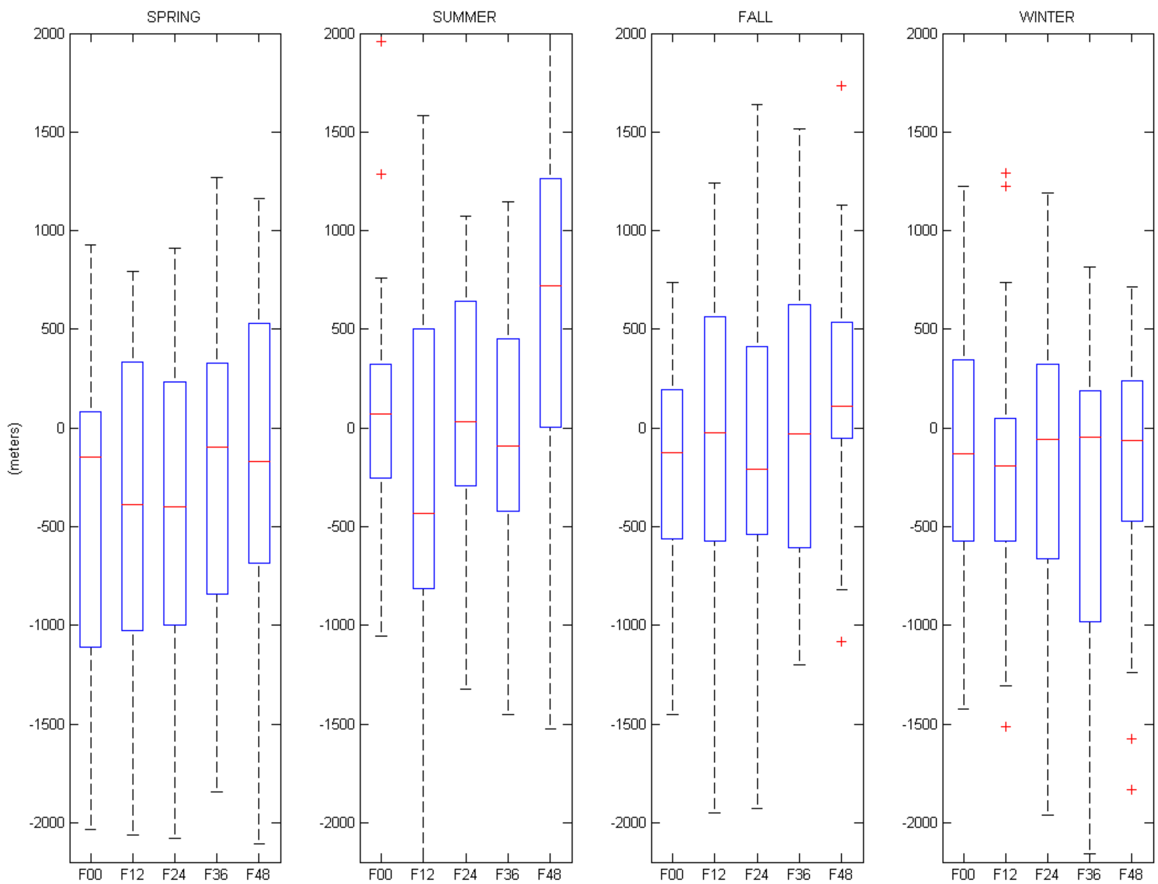

Figure 5-6 Boxplots of forecast error for DRA for forecasts leading up to 00UTC (afternoon). For comparison, mean observed mixing height (m) in spring is 2800, summer is 3200, fall is 1900, and winter is 1100.

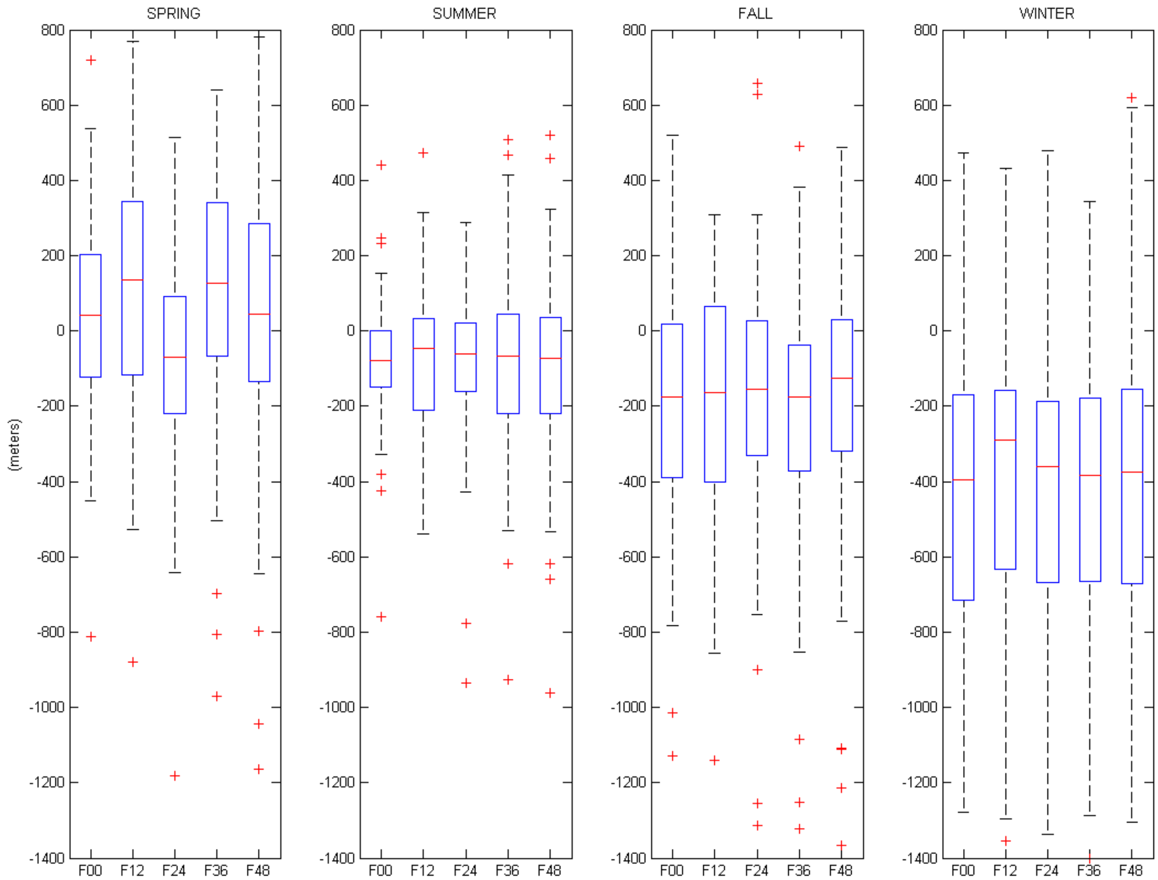

Figure 5-7 Boxplots of forecast error for NKX for forecasts leading up to 00UTC (afternoon). For comparison, mean observed mixing height (m) in spring is 700, summer is 600, fall is 700, and winter is 900.

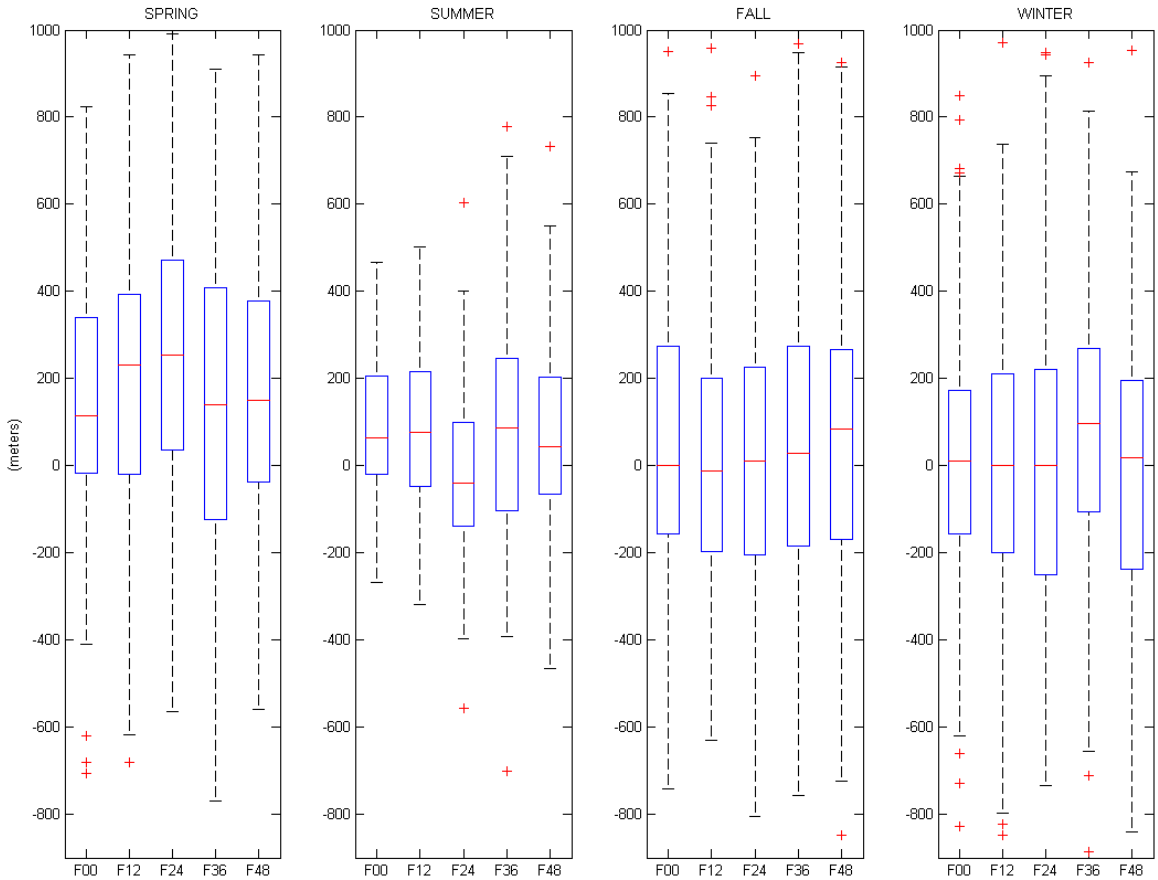

Figure 5-8 Boxplots of forecast error for OAK for forecasts leading up to 00UTC (afternoon). For comparison, mean observed mixing height (m) in spring is 540, summer is 310, fall is 340, and winter is 370.

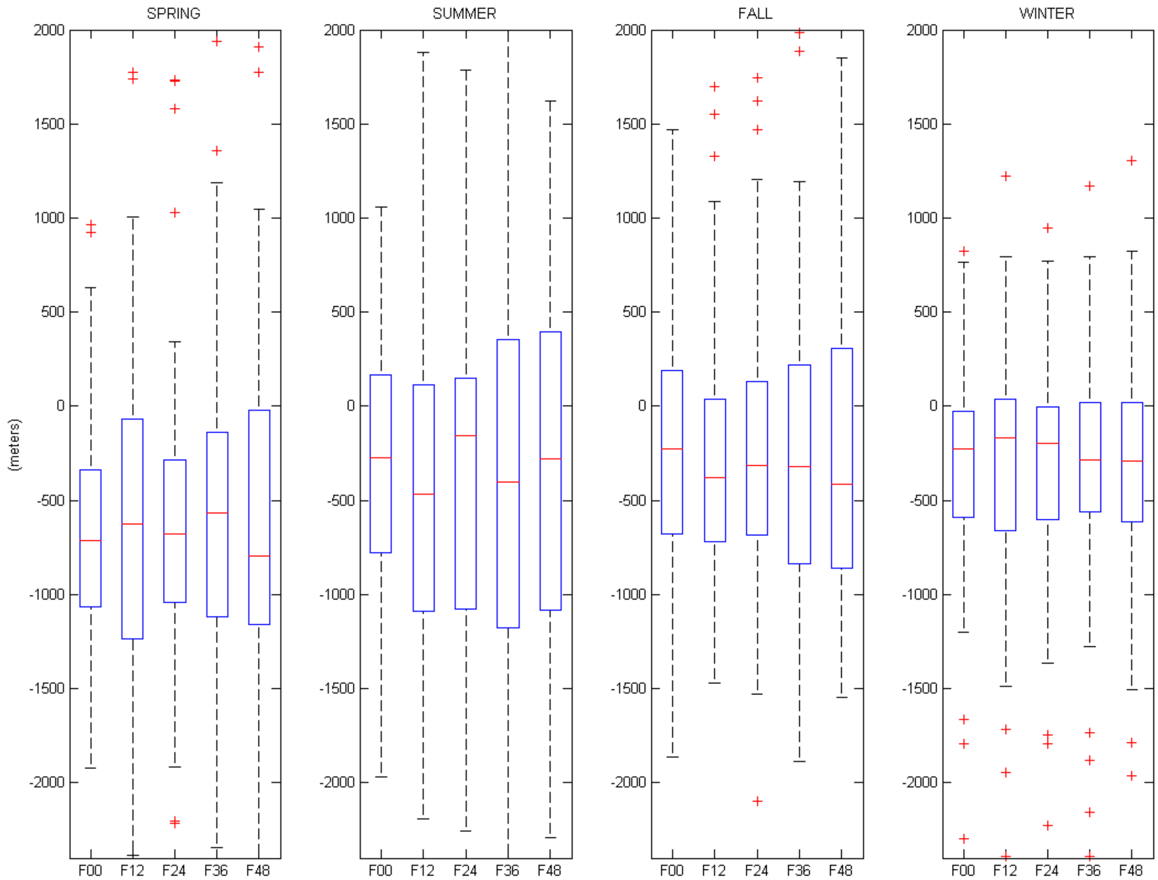

Figure 5-9 Boxplots of forecast error for REV for forecasts leading up to 00UTC (afternoon). For comparison, mean observed mixing height (m) in spring is 2000, summer is 3000, fall is 1600, and winter is 700.

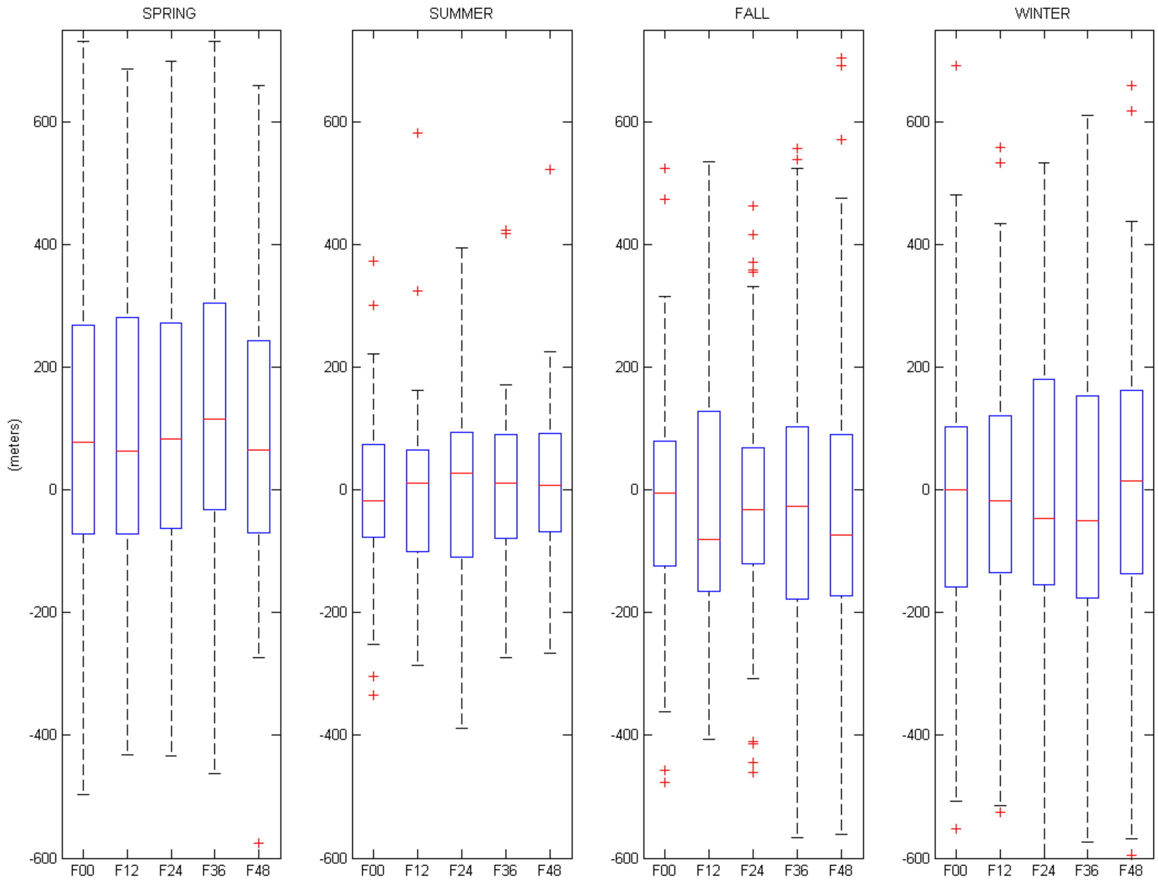

Figure 5-10 Boxplots of forecast error for VBG for forecasts leading up to 00UTC (afternoon). For comparison, mean observed mixing height (m) in spring is 340, summer is 320, fall is 340, and winter is 350.

Forecasts Leading up to 12UTC (Early Morning)

Parcel methods for determining mixing height are really only designed for the convective conditions during the daytime. However, forecasts leading up to 12UTC (early morning) were also included in this study for comparison. The right side of Table 5-4 lists the adjusted R-squared statistic which is nearly zero or undefined in almost every case. Despite such poor R-squared values, Table 5-6 shows that the bias values of the mixing height forecasts leading up to 12UTC (early morning) are very small. Along with bias, Table 5-6 lists the mean observation for comparison. "No eq." (no equation) indicates where no equation could be developed because the predictand values were all zero. Entries in parenthesis indicate forecast equations in which no predictor variables were included. The output of such equations is always zero, but when the standardization of this value is undone, the mixing height forecast becomes the mean observed mixing height from the development data. Outliers are responsible for the higher mean observation during DRA's winter compared to its other seasons.

The following observations can be made regarding bias for forecasts leading up to 12UTC (early morning):

- The bias values are generally extremely small.
- At the Nevada stations DRA and REV, nearly perfect forecasts could be made by simply always forecasting a mixing height of zero for 12UTC.
- At the coastal stations NKX, OAK and VBG, except for "VBG fall", the MOS forecast equations give smaller bias values than would be obtained with forecasts of always zero.

Table 5-6 Bias and mean observation of validation data. Forecast hours (e.g., F12) lead up to 12UTC (early morning).

		DRA		NKX		OAK		REV		VBG	
		Mean Obs. (m agl)	Bias (m)	Mean Obs. (m agl)	Bias (m)	Mean Obs. (m agl)	Bias (m)	Mean Obs. (m agl)	Bias (m)	Mean Obs. (m agl)	Bias (m)
Spring	12Z F00	0	2	95	-42	13	15	3	(0)	17	6
	00Z F12	0	0	96	-52	9	21	3	3	18	16
	12Z F24	0	2	108	-54	12	29	3	4	19	-6
	00Z F36	0	2	94	-39	9	29	3	2	18	1
	12Z F48	0	2	86	-27	9	31	3	(0)	18	1
Summer	12Z F00	0	1	91	13	35	19	12	2	33	-20
	00Z F12	0	1	91	10	34	20	13	-3	34	-14
	12Z F24	0	(0)	84	5	38	9	12	(-6)	33	-19
	00Z F36	0	1	83	11	40	13	0	(6)	27	-12
	12Z F48	0	No eq.	86	28	40	11	0	(6)	31	-18
Fall	12Z F00	0	9	33	34	9	7	4	45	31	(4)
	00Z F12	0	10	33	43	9	7	4	23	31	(3)
	12Z F24	0	19	30	34	8	9	3	23	33	102
	00Z F36	0	14	35	28	8	7	4	26	27	92
	12Z F48	0	9	33	34	8	5	4	22	27	24
Winter	12Z F00	18	No eq.	9	13	8	-6	1	19	19	-1
	00Z F12	18	No eq.	9	12	5	-2	1	17	19	2
	12Z F24	19	No eq.	9	17	8	No eq.	1	19	19	5
	00Z F36	26	No eq.	9	15	8	No eq.	1	16	20	14
	12Z F48	26	No eq.	9	16	8	No eq.	1	24	20	7

Figures 5-11 through 5-15 display the scatterplots of observed versus forecast mixing heights that lead up to 12UTC (early morning). “No equation” is indicated for cases in which the predictand values were all zero so that no regression equation could develop. “No predictors” indicates cases in which no predictor variables were included in the forecast equation. The following observations can be made regarding the scatterplots for forecasts leading up to 12UTC (early morning):

- Many 12UTC scatterplots display a scenario in which there are a significant number of observed mixing heights equal to zero, with forecasted mixing heights greater than zero. This produces a horizontal cluster of data along the x-axis as can been seen in most of the scatterplots in Figures 5-11 through 5-15. Table 5-7 displays the percentage of time that this occurs, and shows high percentages for forecasts leading up to 12UTC (early morning). Since these percentages do not include points which are on the origin, the percentage of data on the x-axis is likely higher.

Table 5-7 Percentage of validation data in which the sounding was zero and the forecast was greater than zero. Forecast hours (e.g., F12) lead up to 00UTC (afternoon) or 12UTC (early morning).

		Forecasts leading up to 00UTC (afternoon)						Forecasts leading up to 12UTC (early morning)				
		DRA	NKX	OAK	REV	VBG		DRA	NKX	OAK	REV	VBG
Spring	00Z F00	0	4	4	3	9	12Z F00	49	53	81	No pre	44
	12Z F12	0	7	4	3	11	00Z F12	0	62	71	61	43
	00Z F24	0	7	4	3	8	12Z F24	42	58	64	60	68
	12Z F36	0	7	6	5	11	00Z F36	40	55	65	58	55
	00Z F48	0	6	6	4	10	12Z F48	45	57	75	No pre	35
Summer	00Z F00	8	2	16	4	5	12Z F00	44	46	67	64	63
	12Z F12	8	3	15	3	5	00Z F12	42	52	65	66	47
	00Z F24	9	4	13	3	5	12Z F24	No pre	66	63	99	56
	12Z F36	13	3	16	3	5	00Z F36	42	64	63	No pre	55
	00Z F48	14	4	17	3	4	12Z F48	No eq.	63	65	No pre	63
Fall	00Z F00	3	3	27	1	7	12Z F00	57	71	74	46	No pre
	12Z F12	3	3	34	1	7	00Z F12	50	58	62	51	No pre
	00Z F24	3	3	34	3	7	12Z F24	36	70	63	63	34
	12Z F36	0	1	30	1	6	00Z F36	53	64	75	51	52
	00Z F48	0	1	35	3	6	12Z F48	27	67	74	58	56
Winter	00Z F00	18	5	41	9	12	12Z F00	No eq.	61	46	71	54
	12Z F12	15	5	32	10	13	00Z F12	No eq.	55	42	72	53
	00Z F24	21	5	40	9	15	12Z F24	No eq.	62	No eq.	65	48
	12Z F36	18	5	43	12	11	00Z F36	No eq.	53	No eq.	61	33
	00Z F48	18	3	41	10	13	12Z F48	No eq.	56	No eq.	67	34

- In Figure 5-11, the DRA scatterplots show excellent results for all available equations. The horizontal cluster along the x-axis is very near the origin. (Notice the extremely reduced scale of the spring and summer scatterplots.)

- In Figure 5-12, the NKX scatterplots show that the mixing heights are often zero while forecasts are greater than zero, but unlike for DRA, the horizontal cluster extends away from the origin for a significant distance. In those cases in which the observation is higher than zero, the equations underforecast producing vertically aligned data clusters in the scatterplots.
- In Figure 5-13, the OAK scatterplots are similar to those for NKX, except that the available fall and winter equations produce better results since the horizontal clusters are near the origin.
- In Figure 5-14, the REV results show very good results in which clusters are near the origin during all seasons except the fall. However, during the fall the errors (in meters) are still relatively small.
- In Figure 5-15, the VBG scatterplots appear to have a large majority of the data clustered near the origin so that forecast errors are relatively small across all seasons. The VBG scatterplots contain outliers in every season.

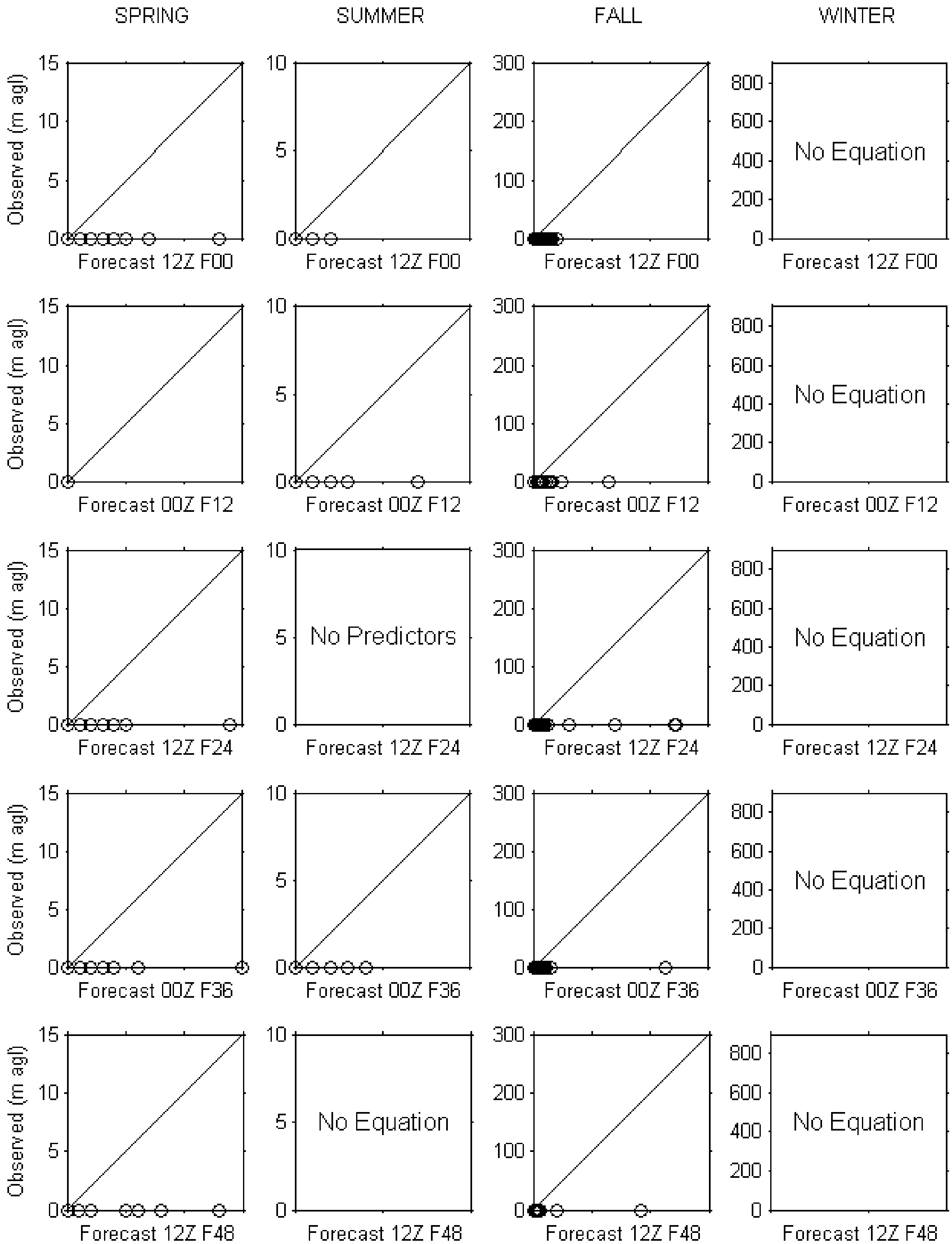

Figure 5-11 Scatterplots of forecasts leading up to 12UTC (early morning) for DRA.

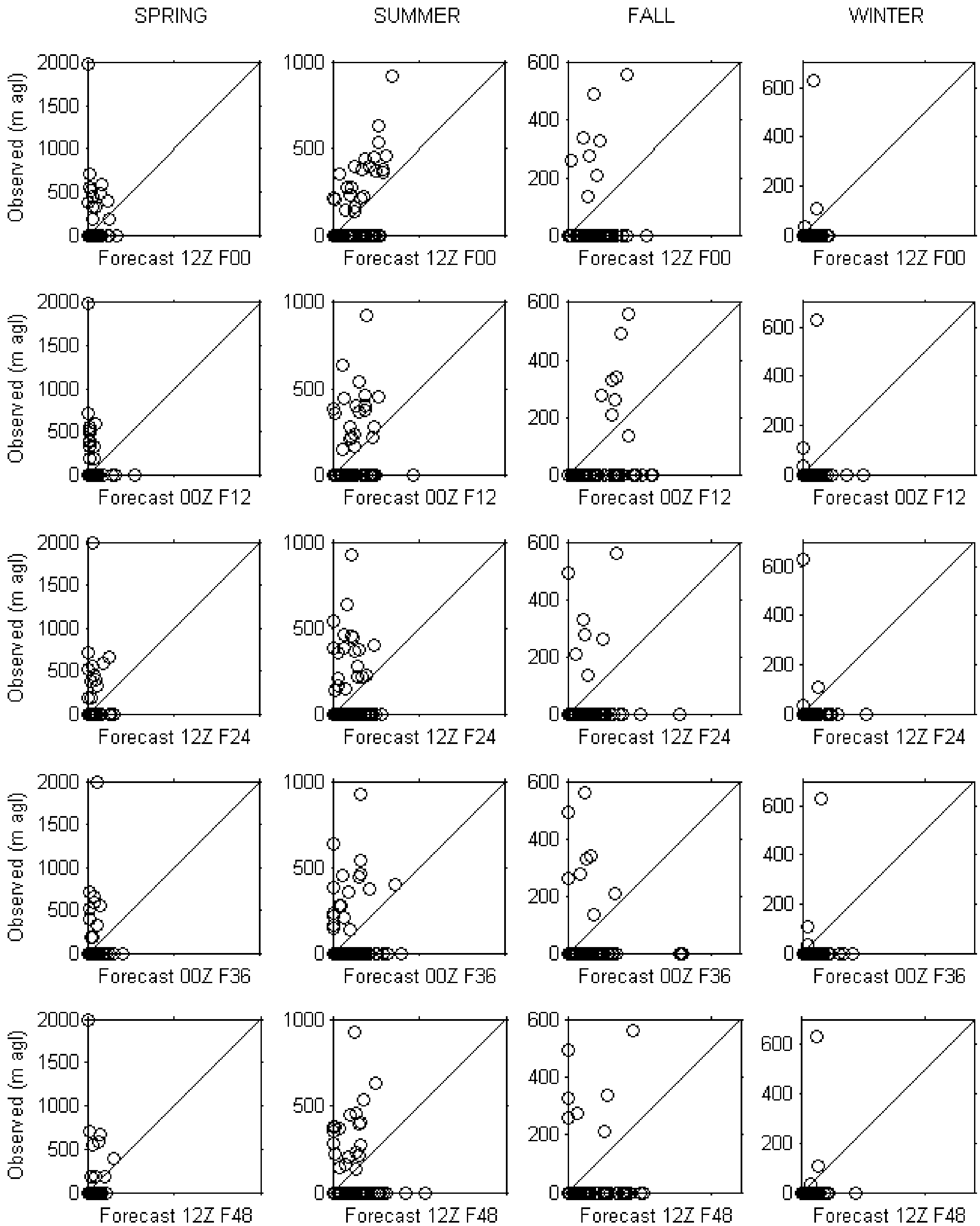

Figure 5-12 Scatterplots of forecasts leading up to 12UTC (early morning) for NKX.

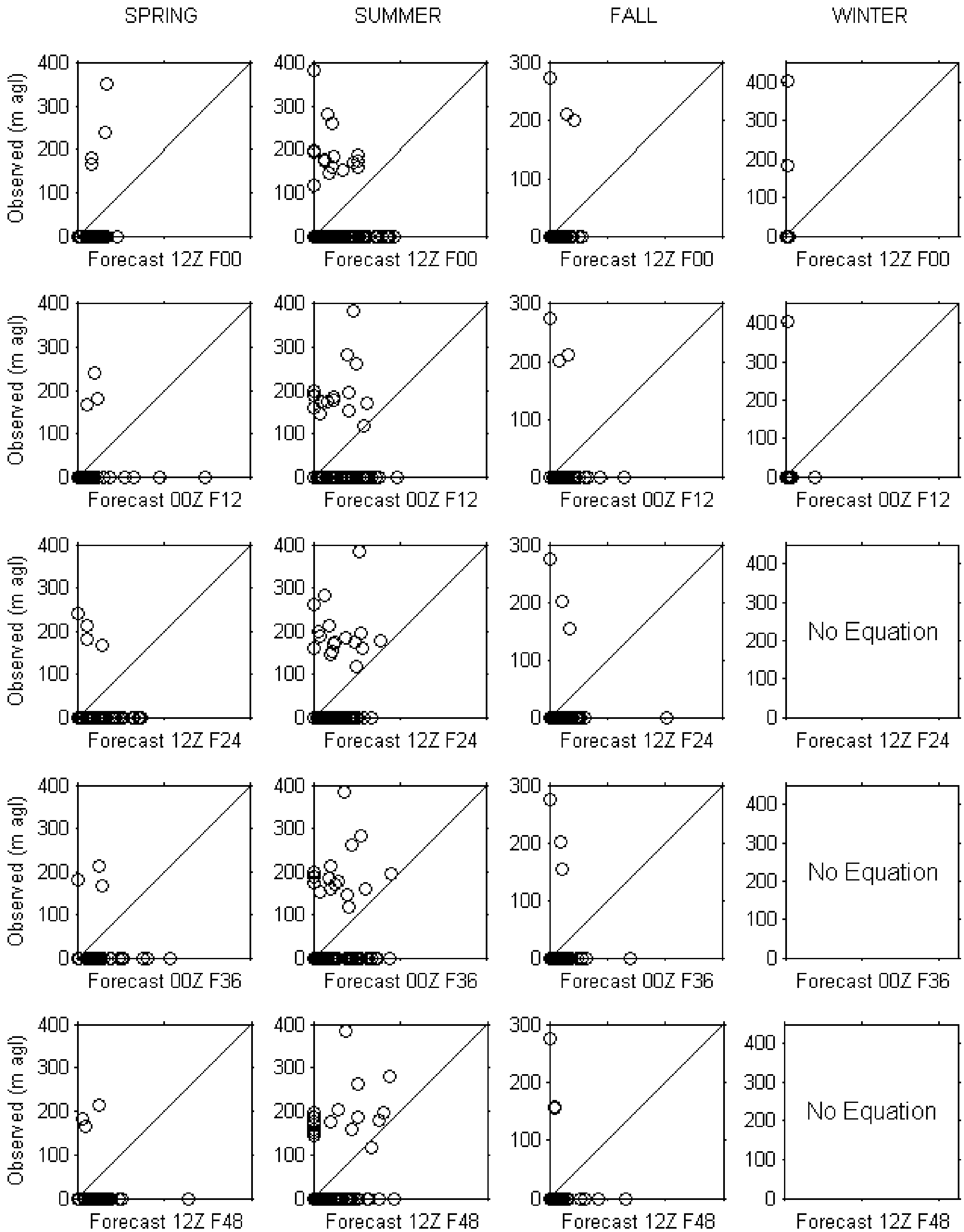

Figure 5-13 Scatterplots of forecasts leading up to 12UTC (early morning) for OAK.

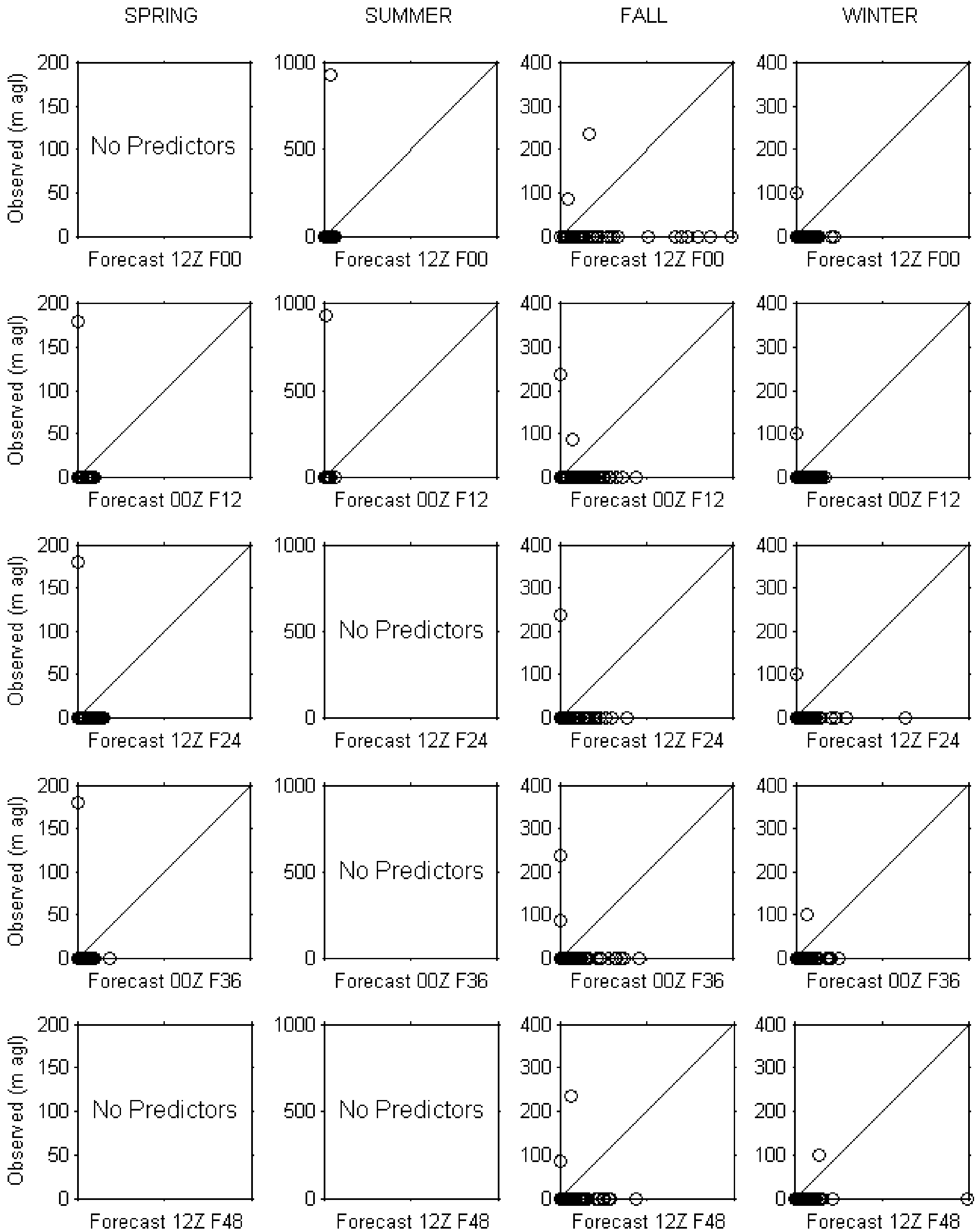

Figure 5-14 Scatterplots of forecasts leading up to 12UTC (early morning) for REV.

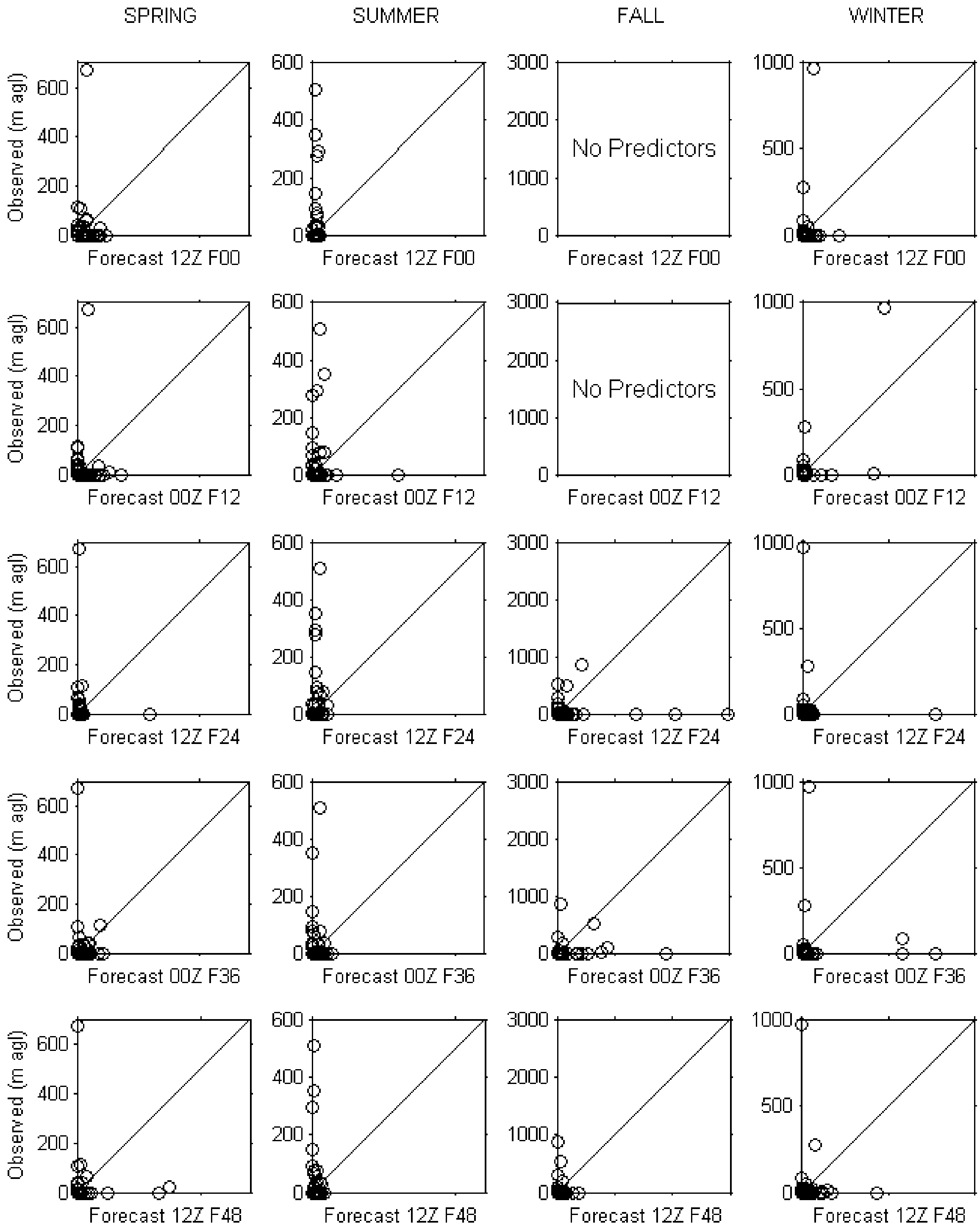

Figure 5-15 Scatterplots of forecasts leading up to 12UTC (early morning) for VBG.

Figures 5-16 through 5-20 display the boxplots of individual forecast errors for forecasts leading up to 12UTC (early morning). “No eq” (no equation) indicates the cases in which no equation could be developed because all predictand values were zero. “No Pre” (no predictors) indicates the cases in which no predictor variables were included in the forecast equations during the regression. The following observations can be made for the boxplots of forecast errors for forecasts leading up to 12UTC (early morning):

- Overall, forecast errors (and observed mixing heights) are much smaller for 12UTC (early morning) than for 00UTC (afternoon).
- At DRA (Figure 5-16), the forecast errors are very small. Even during the fall when the spread is significantly greater, the errors are usually within 30 meters.
- At NKX (Figure 5-17), the boxplots show a smaller spread of errors during winter and spring. The largest spread is in summer.
- At OAK (Figure 5-18), the smallest spread of errors occurs during winter and the largest occurs during summer.
- At REV (Figure 5-19), there are noticeably smaller forecast errors during spring and summer.
- At VBG (Figure 5-20), the error magnitude and spread is consistently small throughout most of the year, with a larger spread during fall.

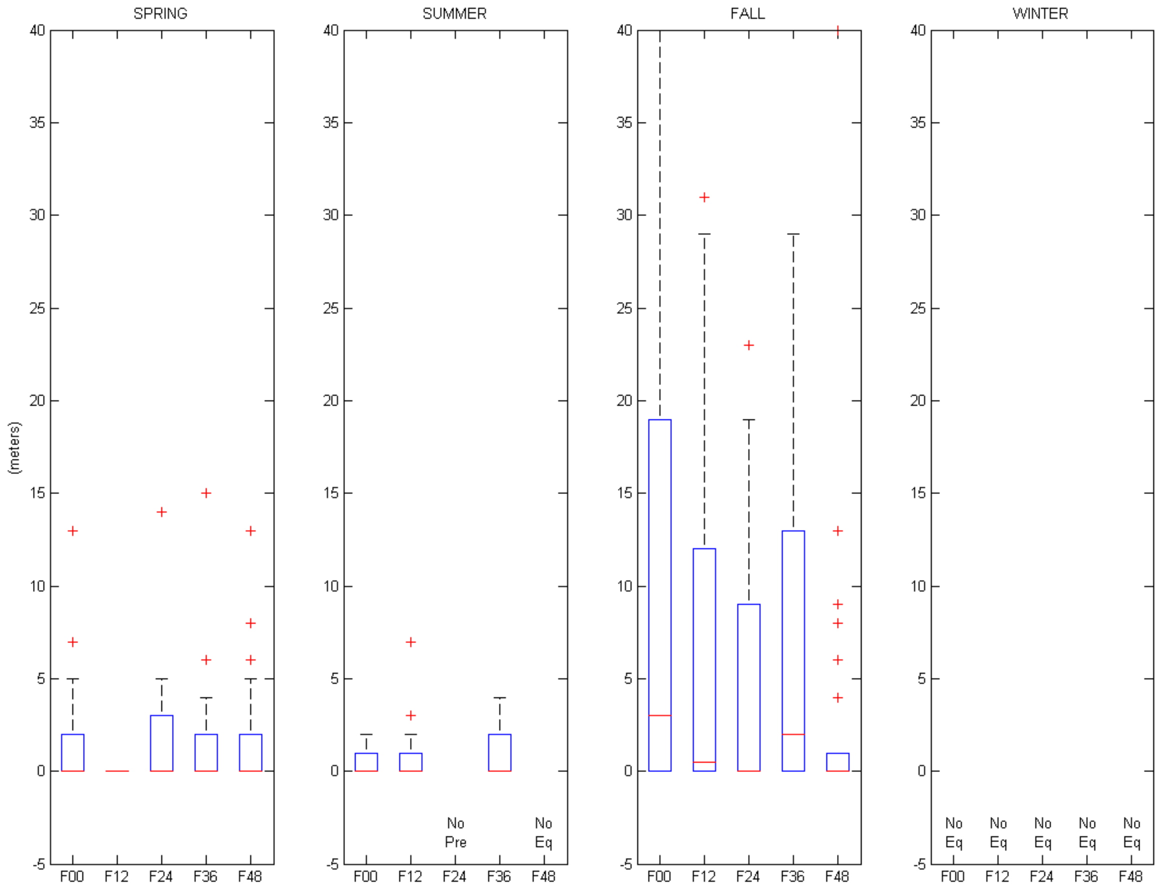

Figure 5-16 Boxplots of forecast error for DRA for forecasts leading up to 12UTC (early morning). For comparison, mean observed mixing height (m) in spring is 0, summer is 0, fall is 0, and winter is 21 (which is due to one non-zero outlier).

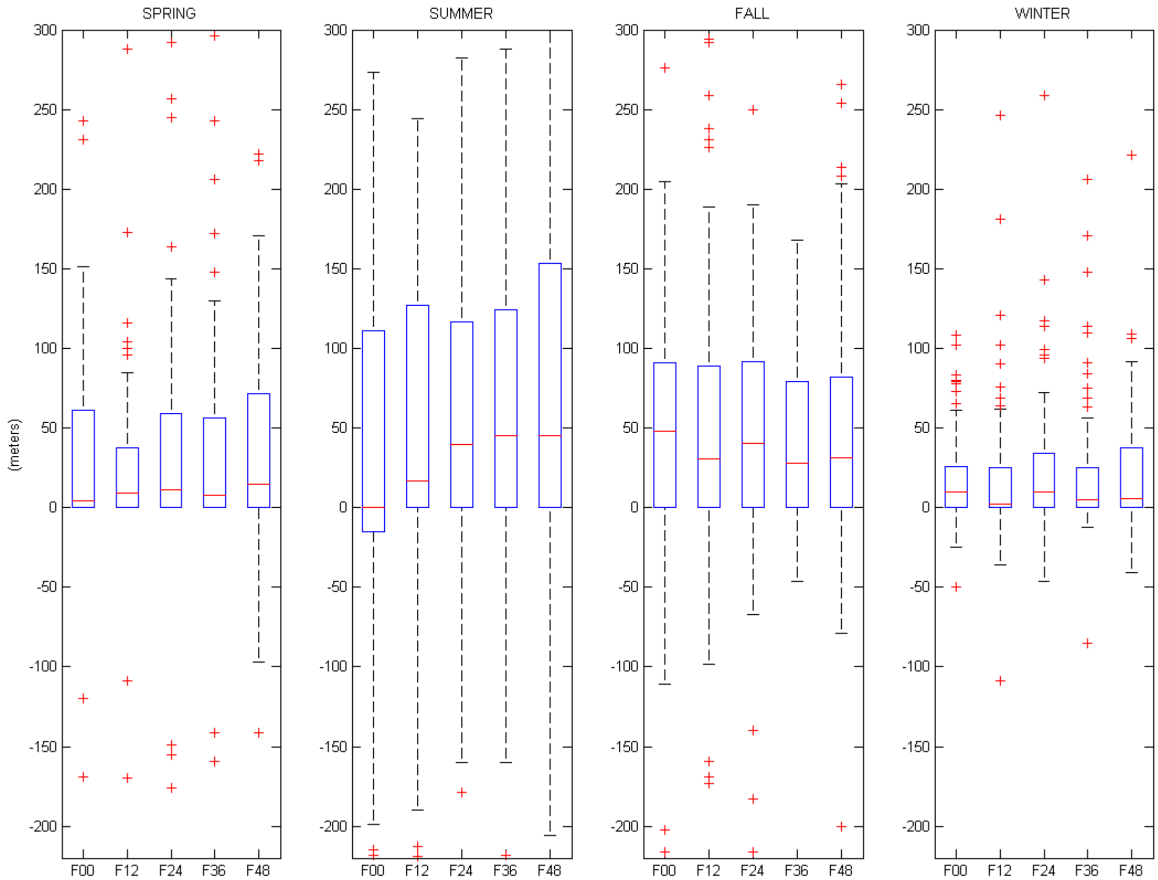

Figure 5-17 Boxplots of forecast error for NKX for forecasts leading up to 12UTC (early morning). For comparison, mean observed mixing height (m) in spring is 96, summer is 87, fall is 33, and winter is 45.

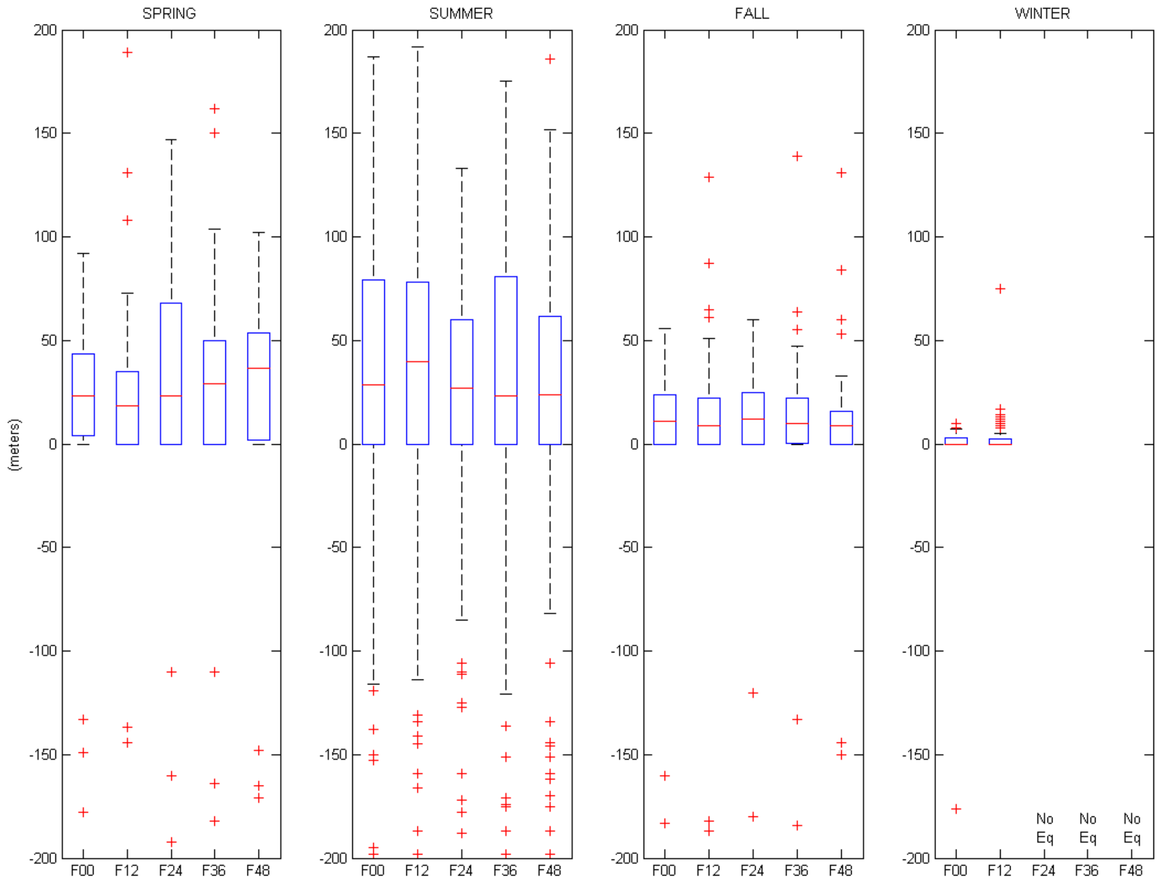

Figure 5-18 Boxplots of forecast error for OAK for forecasts leading up to 12UTC (early morning). For comparison, mean observed mixing height (m) in spring is 10, summer is 37, fall is 8, and winter is 7.

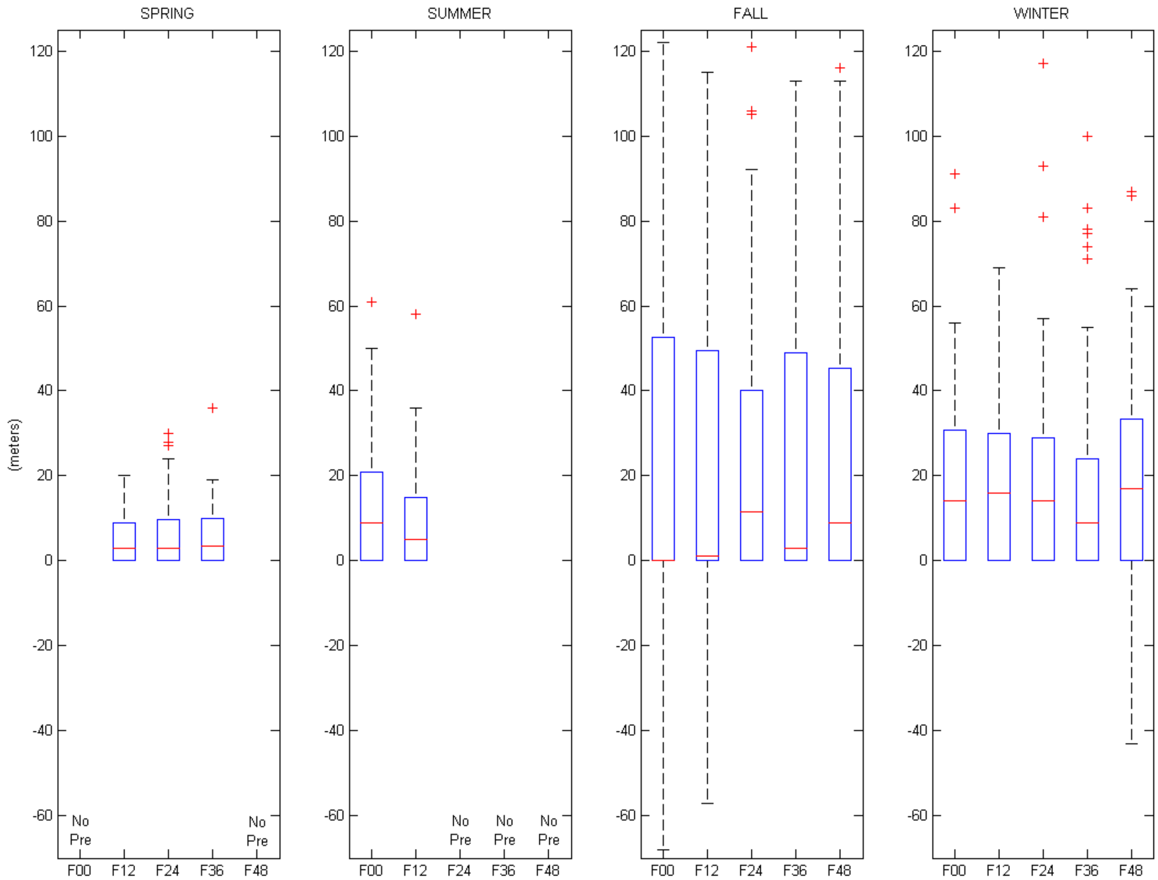

Figure 5-19 Boxplots of forecast error for REV for forecasts leading up to 12UTC (early morning). For comparison, mean observed mixing height (m) in spring is 3, summer is 7, fall is 4, and winter is 1.

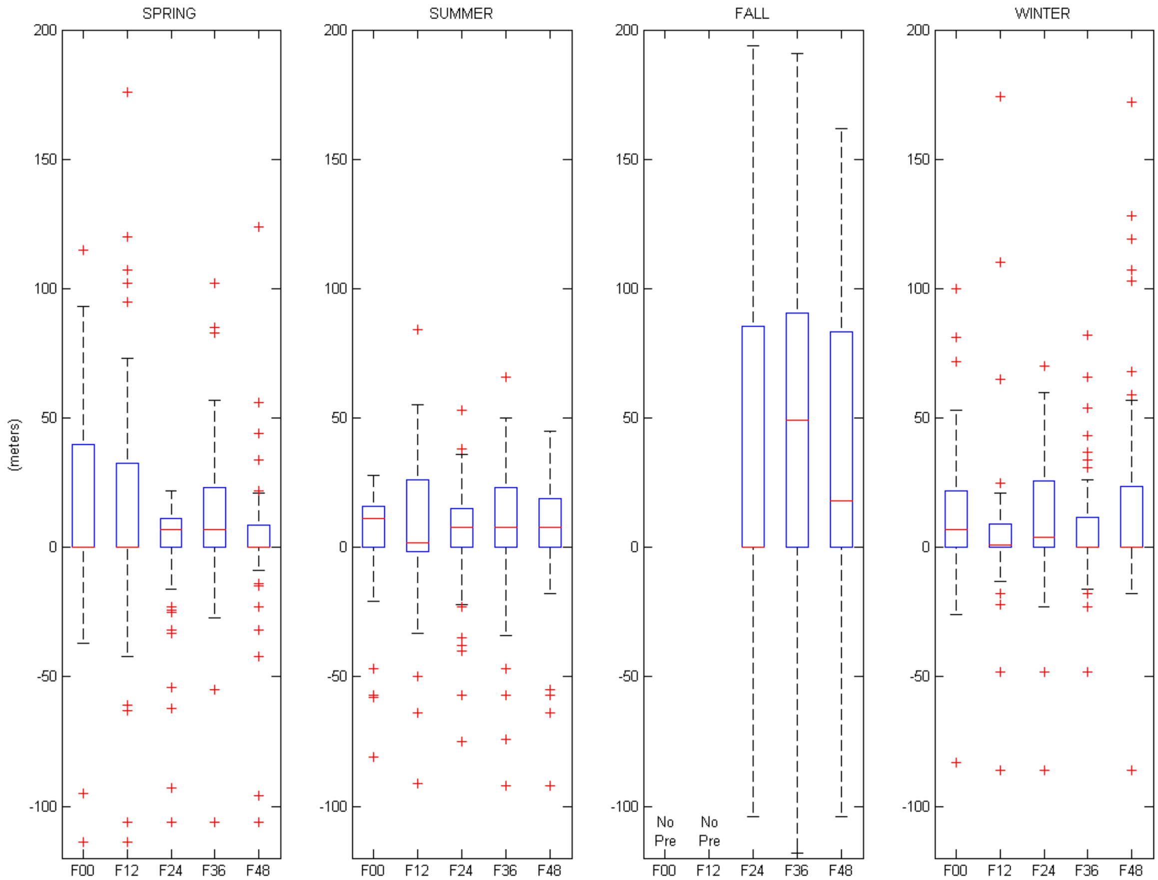

Figure 5-20 Boxplots of forecast error for VBG for forecasts leading up to 12UTC (early morning). For comparison, mean observed mixing height (m) in spring is 18, summer is 32, fall is 30, and winter is 19.

CHAPTER 6

DISCUSSION AND CONCLUSIONS

The results of each method for validation of the MM5 MOS-based forecast equations for mixing height, with observed values determined from a parcel method applied to sounding data, can be summarized as follows:

- Table 6-1 is a condensed version of Table 5-4, showing the adjusted R-squared values for the validation year averaged over all forecast lead times and multiplied by 100. The adjusted R-squared statistic is limited because it is insensitive to scale and can be modified significantly by outliers. If taken at face value as a measure of forecast performance for the equations in this study, the values in the table can be interpreted as a simple index of forecast performance.

Table 6-1 Adjusted R-squared for the validation year averaged over all forecast lead times and multiplied by 100.

	Forecasts leading up to 00UTC					Forecasts leading up to 12UTC				
	DRA	NKX	OAK	REV	VBG	DRA	NKX	OAK	REV	VBG
Spring	7	24	38	10	22	-	-2	-1	-2	-3
Summer	17	25	39	22	41	-	4	-1	-2	-2
Fall	51	21	18	57	13	-	1	-3	-2	-2
Winter	41	41	32	13	24	-	-1	-1	-2	7

The adjusted R-squared results suggest that the forecasts leading up to 12UTC (early morning) show no skill. For forecasts leading up to 00UTC (afternoon), good performance is suggested for DRA fall and winter, NKX winter, OAK spring and summer, REV fall and VBG summer.

- Table 6-2 is a condensed version of Tables 5-5 and 5-6, listing bias averaged over all forecast lead times and the absolute value of bias as a percentage of mean observed mixing height for the cases where bias is greater than 100 m.

Table 6-2 Bias (meters) averaged over all forecast lead times and rounded to the nearest 10 m. For bias over 100m, the absolute value of bias as percentage of mean observed mixing height is also given.

	Forecasts leading up to 00UTC					Forecasts leading up to 12UTC				
	DRA	NKX	OAK	REV	VBG	DRA	NKX	OAK	REV	VBG
Spring	-370:13%	70	170:32%	-610:31%	100	0	-40	30	0	0
Summer	230:7%	-90	60	-360:12%	0	0	10	10	0	-20
Fall	-40	-220:32%	60	-250:16%	-40	10	30	10	30	50
Winter	-210:20%	-460:49%	-10	-320:44%	-40	-	10	0	20	10

The bias or mean error statistic is limited because it only uses average values. Mean errors of less than 100 m or less than about 15% are likely to be considered very good mixing height forecasts. The table shows this to be the case for all forecasts leading up to 12UTC (early morning). For forecasts leading up to 00UTC (afternoon), the bias statistic suggests that forecasts are very good for all cases except DRA winter, NKX fall and winter, OAK spring, and REV winter and spring. All summer forecasts met the criterion for being very good.

- The scatterplots provide a qualitative visual estimation of the performance of the forecast equations. The scatterplots of observed versus forecasted mixing heights for forecasts leading up to 00UTC (afternoon) are fairly in line with the $y = x$ line, looking best for DRA summer and fall, NKX spring and summer, OAK summer, REV fall and VBG in all seasons. Scatterplot validation results suggest that the equations generally produce poor results for forecasts leading up to 12UTC (early morning).

- Validation with boxplots provided an analysis of the magnitude and spread of individual forecast errors. The errors for forecasts leading up to 12UTC (early morning) were usually less than 100 m. Forecasted mixing heights for 00UTC (afternoon) along the California coastline (stations NKX, OAK and VBG) displayed the narrowest spread of errors during summer.

Table 6-3 marks those equations which the results of this study suggest reasonable mixing height forecasts. Decisions regarding the content of this table were based on synthesizing the results from the different validation methods, specifically described by the following:

- None of the equations for forecasts leading up to 12UTC (early morning) were included. The goodness of fit measures for these equations suggest that they are poorly fit, and several of them contained no predictor variables or could not be developed. The low bias statistic and narrow spread of forecast errors associated with these forecasts support inclusion of these equations, but the R-squared values and especially the scatterplots support their exclusion. The scatterplots and Table 5-7 show that a large percentage of the data lies on the x-axis instead of near the $y = x$ line. Points which are not on the x-axis tend to cluster near the y-axis. The conclusion is that too many of the observed mixing heights, as determined by the parcel method used in this study, are equal to zero in the early morning. This lack of variance of the predictand prevents meaningful forecast equations to develop. The remaining points refer only to forecasts leading up to 00UTC (afternoon).

- DRA summer and fall scatterplots look fairly good, bias values are low and R-squared is high in fall. The lesser R-squared in summer is attributable to outliers as seen in the scatterplots. Winter is included to a lesser extent because R-squared and scatterplots show fair results. Spring data is too scattered (very low R-squared) and interquartile range (the box in the boxplots) is more than 1000 m.
- NKX spring and summer have low bias and scatterplots look good, but results for spring F48 and summer F36 and F48 are worse. Fall and winter bias and bias as percentage of mean observed value (Table 6-2) are too high. Even though winter R-squared is good, the spread in the boxplots seems too large.
- OAK summer looks good for all validation methods. Fall and winter scatterplots display a tendency toward clustering along the x- and y-axis similar to the 12UTC cases. Spring R-squared is good and bias is usually within 200 m, but the boxplots seem to have too much spread so this case has been marginally excluded.
- REV fall shows good scatterplot results and high R-squared. Summer has reduced R-squared and rounder clusters in the scatterplots. Bias is a fairly

low 12% on average. This is a borderline case which has been included, but F36 and F48 are excluded due to somewhat greater spreads. Spring and winter show too much variation, low R-squared and bias which is too high.

- VBG summer and fall scatterplots look good and bias values are low. Fall is questionable because of its low R-squared, but has been marginally included because of the narrow spread of the interquartile range in the boxplots. Spring and winter scatterplots are not as good as those of summer, but bias values are small and the boxplots show only a slightly larger range (whisker end to whisker end) than the fall. They have been excluded because the interquartile range (box within the boxplot) is more spread out.

Table 6-3 Equations that provide reasonable results. "X" means equation is included, "-" means equation is excluded, and parenthesis means the decision was near the margin.

		Forecasts leading up to 00UTC (afternoon)						Forecasts leading up to 12UTC (early morning)				
		DRA	NKX	OAK	REV	VBG		DRA	NKX	OAK	REV	VBG
Spring	00Z F00	-	X	(-)	-	-	12Z F00	-	-	-	-	-
	12Z F12	-	X	(-)	-	-	00Z F12	-	-	-	-	-
	00Z F24	-	X	(-)	-	-	12Z F24	-	-	-	-	-
	12Z F36	-	X	(-)	-	-	00Z F36	-	-	-	-	-
	00Z F48	-	-	(-)	-	-	12Z F48	-	-	-	-	-
Summer	00Z F00	X	X	X	(X)	X	12Z F00	-	-	-	-	-
	12Z F12	X	X	X	(X)	X	00Z F12	-	-	-	-	-
	00Z F24	X	X	X	(X)	X	12Z F24	-	-	-	-	-
	12Z F36	X	-	X	-	X	00Z F36	-	-	-	-	-
	00Z F48	X	-	X	-	X	12Z F48	-	-	-	-	-
Fall	00Z F00	X	-	-	X	(X)	12Z F00	-	-	-	-	-
	12Z F12	X	-	-	X	(X)	00Z F12	-	-	-	-	-
	00Z F24	X	-	-	X	(X)	12Z F24	-	-	-	-	-
	12Z F36	X	-	-	X	(X)	00Z F36	-	-	-	-	-
	00Z F48	X	-	-	X	(X)	12Z F48	-	-	-	-	-
Winter	00Z F00	(X)	-	-	-	-	12Z F00	-	-	-	-	-
	12Z F12	(X)	-	-	-	-	00Z F12	-	-	-	-	-
	00Z F24	(X)	-	-	-	-	12Z F24	-	-	-	-	-
	12Z F36	(X)	-	-	-	-	00Z F36	-	-	-	-	-
	00Z F48	(X)	-	-	-	-	12Z F48	-	-	-	-	-

The final recommendations regarding the reasonableness of the equations developed in this study, based on a synthesis of all validation methods, are the following:

- Summer equations at all five stations can be used for forecasts leading up to 00UTC (afternoon). This includes all forecast lead-times with the exception of NKX F36 and F48, and REV F36 and F48.
- Fall equations at the Nevada stations DRA and REV can be used for forecasts leading up to 00UTC (afternoon). This includes all forecast lead-times.

Since the distance away from station locations for which the equations maintain their forecast quality is unknown, it is recommended that they be used only at or near their corresponding MM5 gridpoint or sounding location. Fortunately, most of the sounding locations are near cities. REV is near Reno, OAK is near Oakland and NKX is near San Diego. For operational purposes, the summer equations at all stations and the fall equations at the Nevada stations (DRA and REV) can be used to obtain reasonable mixing height forecasts leading up to 00UTC (afternoon). The summer equations at stations NKX and REV give reasonable forecasts up to a 24-hour lead time. Mixing height forecasts from the MOS equations could easily be adjusted to account for the bias determined in this study. Decision-makers should keep in mind that the forecast skill for these equations show promise, but are not perfect. Perhaps forecasts from these equations could be used in combination with other mixing height forecast sources, such as from the NWS fire weather forecast or the CANSAC website (both of which do not use MOS equations), to gain more confidence in a particular forecast.

These results are also dependent on the way in which the observed mixing heights were determined. Although wind-related variables were part of the predictors, the observed mixing heights were based only on the buoyancy of air parcels. Afternoon equations for the cold seasons did not work out as well as those for the warmer seasons. During the fall, there is a striking difference in equation performance between the good results at the inland Nevada stations and the poorer results at the California coastal stations. It is likely that the marine boundary layer influences the mixing height above the coastal stations in a way that is dissimilar to the effects of buoyancy during this season (and perhaps others as well).

Future work could consider different methods of determining the observed mixing height and the effect these different methods have on the predictor variables included in the MOS equations and the results of the validation. Besides parcel methods, other existing methods consider the mixing height as the top of an inversion, take wind shear into account by using the Richardson number, or use the height of the nocturnal low-level jet.

Since prescribed burns typically occur during particular seasons depending on location, the corresponding seasonal forecast equations are more important for that application. Wildland fires also occur more often during particular seasons. A field study could perform soundings within fire-prone regions in order to develop mixing height forecast equations for those specific locations of concern.

References

Berman, S., Ku, J., and Rao, S.T., 1999: Spatial and temporal variation in the mixing depth over the northeastern United Stated during the summer of 1995. *Journal of Applied Meteorology* **38**, 1661-1673.

Cheng, S.Y., Jin, Y.Q., Liu, L., Huang, G.H., Hao, R.X., and Jansson, C.R.E., 2002: Estimation of atmospheric mixing heights over large areas using data from airport meteorological stations. *J. Environ. Sci. Health* **A37(6)**, 991-1007.

Coulter, R.L., 1979: A comparison of three methods for measuring mixing-layer height. *Journal of Applied Meteorology* **18**, 1495-1499.

Coulter, R.L., and Holdridge, D.J., 1998: A procedure for the automatic estimation of mixed layer height. *Atmospheric Radiation Measurement (ARM) Science Team Meeting*, March 24-26 1998, Tucson, AZ, Argonne National Lab, IL.

Crespi, S.N., Artinano, B., and Cabal, H., 1995: Synoptic classification of the mixed-layer height evolution. *Journal of Applied Meteorology* **34**, 1666-1677.

Fay, B., Schrodin, R., Jacobsen, I., and Engelbart, D., 1997: Validation of mixing heights derived from the operational NWP models at the German Weather Service. *The Determination of Mixing Height- Current Progress and Problems, EURASAP workshop proceedings*, October 1-3 1997, Riso National Laboratory, Denmark, 55-58.

Fearon, M.G., 2000: The use of nonlocal static stability to determine mixing height from NCEP Eta model output over the western U.S. *Thesis at University of Nevada-Reno*, 134 pp.

Hanna, S.R., Burkhart, C.L., and Paine, R.J., 1985: Mixing height uncertainties. *Proc. 7th AMS Symp. Turb. & Diff.*, Boulder, 82-85.

Hanna, S.R., and Yang, R., 2001: Evaluations of mesoscale models' simulations of near-surface winds, temperature gradients, and mixing depths. *Journal of Applied Meteorology* **40**, 1095-1104.

Holzworth, G.C., 1964: Estimates of mean maximum mixing depths in the contiguous United States. *Monthly Weather Review* **92(5)**, 235-242.

Hsu, S.A., 1979: An operational forecasting model for the variation of mean maximum mixing heights across the coastal zone. *Boundary-Layer Meteorology* **16**, 93-98.

Leahey, D.M., and Friend, J.P., 1971: A model for predicting the depth of the mixing layer over an urban heat island with applications to New York City. *Journal of Applied Meteorology* **10**, 1162-1173.

Lokoshchenko, M.A., 2002: Long-term sodar observations in Moscow and a new approach to potential mixing determination by radiosonde data. *Journal of Atmospheric and Oceanic Technology* **19**, 1151-1162.

Marsik, F.J., Fischer, K.W., McDonald, T.D., and Samson, P.J., 1995: Comparison of methods for estimating mixing height used during the 1992 Atlanta Field Intensive. *Journal of Applied Meteorology* **34**, 1802-1814.

Martin, C.L., Fitzjarrald, D., Garstang, M., Oliveira, A.P., Greco, S., and Browell, E., 1988: Structure and growth of the mixing layer over the Amazonian rain forest. *Journal of Geophysical Research* **93(D2)**, 1361-1375.

McElroy, J.L., and Smith, T.B., 1991: Lidar descriptions of mixing-layer thickness characteristics in a complex terrain/coastal environment. *Journal of Applied Meteorology* **30**, 585-597.

Melas, D., 1990: Sodar estimates of surface heat flux and mixed layer depth compared with direct measurements. *Atmospheric Environment* **24A(11)**, 2847-2853.

Miller, M.E., 1967: Forecasting afternoon mixing depths and transport wind speeds. *Monthly Weather Review* **95(1)**, 35-44.

Murphy, A.H., 1995: The coefficients of correlation and determination as measures of performance in forecast verification. *Weather and Forecasting* **10**, 681-688.

National Weather Service, 2006: Central Region Headquarters, Fire Weather Operations Plan for Central Kentucky and Southern Indiana, www.crh.noaa.gov/images/lmk/fire_wx/fire_wx_plan.pdf

Piringer, M., Baumann, K., and Langer, M., 1998: Summertime mixing heights at Vienna, Austria, estimated from vertical soundings and by a numerical model. *Boundary-Layer Meteorology* **89**, 25-45.

Russell, P.B., Uthe, E.E., and Ludwig, F.L., 1974: A comparison of atmospheric structure as observed with monostatic acoustic sounder and lidar techniques. *Journal of Geophysical Research* **79(36)**, 5555-5566.

Russell, P.B., and Uthe, E.E., 1978: Regional patterns of mixing depth and stability: sodar network measurements for input to air quality models. *Bulletin American Meteorological Society* **59(10)**, 1275-1287.

Seibert, P., Beyrich, F., Gryning, S., Joffre, S., Rasmussen, A., and Tercier, P., 1997: Mixing height determination for dispersion modelling. *COST Action 710, Preprocessing of Meteorological Data for Dispersion Modelling, Report of Working Group 2*. L-2985 Luxembourg: European Commission, EUR 18195 EN (ISBN 92-828-3302-X).

Seibert, P., Beyrich, F., Gryning, S., Joffre, S., Rasmussen, A., and Tercier, P., 2000: Review and intercomparison of operational methods for the determination of mixing height. *Atmospheric Environment* **34**, 1001-1027.

Steyn, D.G., and Oke, T.R., 1982: The depth of the daytime mixed layer at two coastal sites: a model and its validation. *Boundary-Layer Meteorology* **24**, 161-180.

Steyn, D.G., Baldi, M., and Hoff, R.M., 1999: The detection of mixed layer depth and entrainment zone thickness from lidar backscatter profiles. *Journal of Atmospheric and Oceanic Technology* **16**, 953-959.

Stull, R.B., 1988: An Introduction to Boundary Layer Meteorology. Kluwer Academic Publishers, Dordrecht, 666 pp.

Stull, R.B., 1991: Static stability- an update. *Bulletin American Meteorological Society* **72(10)**, 1521-1529.

Van Pul, W.A.J., Holtslag, A.A.M., and Swart, D.P.J, 1994: A comparison of ABL heights inferred routinely from lidar and radiosondes at noontime. *Boundary-Layer Meteorology* **68**, 173-191.

White, A.B., and Senff, C.J., 1999: A comparison of mixing depths observed by ground-based wind profilers and an airborne lidar. *Journal of Atmospheric and Oceanic Technology* **16**, 584-590.

Wilks, D.S., 2006: Statistical Methods in the Atmospheric Sciences. Academic Press, 627 pp.

Appendix A

Regression Equations Variables and Coefficients

Y-intercepts are negligible and omitted from this listing, being on the order of 1e-15.

Station DRA: Forecasts Leading up to 00UTC (afternoon)

<u>DRA Spring 00Z F00</u>

SOIT1	2.159
V(15)	-0.19496
V(25)	0.68416
V(30)	-0.37434
T(17)	-1.7298

<u>DRA Spring 12Z F12</u>

PBLHT	0.58513
SHFLX	-0.45037
LHFLX	0.57305
Q2	0.72058
U(1)	0.30084
U(17)	-0.4325
U(28)	0.22738
T(22)	-0.51032
Q(16)	-0.18437
TK(8)	0.43619
TK(11)	-0.55329
TK(26)	0.13677
RT(12)	0.23976
RT(23)	0.34454
RT(30)	-0.19131
W(32)	-0.1903

<u>DRA Spring 00Z F24</u>

LHFLX	0.72726
Q2	0.91705
V(24)	0.65181
V(31)	-0.40889
T(18)	-1.0465
RT(17)	0.24964
RT(24)	0.14298
W(4)	-0.15659

<u>DRA Spring 12Z F36</u>

LHFLX	0.62625
Q2	0.51801
U(9)	0.26892
U(17)	-0.38636
T(22)	-0.721
TK(18)	-0.24328
RT(10)	-0.25992
RT(11)	0.36953
RT(24)	0.18907

<u>DRA Spring 00Z F48</u>

SOIT4	1.1803
V(19)	-0.4562
V(24)	1.195
V(28)	-0.65118
T(17)	-0.60625
Q(24)	-0.32035
TK(19)	-0.31209
RT(20)	0.21797
W(10)	-0.24847
W(28)	0.20803
W(31)	-0.18542

DRA Summer 00Z F00

GRNDT	0.81388
U(14)	-0.1099
V(24)	-0.16281
T(8)	9.5139
T(9)	-9.2203
T(19)	-0.58242
Q(21)	0.14799
Q(24)	-0.33446
Q(31)	0.20205
W(1)	0.28914

DRA Summer 12Z F12

LHFLX	0.38973
U(15)	0.16397
U(20)	-0.28872
V(20)	0.23743
V(23)	-0.29878
T(24)	-0.25096
Q(20)	-0.32534
TK(1)	-0.15159
TK(13)	0.41824
TK(15)	-0.76122
TK(18)	0.38246
TK(21)	0.14632
RT(4)	-0.50053
RT(9)	0.4852
RT(21)	0.24384
RT(24)	-0.21515
RT(28)	0.15496

DRA Summer 00Z F24

LHFLX	0.52663
Q(25)	-0.21113
Q(28)	-0.27692
TK(16)	0.19456
RT(18)	-0.15664
RT(23)	0.46112
RT(28)	0.23212
W(10)	-0.39531
W(19)	-0.21466

DRA Summer 12Z F36

GRNDT	0.53148
PBLHT	-0.1846
T(23)	-0.38956
Q(2)	-0.19244
Q(25)	-0.17822
RT(14)	0.17063
RT(30)	0.19534
W(21)	0.17387
24PER	0.19689

DRA Summer 00Z F48

LHFLX	0.41697
SWOUT	0.1784
V(1)	-0.38488
Q(28)	-0.34484
TK(19)	-0.33028
RT(7)	-0.8943
RT(8)	0.70667
RT(21)	0.1397
RT(31)	-0.31466
W(19)	-0.22357
W(23)	-0.14224
W(30)	-0.34767
24PER	0.17184

DRA Fall 00Z F00

GRNDT	1.5906
V(19)	-0.12677
T(14)	-0.6907
T(18)	-0.37631
T(29)	0.14726
Q(7)	-0.16317
24PER	0.15788

DRA Fall 12Z F12

LWOUT	-0.27013
SOIT3	1.3462
T(19)	-0.69347
Q(9)	-0.20578
Q(19)	-0.29605
Q(30)	-0.098769
TK(14)	-0.18468
TK(19)	0.10299
RT(17)	0.13206
RT(18)	-0.24519
RT(29)	0.15787
W(30)	-0.12211
24PER	0.18887

DRA Fall 00Z F24

SWDWN	0.30926
SOIT4	0.59042
T(22)	-0.68756
T(26)	0.71148
T(27)	-0.64228
Q(1)	-0.11244
Q(17)	0.19757
Q(19)	-0.22215
Q(23)	-0.34809
Q(24)	0.23167
TK(14)	-0.15319
TK(16)	0.16555
RT(6)	-0.15134
RT(11)	0.17887
24PER	0.3159

DRA Fall 12Z F36

SOIT4	0.71716
V(3)	-0.1128
T(20)	-0.31025
Q(17)	0.24819
Q(18)	-0.40862
Q(26)	-0.16061
RT(17)	-0.13946
24PER	0.30568

DRA Fall 00Z F48

SOIT6	0.67
T(21)	-0.56383
Q(19)	-0.24169
Q(23)	-0.30802
TK(18)	-8.2717
TK(19)	8.1587
RT(25)	-0.19036
PP(23	0.39173
24PER	0.26372

DRA Winter 00Z F00

SOIT4	0.77023
T(16)	-0.94314
Q(1)	-0.24094
Q(17)	-0.18142
Q(21)	-0.12967

DRA Winter 12Z F12

LHFLX	0.23577
SOIT3	0.41274
T(14)	-0.62887
Q(3)	-1.0024
Q(7)	0.80125
Q(21)	-0.25818
RT(8)	-0.19874
RT(12)	-0.14378
RT(18)	0.19319
W(27)	-0.14228

DRA Winter 00Z F24

REGIM	-0.38179
LHFLX	0.55332
SOIT5	0.71545
Q2	-0.42603
T(13)	-0.69775
Q(22)	-0.37596
TK(14)	-0.13635
RT(3)	-0.18025
RT(15)	0.23434
RT(19)	-0.15042
W(23)	0.15984
W(28)	-0.20054

DRA Winter 12Z F36

SWDWN	0.36095
V(25)	-0.16888
T(9)	0.68412
T(13)	-1.1016
Q(21)	-0.13998
TK(18)	-59.1745
TK(20)	59.2875
RT(6)	-0.26994
RT(15)	-0.32383
RT(17)	0.25623
W(19)	-0.17944
W(28)	-0.17704
W(32)	0.15632

DRA Winter 00Z F48

SWDWN	0.35146
V(26)	-0.27058
T(2)	0.84005
T(12)	-1.2465
TK(9)	-0.18857
W(20)	0.25782

Station DRA: Forecasts Leading up to 12UTC (early morning)

DRA Spring 12Z F00

U(15)	0.44285
U(22)	-0.60174
V(1)	0.58115
V(13)	0.75721
V(16)	-0.93097
V(25)	0.5158
T(7)	-0.70526
T(25)	0.54919
T(30)	0.20322
W(1)	-0.61037

DRA Spring 00Z F12

PBLHT	-3.2705e-008
U(6)	-1.6422e-008
U(29)	9.0395e-009
V(11)	-9.165e-009
TK(2)	-4.8376e-008
TK(3)	1.2453e-007
TK(6)	3.8794e-008
TK(9)	-8.5692e-008
TK(10)	2.8415e-008
TK(22)	1
TK(23)	-1.3349e-006
RT(6)	1.0678e-008
RT(11)	1.0306e-008
RT(17)	-1.4611e-008
W(11)	2.5198e-008
W(20)	1.3758e-008
W(29)	-1.0245e-008
W(30)	2.1619e-008
W(32)	-1.5042e-008

DRA Spring 12Z F24

GRNDT	-0.55531
SHFLX	0.32073
LWDWN	0.95782
LWOUT	0.54479
U(4)	-0.15078
U(16)	0.28038
U(20)	-0.20291
U(24)	-0.18111
T(21)	-0.27504
Q(19)	-0.65722
Q(22)	0.1998
RT(1)	0.16405
RT(12)	0.24299
RT(15)	0.28781
RT(21)	-0.76462

DRA Spring 00Z F36

REGIM	-0.16302
LHFLX	-0.43656
U(29)	-0.15191
TK(1)	0.95573
RT(22)	0.19124
W(21)	-0.24435
W(30)	0.18589

DRA Spring 12Z F48

LHFLX	-0.56758
U(14)	0.2894
U(25)	-0.14237
V(15)	-0.35391
V(20)	-0.46971
V(21)	0.8154
V(29)	-0.35501
V(31)	0.44237
T(2)	0.72611
T(16)	-0.67138
T(26)	0.21263
Q(22)	-0.26765
Q(25)	0.12996
TK(1)	1.4293
TK(6)	-0.18973
TK(10)	0.5394
TK(11)	-1.6075
TK(12)	1.0473
TK(17)	-0.50695
TK(20)	-0.13414
TK(22)	0.13871
RT(19)	0.1686
RT(20)	0.15201
RT(30)	0.19161
W(25)	-0.18426

<u>DRA Summer 12Z F00</u>

U(17)	-0.18434

<u>DRA Summer 00Z F12</u>

SHFLX	-0.17379
W(17)	0.24943
W(21)	0.21621

<u>DRA Summer 12Z F24</u>

(none)

<u>DRA Summer 00Z F36</u>

U(5)	-1.8614
U(6)	2.67
U(10)	-2.6424
U(11)	1.6983
W(21)	0.22572

<u>DRA Summer 12Z F48</u>

(none)

<u>DRA Winter 12Z F00</u>

(none)

<u>DRA Winter 00Z F12</u>

(none)

<u>DRA Winter 12Z F24</u>

(none)

<u>DRA Winter 00Z F36</u>

(none)

<u>DRA Winter 12Z F48</u>

(none)

DRA Fall 12Z F00

U(12)	-0.90443
U(16)	0.36338
V(29)	-0.25759
Q(21)	0.17905
W(1)	0.86767

DRA Fall 00Z F12

PBLHT	-0.62326
LWOUT	-0.17614
U(7)	-0.31308
TK(1)	-0.70449
TK(3)	1.3121
TK(6)	-0.65378
TK(8)	3.3399
TK(9)	-3.7539
TK(10)	2.3843
TK(11)	-1.3822
TK(12)	-0.69441
TK(13)	1.0556
RT(14)	0.12469
RT(19)	-0.11535
RT(21)	-0.21486
W(24)	-0.12513
W(31)	-0.14701
W(32)	-0.11628

DRA Fall 12Z F24

PBLHT	-1.0205
TK(1)	0.19552
TK(3)	1.726
TK(4)	-2.5115
TK(6)	6.6315
TK(7)	-14.8901
TK(8)	14.9532
TK(9)	-5.241
TK(10)	-0.63625
TK(11)	1.45
TK(17)	0.091699
RT(12)	0.29588
RT(14)	-0.18699
RT(20)	0.28279
RT(21)	-0.30154
W(13)	0.56524
W(14)	-0.54697
W(21)	-0.13603
W(28)	-0.13357
W(32)	-0.1624

DRA Fall 00Z F36

PBLHT	-0.25821
LHFLX	-0.21314
LWOUT	0.18047
U(7)	-0.10637
V(5)	0.16362
T(28)	-0.08173
TK(7)	0.57337
TK(8)	1.0489
TK(9)	-0.39625
TK(11)	-0.67925
TK(12)	1.5877
TK(13)	-1.5057
TK(23)	0.08696
TK(25)	0.13003
RT(3)	-0.068411
RT(6)	0.076226
RT(9)	-0.21483
RT(10)	0.15291
RT(26)	-0.11455
RT(30)	-0.092407
PP(17	0.098926
24PER	-0.54012

DRA Fall 12Z F48

PBLHT	-1.35
UST	-0.24635
U(20)	-0.21288
V(1)	-0.45873
TK(4)	1.1737
TK(7)	1.334
TK(15)	-0.17037
TK(17)	0.31952
RT(21)	0.14209
RT(25)	-0.22733
W(19)	-0.19698

Station NKX: Forecasts Leading up to 00UTC (afternoon)

NKX Spring 00Z F00

SOIT4	0.73097
U(3)	0.17695
T(13)	-1.1392
Q(9)	0.28695
Q(19)	-0.16662
Q(30)	0.14143
W(21)	0.12481

NKX Spring 12Z F12

SOIT5	0.41384
U(21)	-0.30715
U(23)	0.41706
U(31)	-0.20345
T(10)	-0.31136
T(13)	-0.54405
Q(17)	-0.21424
TK(9)	0.19108
TK(16)	-0.27375
TK(23)	0.15778
RT(4)	0.11812
RT(18)	-0.28982
RT(22)	0.1892
W(14)	0.21231
W(31)	-0.22136

NKX Spring 00Z F24

U(23)	0.37061
U(31)	-0.27473
T(10)	-0.31188
T(28)	0.21093
Q(18)	-0.21274
Q(28)	-0.21074
Q(29)	0.15006
TK(9)	0.21799
TK(21)	-0.31915
RT(6)	-0.11047
RT(11)	-0.14782
RT(22)	0.15405
W(10)	-0.14749

NKX Spring 12Z F36

SOIT5	0.35586
T(11)	-0.82217
T(29)	0.17021
Q(18)	-0.18288
TK(14)	0.13685
RT(12)	0.23641
RT(15)	-0.14074
RT(17)	-0.2518
RT(18)	0.18587
W(23)	0.13012

NKX Spring 00Z F48

U(1)	1.2499
U(5)	-1.5236
U(13)	0.28267
T(8)	0.36863
T(12)	-0.98583
T(31)	0.22615
Q(21)	-0.21604
TK(12)	-0.19689
TK(25)	-0.15872
TK(26)	-0.13132
RT(15)	0.19407
RT(16)	-0.08995
RT(20)	0.28063
PP(31	0.33431

NKX Summer 00Z F00

GRNDT	1.1532
V(1)	0.11206
V(16)	-0.26553
V(24)	0.15199
T(7)	-1.0332
T(12)	-0.80975
T(23)	-0.14272
PP(17	0.29192
W(22)	0.1632

NKX Summer 12Z F12

V(8)	0.20387
V(17)	-0.16686
V(31)	0.20777
Q(31)	0.1796
RT(10)	0.21968
PP(29	-0.42435
W(9)	-0.17705
24PER	0.19316

NKX Summer 00Z F24

SOIT6	0.28477
U(21)	-0.27275
V(11)	0.16199
V(18)	-0.36803
V(20)	0.19257
V(31)	0.20517
T(10)	-0.77094
T(28)	-0.34073
T(30)	0.14354
Q(10)	-0.31793
Q(13)	0.21247
TK(12)	-0.2139
TK(20)	-0.149
24PER	0.11404

NKX Summer 12Z F36

SHFLX	-0.22208
U(27)	-0.25671
V(18)	-0.22173
V(31)	0.29361
T(7)	-0.59267
T(26)	-0.35783
TK(12)	0.13428
TK(15)	-0.12319
RT(10)	0.13253
RT(18)	-0.17503
W(21)	0.17397

NKX Summer 00Z F48

U(27)	-0.23835
V(14)	0.53269
V(15)	-0.63968
V(31)	0.22711
T(7)	-0.29542
Q(30)	0.15204
TK(17)	0.10905
TK(20)	-0.12818
RT(9)	-0.12259
RT(12)	0.15333
PP(30	-0.4387
W(8)	0.13294
W(20)	0.12357

NKX Fall 00Z F00

U(18)	0.6075
U(19)	-1.2218
U(21)	0.78547
V(18)	-0.1508
T(30)	0.31813
Q(12)	0.3337
Q(16)	-0.17746
PP(18	-0.20279
W(1)	0.18835

NKX Fall 12Z F12

PBLHT	0.25632
UST	0.30474
Q2	0.5057
U(1)	0.23491
V(5)	0.13902
V(20)	-0.24715
V(31)	0.27383
T(25)	-0.20775
Q(16)	-0.14785
Q(22)	-0.15207
Q(24)	0.26006
RT(9)	-0.10861
RT(27)	0.12568
PP(16	3.2021
PP(17	-3.7157

NKX Fall 00Z F24

UST	0.4012
U(1)	0.18764
U(9)	0.39177
U(16)	-0.17933
V(17)	-0.1354
Q(21)	-0.11581
TK(1)	-0.54169
TK(7)	0.68362
TK(30)	0.1013
TK(31)	0.14175
RT(14)	-0.13742
RT(20)	0.32073
PP(17	-0.45436
W(13)	-0.14152
W(27)	-0.37959
W(28)	0.2822

NKX Fall 12Z F36

TK(7)	0.16917
TK(19)	-0.16579
RT(13)	-0.1417
RT(14)	0.14647
RT(15)	-0.18083
RT(27)	0.11139
PP(16	-0.33229
W(27)	-0.1531
24PER	0.20549

NKX Fall 00Z F48

PBLHT	0.25346
U(9)	0.21778
V(17)	-0.14789
TK(2)	-0.16088
TK(12)	0.19482
TK(15)	-0.12702
RT(6)	0.13263
RT(8)	0.13054
RT(18)	0.1991
RT(21)	0.21538
PP(17	-0.42772
24PER	0.10459

NKX Winter 00Z F00

SOIT1	0.67008
U(4)	0.19586
U(16)	-0.29127
U(19)	0.5096
U(29)	-0.28573
T(13)	-2.9488
T(14)	2.5089
T(16)	-0.67411
Q(20)	-0.18413
Q(28)	0.13009
W(30)	0.18147

NKX Winter 12Z F12

SOIT3	0.72695
U(18)	-0.47333
U(19)	0.71932
U(27)	-0.27948
V(27)	0.13983
T(11)	-1.2071
Q(13)	-0.24937
Q(19)	-0.14013
Q(30)	-0.13624
TK(12)	0.24044
TK(16)	-0.13397
TK(19)	0.20086
RT(3)	0.22839
RT(15)	0.11414
RT(16)	-0.16679

NKX Winter 00Z F24

LHFLX	0.31047
U(20)	0.33633
U(30)	-0.24078
T(11)	-0.54786
Q(19)	-0.29504
TK(14)	-0.13086
RT(14)	-0.12631
W(7)	0.20806

NKX Winter 12Z F36

LHFLX	0.29289
U(13)	0.23003
U(22)	0.27328
U(29)	-0.29606
T(11)	-0.59207
Q(20)	-0.23336
W(31)	-0.14339

NKX Winter 00Z F48

LHFLX	0.15384
LWOUT	0.24369
U(17)	-0.35824
U(20)	0.79341
U(28)	-0.28208
T(12)	-0.57081
RT(10)	0.1527
RT(19)	0.26287
W(22)	0.1999

Station NKX: Forecasts Leading up to 12UTC (early morning)

NKX Spring 12Z F00

SOIT1	0.16207
Q(12)	0.48148
Q(14)	-0.50087
Q(28)	-0.14621
24PER	0.29236

NKX Spring 00Z F12

TK(29)	0.23994
RT(11)	-0.38276
RT(29)	-0.15333
24PER	0.34208

NKX Spring 12Z F24

SOIT2	0.19658
V(22)	-0.30648
V(29)	0.43835
Q(20)	-0.14535
RT(5)	-0.23361
24PER	0.29125

NKX Spring 00Z F36

V(30)	0.19913
T(27)	0.20938
T(31)	0.25633
Q(11)	0.2487
Q(15)	-0.19026
TK(25)	0.2127
RT(2)	-0.34334
RT(3)	0.18583
RT(6)	-0.17183
RT(21)	-0.14172
RT(30)	0.17456
W(29)	0.14436
24PER	0.13445

NKX Spring 12Z F48

U(7)	-0.13997
Q(6)	0.33038
Q(15)	-0.26643
RT(11)	0.17335
24PER	0.29757

NKX Summer 12Z F00

GRNDT	23769.0492
SOIT1	-23768.6905
U(14)	-0.15657
U(31)	0.24562
V(17)	0.16749
T(28)	0.39076
Q(12)	-0.44184
PP(18	-0.35985
W(4)	0.153

NKX Summer 00Z F12

U(20)	0.17257
U(31)	0.28201
V(28)	0.29775
T(28)	0.19252
RT(4)	-0.21915
RT(17)	-0.30212
W(20)	0.23476

NKX Summer 12Z F24

V(21)	-0.23543
V(26)	0.37478
T(30)	0.1656
Q(27)	-0.2041
RT(3)	-0.18341

NKX Summer 00Z F36

V(21)	-0.32131
V(27)	0.47445
T(31)	0.243
RT(3)	-0.18292
RT(20)	-0.24017
RT(29)	0.15604
PP(1)	-0.14584

NKX Summer 12Z F48

U(13)	-0.25628
U(15)	0.44666
U(30)	0.27405
V(18)	0.74449
V(19)	-0.58849
T(30)	0.18226
Q(4)	0.18207
TK(8)	-0.26009
TK(14)	0.14605
TK(16)	0.15185
RT(9)	-0.32272

NKX Fall 12Z F00

V(1)	0.19299
Q(1)	0.34806
Q(14)	-0.4515
PP(11	-0.17637

NKX Fall 00Z F12

U(17)	-0.12929
Q(8)	0.78064
Q(10)	-0.43739
Q(14)	-0.51578
Q(17)	0.41754
TK(28)	0.20045
RT(3)	-0.21454
RT(5)	-0.19711
RT(25)	0.15682
PP(10	-0.18041

NKX Fall 12Z F24

Q(3)	0.35936
Q(11)	-0.31459
Q(29)	0.18474
RT(9)	-0.13881
RT(28)	0.23458
PP(1)	-0.24

NKX Fall 00Z F36

T(28)	-0.20348
Q(30)	0.22519
TK(22)	0.23331
TK(26)	0.24267
RT(6)	-0.29083
RT(8)	-0.10794
RT(19)	-0.25902
PP(9)	-0.24814
W(25)	0.14035

NKX Fall 12Z F48

U(30)	-0.13747
Q(1)	0.50694
Q(12)	-0.53703
Q(18)	0.2249
Q(22)	-0.15807
Q(29)	0.15321
PP(9)	-0.21395

NKX Winter 12Z F00

SOIT6	0.31177
U(16)	0.14899
T(7)	-0.25178
T(27)	0.27618
Q(15)	0.22032
Q(23)	-0.1985

NKX Winter 00Z F12

U(16)	0.22174
T(28)	0.31637
RT(12)	-0.35481
RT(15)	-0.23249

NKX Winter 12Z F24

T(27)	0.17997
Q(16)	0.55895
Q(18)	-0.41841
TK(21)	0.1248
TK(25)	-0.1206
RT(7)	-0.29005
RT(15)	-0.32416
RT(18)	0.12451
RT(20)	-0.38777

NKX Winter 00Z F36

LWDWN	0.16422
T(27)	0.13393
TK(21)	0.30467
RT(1)	-0.14314
RT(13)	-0.31222
RT(16)	-0.35773
RT(17)	-0.11641

NKX Winter 12Z F48

V(29)	-0.13894
T(28)	0.15019
Q(12)	0.21388
TK(29)	0.32659
RT(4)	-0.22124
RT(16)	-0.26934
W(16)	-0.23513
W(17)	0.71501
W(18)	-0.39027
W(23)	0.21089
W(30)	-0.12807

Station OAK: Forecasts Leading up to 00UTC (afternoon)

OAK Spring 00Z F00

SOIT1	0.83165
V(12)	-0.15716
T(8)	-0.73135
T(16)	-0.62572
Q(17)	-0.14505

OAK Spring 12Z F12

U(29)	0.54248
U(30)	-0.67054
V(10)	-0.20666
T(6)	-0.2279
T(14)	1.0134
T(15)	-1.3931
Q(16)	-0.2396
TK(20)	0.12004
TK(27)	-0.14662
RT(11)	0.18515
RT(12)	0.1451
RT(13)	0.26951
RT(16)	-0.13979
W(27)	-0.22053
W(30)	0.12722

OAK Spring 00Z F24

SHFLX	0.45745
U(13)	-0.22365
U(20)	0.5289
U(30)	-0.33252
V(12)	-0.25985
T(13)	1.2192
T(14)	-1.8505
TK(2)	-0.22609
TK(20)	0.27618
RT(15)	-0.22284
RT(17)	0.12536
RT(31)	-0.1578
W(10)	0.17445
W(19)	0.14274

OAK Spring 12Z F36

PBLHT	0.31557
U(21)	0.26465
U(31)	-0.17789
V(26)	-0.17651
T(16)	-0.87049
T(19)	0.41726
RT(2)	0.25833
RT(12)	0.23939
RT(14)	-0.19017
RT(24)	0.11219
W(30)	0.1408
24PER	-0.13541

OAK Spring 00Z F48

SWDWN	0.35524
U(26)	0.16256
T(10)	-0.62028
T(21)	0.26809
TK(14)	0.20405
RT(16)	-0.16111
RT(31)	-0.40959
W(21)	0.13127

OAK Summer 00Z F00

U(3)	0.16537
U(16)	-0.14819
V(29)	0.11644
T(11)	-0.67044
T(19)	-0.28777
T(28)	0.14422

OAK Summer 12Z F12

GRNDT	0.28503
U(21)	-0.18276
U(23)	0.43613
U(31)	-0.16746
V(8)	0.1241
V(15)	0.14076
T(10)	-1.0082
T(28)	0.10014
Q(10)	-0.1522
Q(22)	-0.13505
RT(11)	-0.11675
RT(17)	0.14195
RT(18)	-0.13071
RT(20)	0.22713

OAK Summer 00Z F24

PBLHT	0.2292
LWDWN	-0.2631
V(19)	0.24946
T(11)	-0.16952
T(27)	0.11456
Q(13)	0.12333
TK(11)	0.85115
TK(12)	-0.80966
TK(14)	-0.34332
RT(25)	0.14947
PP(22	-0.2635
W(13)	0.19695
24PER	0.22567

OAK Summer 12Z F36

PBLHT	0.24638
SWOUT	-0.18749
U(13)	0.1801
U(24)	0.26061
V(8)	0.28126
V(21)	0.24845
T(9)	-0.2926
Q(9)	-0.13967
RT(6)	-0.096283
RT(18)	0.16414
RT(19)	-0.14825
W(10)	-0.19757
W(18)	-0.1605
W(32)	-0.19212
24PER	0.236

OAK Summer 00Z F48

U(31)	-0.12131
T(11)	-0.44949
Q(10)	-0.15327
TK(8)	0.21482
RT(12)	0.13775
RT(13)	-0.27179
RT(21)	-0.13894
W(13)	-0.092305
W(29)	-0.087818
W(32)	-0.13969
24PER	0.23391

OAK Fall 00Z F00

SOIT4	1.3266
V(11)	0.26621
T(7)	-1.3734
T(12)	-0.47817
Q(7)	-0.19019
Q(20)	-0.14405
Q(29)	0.12508
PP(19	-0.21234
W(16)	-0.39307
24PER	-0.18626

OAK Fall 12Z F12

PBLHT	0.29994
SOIT5	0.39836
T(8)	-0.6708
RT(13)	-0.13611
RT(22)	-0.17932
RT(30)	-0.13515
PP(21	-0.17443
W(11)	-0.21873
W(31)	-0.19857

OAK Fall 00Z F24

SOIT1	0.41328
V10	0.22299
U(14)	-0.33694
U(28)	0.20768
T(9)	-0.734
Q(25)	-0.20171
RT(10)	0.14768
RT(19)	0.26686
RT(26)	0.17033
RT(30)	0.20098
PP(20	-0.30556
W(18)	-0.14784

OAK Fall 12Z F36

SOIT1	6.0861
SOIT2	-6.591
SOIT6	0.76678
V(9)	-0.62385
V(10)	0.87746
T(9)	-0.59571
Q(19)	-0.1633
Q(22)	-0.17945
TK(5)	0.89875
TK(7)	-0.60599
TK(15)	-0.20926
RT(12)	0.11403
RT(19)	0.26877
RT(24)	0.1293
PP(20	-0.28691
W(19)	-0.21381
W(32)	-0.21126

OAK Fall 00Z F48

SWOUT	0.18256
V(20)	0.41796
V(23)	-0.82006
V(27)	0.27086
Q(13)	-0.24144
TK(18)	-0.22289
RT(2)	0.39573
RT(6)	-0.28655
RT(13)	-0.13617
RT(17)	-0.20207
PP(21	-0.55919
W(29)	-0.17741

<u>OAK Winter 00Z F00</u>

SOIT1	1.1695
U(26)	0.18211
V(18)	-0.22654
T(5)	-1.081
T(14)	-0.21696
Q(4)	-0.25815
Q(30)	0.18303

<u>OAK Winter 12Z F12</u>

PBLHT	0.21953
SWDWN	0.19524
V(18)	-0.2198
T(13)	-0.39459
Q(19)	-0.19159
Q(28)	0.13652
TK(15)	0.18417
RT(11)	-0.20933

<u>OAK Winter 00Z F24</u>

PBLHT	0.263
SHFLX	0.14251
V(1)	-0.29163
V(22)	-0.21655
T(17)	-0.2268
RT(8)	0.14148
RT(12)	-0.12277
RT(16)	-0.16498
RT(19)	-0.25072
W(17)	-0.13086
24PER	0.15784

<u>OAK Winter 12Z F36</u>

SHFLX	0.83685
SWOUT	0.32486
U(29)	0.11865
V(21)	-0.19475
T(11)	-0.35421
TK(23)	0.17327
RT(1)	-0.55783
RT(8)	-0.1489
RT(16)	-0.12746
W(18)	-0.11423
W(27)	-0.20834

<u>OAK Winter 00Z F48</u>

SHFLX	0.19296
SOIT5	0.227
V(18)	-0.24863
T(13)	-0.43644
Q(1)	-0.30217
RT(13)	-0.13225
W(26)	-0.21801
W(29)	0.13177

Station OAK: Forecasts Leading up to 12UTC (early morning)

OAK Spring 12Z F00

W(4)	0.19603

OAK Spring 00Z F12

U(13)	0.18447
TK(11)	0.16471
TK(20)	0.2301

OAK Spring 12Z F24

LWOUT	-0.27822
V(29)	-0.19653
Q(11)	0.14538
RT(20)	-0.41158
W(17)	-0.20119
W(31)	0.24181

OAK Spring 00Z F36

Q(17)	-0.37374
Q(18)	0.48241
RT(11)	-0.31938
RT(29)	-0.1862

OAK Spring 12Z F48

RT(10)	-0.21397
RT(21)	-0.23972
RT(22)	0.20268
W(23)	-0.16028

OAK Summer 12Z F00

U(17)	-0.25826
T(6)	-0.28026
T(12)	-0.36377
T(28)	0.41398
Q(25)	0.18533
W(1)	0.1943
W(25)	-0.1426

OAK Summer 00Z F12

U(26)	0.6566
U(27)	-0.81027
T(8)	-0.17771
T(29)	0.27175
RT(3)	-0.17996
RT(10)	-0.18755
PP(13	-0.18827
W(1)	0.20261
W(15)	-0.48084
W(16)	0.70577
W(18)	-0.20505

OAK Summer 12Z F24

V(10)	0.17624
V(26)	-0.41262
V(31)	0.29306
RT(3)	0.16149
RT(16)	0.19072
RT(30)	-0.19485
W(7)	0.26387

OAK Summer 00Z F36

U(27)	-0.2021
V(1)	-0.27629
V(27)	-0.72438
V(29)	0.56151
T(11)	-0.18698
T(30)	0.17756
Q(9)	-0.2464
Q(25)	0.17845
RT(8)	-0.16812
RT(10)	-0.20312
RT(11)	-0.20854
RT(13)	-0.25261
PP(1)	-0.20366
W(1)	0.43225

OAK Summer 12Z F48

UST	0.24356
RT(5)	0.19929
RT(10)	0.12971
RT(12)	-0.34063
RT(16)	0.19759
RT(19)	-0.21313
RT(20)	-0.15735
PP(13	-0.19641

OAK Fall 12Z F00

SOIT4	-0.29983
V(29)	0.30009
T(27)	0.31245

OAK Fall 00Z F12

V(30)	0.23558
TK(17)	0.28312
RT(7)	-0.14906
RT(17)	-0.14732

OAK Fall 12Z F24

V(30)	0.21469
T(28)	0.20115
TK(29)	0.29664
RT(4)	-0.21716
RT(8)	-0.20136

OAK Fall 00Z F36

V(21)	0.24445
RT(6)	-0.30343
RT(8)	-0.20845

OAK Fall 12Z F48

V(29)	0.1731
TK(29)	0.26763
RT(7)	-0.25181

OAK Winter 12Z F00

U(18)	0.22062

OAK Winter 00Z F12

Q(21)	0.15583
Q(28)	-0.2515
TK(11)	-0.18269
RT(28)	-0.57081
W(9)	0.23959

OAK Winter 12Z F24

(none)

OAK Winter 00Z F36

(none)

OAK Winter 12Z F48

(none)

Station REV: Forecasts Leading up to 00UTC (afternoon)

REV Spring 00Z F00

SOIT1	18.0234
SOIT2	-16.66
U(20)	-0.16988
V(30)	-0.63587
V(31)	0.73981
T(7)	-3.403
T(8)	6.727
T(13)	-3.4971
T(16)	-0.87762
T(20)	-0.79056
T(23)	0.84565

REV Spring 12Z F12

LHFLX	0.31221
TK(25)	0.14131
RT(19)	-0.21209
RT(20)	-0.21032
24PER	0.2041

REV Spring 00Z F24

LHFLX	0.4169
TK(18)	0.15445
RT(13)	0.25582
RT(25)	0.15802
W(10)	-0.18968

REV Spring 12Z F36

T(5)	0.91316
T(18)	-0.53835
TK(17)	-0.21769
RT(26)	0.16657

REV Spring 00Z F48

T(5)	2.2218
T(11)	-1.8817

REV Summer 00Z F00

GRNDT	1.8045
U(19)	0.16145
T(8)	0.95244
T(15)	-1.702
T(18)	1.4699
T(19)	-2.0369
T(29)	0.13845

REV Summer 12Z F12

SWDWN	-0.22887
SOIT4	2.016
SOIT5	-1.7892
U(16)	-0.15616
Q(28)	-0.33506
RT(9)	-0.21434
RT(24)	-0.13447
RT(30)	-0.17723
W(19)	0.18323
24PER	0.16593

REV Summer 00Z F24

Q2	0.38086
V(1)	0.19817
V(28)	0.24145
V(31)	-0.37988
RT(21)	-0.23211
RT(26)	0.24733

REV Summer 12Z F36

T(6)	0.41147
Q(20)	-0.30412
Q(30)	-0.24346
RT(22)	-0.18412
RT(29)	-0.16917
W(3)	-0.18526
W(28)	0.15736

REV Summer 00Z F48

SOIT6	-0.55022
T(5)	-4.7236
T(7)	5.769
T(31)	0.27501
Q(4)	0.51222
Q(11)	-0.37633
Q(31)	-0.219
TK(14)	-0.24282
RT(27)	0.26063
PP(26	-0.39561
W(11)	0.16336

REV Fall 00Z F00

SOIT3	0.90023
U(22)	-0.18519
U(30)	0.30297
T(18)	-0.41201
Q(5)	-0.17536
Q(21)	-0.18629
Q(30)	0.13147
24PER	0.25667

REV Fall 12Z F12

PBLHT	0.13915
Q2	0.67811
U10	0.14066
T(18)	-0.25695
Q(20)	-0.2043
Q(25)	0.12098
W(24)	-0.10046
24PER	0.14398

REV Fall 00Z F24

LHFLX	0.22613
Q2	0.71962
T(20)	-0.45937
T(27)	-0.13399
Q(20)	-0.19216
Q(26)	0.21171
TK(28)	0.13236
RT(23)	-0.16235
W(26)	-0.11158
24PER	0.16775

REV Fall 12Z F36

SOIT6	0.41378
Q2	0.45975
U(31)	0.1282
T(20)	-0.36904
Q(19)	-0.19919
TK(19)	-0.20722
RT(15)	0.11263
RT(17)	0.18026
RT(23)	0.13032
24PER	0.13894

REV Fall 00Z F48

Q2	0.65533
U(30)	-0.39598
U(31)	0.5458
T(20)	-0.29674
RT(24)	0.1556
W(12)	-0.17383
24PER	0.23965

REV Winter 00Z F00

SOIT1	0.38383
T(17)	-0.35989
Q(19)	-0.21391
Q(29)	-0.1403
W(20)	-0.18024
24PER	0.32957

REV Winter 12Z F12

SWDWN	0.30894
U(25)	0.16505
Q(12)	0.19116
Q(18)	-0.32531
RT(18)	0.1213
24PER	0.376

REV Winter 00Z F24

PBLHT	0.20557
SWDWN	0.18139
SWOUT	0.22008
V(14)	-0.19934
Q(18)	-0.1626
Q(24)	-0.32158
Q(27)	0.19906
Q(31)	-0.21968
TK(16)	0.13374
24PER	0.27124

REV Winter 12Z F36

LHFLX	0.43577
T(18)	-0.37596
Q(31)	-0.33245
TK(1)	-0.32594
24PER	0.25621

REV Winter 00Z F48

SWDWN	0.19162
T(20)	-0.25421
Q(31)	-0.21418
TK(14)	0.36461
TK(15)	-0.17277
RT(15)	-0.20336
W(29)	-0.15184
24PER	0.38154

Station REV: Forecasts Leading up to 12UTC (early morning)

REV Spring 12Z F00
(none)

REV Spring 00Z F12

U(27)	-0.21281
U(31)	0.30045
RT(2)	-0.14036

REV Spring 12Z F24

U(27)	-0.29947
U(31)	0.35442
Q(12)	-0.2467
PP(14	0.16979

REV Spring 00Z F36

U(28)	-0.2219
U(31)	0.33546
PP(1)	0.16317

REV Spring 12Z F48
(none)

REV Summer 12Z F00

U(31)	0.24228
V(21)	0.16992
Q(24)	0.19841
Q(30)	0.19822

REV Summer 00Z F12

U(29)	0.37676
U(31)	-0.25135

REV Summer 12Z F24
(none)

REV Summer 00Z F36
(none)

REV Summer 12Z F48
(none)

REV Fall 12Z F00

Q(11)	0.89696
Q(13)	-4.4263
Q(14)	6.37
Q(15)	-3.2126
Q(16)	0.49714
Q(25)	0.15972

REV Fall 00Z F12

Q(28)	0.24608

REV Fall 12Z F24

Q(27)	0.19766

REV Fall 00Z F36

Q(29)	0.26764

REV Fall 12Z F48

Q(28)	0.21046

REV Winter 12Z F00

V(19)	-0.30937
V(24)	1.4419
V(26)	-0.74335
W(25)	-0.239

REV Winter 00Z F12

V(23)	0.5381
V(29)	-0.31513
RT(19)	-0.19246

REV Winter 12Z F24

LWOUT	-0.16805
T(17)	0.26793
T(25)	-0.33839
TK(14)	1.3749
TK(15)	-1.1376
RT(20)	-0.33478

REV Winter 00Z F36

U(29)	-0.18244
T(24)	-0.40025
Q(29)	0.41627
Q(31)	-0.3314
RT(1)	-0.16709

REV Winter 12Z F48

V10	-0.65598
U(18)	0.62747
U(21)	-0.46474
V(2)	0.48579
V(17)	0.24757
Q(17)	-0.24942
TK(14)	-0.3621
RT(7)	0.42396
RT(12)	0.13863
RT(17)	-0.65263
RT(23)	-0.14456

Station VBG: Forecasts Leading up to 00UTC (afternoon)

VBG Spring 00Z F00

SOIT2	0.53972
U(12)	0.293
T(8)	-0.31704
Q(1)	-0.39824
Q(9)	0.39947
Q(14)	-0.17986
PP(22	-0.48456

VBG Spring 12Z F12

PBLHT	-0.16621
LWOUT	0.20948
SOIT4	0.51342
U(11)	0.45618
U(31)	-0.12258
T(5)	-0.27371
Q(4)	-0.41082
Q(8)	0.2011
RT(12)	-0.23282
RT(16)	0.23302
RT(27)	-0.11489
RT(29)	-0.1503
PP(22	-0.51137
W(12)	-0.54062
W(14)	0.19177
W(23)	0.13925

VBG Spring 00Z F24

LWOUT	0.18089
U10	1.0247
U(3)	-0.84116
U(13)	0.17724
U(31)	-0.16322
V(18)	-0.33872
V(24)	0.29711
TK(21)	-0.19674
RT(20)	0.26495
PP(22	-0.60403
W(11)	-0.19756
W(31)	-0.20323

VBG Spring 12Z F36

GRNDT	0.29571
U(30)	-0.20131
T(13)	-0.65198
Q(20)	0.21754
TK(8)	0.16184
TK(13)	0.095189
TK(15)	0.12152
TK(16)	0.10368
TK(22)	-0.21785
RT(8)	-0.13628
RT(12)	-0.20393
RT(17)	-0.23469
RT(20)	-0.28209
PP(21	-0.26069
W(1)	0.45795
W(10)	-0.17494
W(25)	0.113

VBG Spring 00Z F48

V(12)	-0.26475
RT(1)	0.96171
RT(2)	-0.57396
RT(6)	-0.12619
RT(21)	-0.12934
PP(22	-0.77692
W(11)	-0.1616

VBG Summer 00Z F00

SOIT1	6.7814
SOIT2	-6.4648
V(24)	0.18278
T(6)	-0.2304
T(10)	-0.74526
T(16)	0.22193
Q(29)	0.21063

VBG Summer 12Z F12

V10	-1.526
U(12)	-0.1134
V(4)	1.9249
T(8)	-0.25763
Q(7)	-0.17243
Q(24)	-0.37494
TK(8)	0.15578
RT(5)	-0.31038
RT(6)	-0.12602
RT(15)	-0.12822
RT(24)	0.21467
W(3)	0.41616

VBG Summer 00Z F24

V(6)	0.43609
Q(28)	-0.13542
TK(10)	0.1273
TK(29)	-0.14883
RT(7)	0.25103
RT(9)	0.31577
RT(26)	0.15387
W(5)	0.31765
W(29)	0.29872
W(31)	-0.18584
24PER	0.2076

VBG Summer 12Z F36

V(6)	0.49439
V(27)	0.14891
T(7)	-0.28964
Q(23)	-0.16782
RT(18)	0.25184
RT(30)	-0.1616
W(10)	0.27654
24PER	0.16902

VBG Summer 00Z F48

V(7)	0.53062
T(9)	-0.41645
T(30)	0.33112
T(31)	-0.18836
Q(12)	-0.28498
TK(5)	0.39146
RT(20)	-0.12696

VBG Fall 00Z F00

SOIT4	0.36892
U(13)	0.15185
T(8)	-0.66357
T(24)	-0.17958
T(28)	0.28003
Q(20)	-0.16195

VBG Fall 12Z F12

SOIT4	-0.47402
Q2	0.65913
U10	0.21765
T(6)	-0.55099
T(29)	0.20838
Q(20)	-0.12432
TK(5)	-0.20353
TK(8)	0.29261
RT(10)	-0.19431
RT(11)	0.17665
RT(17)	-0.19072
RT(20)	0.2721
W(15)	-0.1307
W(32)	-0.15504

VBG Fall 00Z F24

SOIT1	1.1916
SOIT4	-0.56651
U(8)	0.37187
T(7)	-0.74239
T(23)	-0.84376
T(25)	0.63701
Q(15)	-0.13167
TK(13)	0.1915
RT(6)	-0.16313
RT(20)	0.11413

VBG Fall 12Z F36

U10	1.4312
U(4)	-0.97473
T(22)	-0.16622
Q(8)	0.43059
Q(11)	-0.2931
TK(13)	0.24125
RT(4)	-0.2191
RT(9)	0.15362
RT(18)	-0.18084
RT(23)	0.15276
W(28)	0.12987

VBG Fall 00Z F48

SWOUT	0.26295
SOIT2	1.0403
T(7)	-1.0508
T(21)	-0.35133
Q(20)	-0.1892
RT(8)	-0.32008
RT(22)	0.2017

VBG Winter 00Z F00

U(2)	0.26137
T(12)	-0.42029
Q(15)	-0.22334
Q(29)	0.20662
W(15)	-0.2369
W(20)	0.31356
24PER	0.2845

VBG Winter 12Z F12

SHFLX	0.42147
UST	-0.26841
T(13)	-0.50701
TK(25)	-0.11814
RT(12)	-0.24868
RT(17)	-0.13653
W(24)	0.15323
24PER	0.17694

VBG Winter 00Z F24

SOIT3	0.52397
U(21)	-0.5741
U(22)	0.44349
V(16)	-0.42578
V(24)	0.36778
T(7)	-0.94741
RT(9)	-0.15607
RT(12)	-0.10849
RT(13)	-0.20555
RT(18)	-0.15122
RT(21)	0.12836
W(15)	0.14525
24PER	0.26813

VBG Winter 12Z F36

V(3)	-0.39159
V(20)	0.51393
V(22)	-0.31268
T(3)	-0.35293
Q(21)	-0.16644
TK(13)	-0.14787
TK(20)	-0.26154
TK(21)	-0.13418
RT(1)	0.21231
RT(9)	0.14888
RT(13)	0.10667
W(16)	0.35724
24PER	0.24213

VBG Winter 00Z F48

T(3)	-0.3641
Q(17)	-0.19833
TK(8)	-0.20576
TK(18)	0.19877
24PER	0.37001

Station VBG: Forecasts Leading up to 12UTC (early morning)

VBG Spring 12Z F00

SOIT1	0.21707
Q(13)	0.66068
Q(14)	-0.83184
W(25)	-0.4593
W(27)	0.57158

VBG Spring 00Z F12

LHFLX	0.16267
U(9)	0.23934
U(14)	-0.32241
U(16)	0.21704
V(17)	0.18309
TK(9)	-0.28136
TK(13)	-0.27376
TK(14)	1.1333
TK(18)	0.096382
TK(19)	0.077717
TK(22)	0.17695
RT(3)	0.068255
RT(6)	-0.21582
RT(19)	0.075438
RT(20)	-0.2507
RT(22)	0.1003
W(12)	-0.10494
W(17)	0.27466
W(19)	-0.48734
W(23)	-0.14734
W(28)	0.087855
W(31)	-0.16628

VBG Spring 12Z F24

RT(9)	-0.40608

VBG Spring 00Z F36

RT(9)	-0.39713

VBG Spring 12Z F48

U(16)	0.13909
RT(4)	-0.11366
RT(10)	-0.74818

VBG Summer 12Z F00

V(1)	0.17039

VBG Summer 00Z F12

LWOUT	0.26822
Q(22)	0.27047
Q(24)	-0.26571
Q(25)	-0.15574
TK(19)	-0.35973
RT(4)	-0.10836
RT(5)	-0.10141
RT(23)	0.86998
RT(24)	-0.27461
RT(26)	-0.57604

VBG Summer 12Z F24

W(25)	0.33029
W(32)	0.16853

VBG Summer 00Z F36

Q(10)	-0.18195
Q(24)	0.30193
Q(26)	-0.19013
RT(4)	-0.15847
RT(16)	-0.27278

VBG Summer 12Z F48

Q(8)	-0.1861
Q(23)	0.18019
RT(15)	-0.27085

VBG Fall 12Z F00
(none)

VBG Fall 00Z F12
(none)

VBG Fall 12Z F24

PBLHT	1.6649
REGIM	-0.71496
SHFLX	0.18756
V(9)	-0.17407
V(30)	0.079081
T(31)	-0.066431
Q(23)	-0.097289
Q(29)	0.10008
TK(3)	-0.43482
TK(5)	-1.2464
TK(7)	1.2935
TK(8)	-0.6711
TK(9)	0.094059
RT(7)	-0.097413
RT(12)	-0.093905
RT(21)	0.17503
RT(22)	-0.066954
W(3)	-0.25273
W(21)	-0.13952
W(22)	0.083094

VBG Fall 00Z F36

PBLHT	1.0236
REGIM	-0.29173
Q(25)	-0.10585
TK(2)	-0.25452
TK(5)	-2.3777
TK(6)	5.0901
TK(7)	-3.4167
TK(9)	0.13687
TK(14)	0.10783
TK(16)	-0.25818
TK(24)	-0.13741
RT(6)	-0.29598
RT(7)	0.08866

VBG Fall 12Z F48

Q(28)	0.19556
RT(29)	0.26241

VBG Winter 12Z F00

U(6)	0.16956
24PER	0.1883

VBG Winter 00Z F12

RT(11)	-0.54385
RT(12)	0.15047
24PER	0.16413

VBG Winter 12Z F24

RT(5)	-0.69817
RT(7)	0.16408

VBG Winter 00Z F36

T(27)	-0.10691
RT(5)	0.16997
RT(9)	0.21122
RT(10)	-0.88656
W(23)	0.11343

VBG Winter 12Z F48

LWDWN	0.1822
SOIT2	0.64939
V10	0.30973
V(7)	-0.2418
V(17)	-0.18665
T(1)	1.0038
T(2)	-5.4642
T(3)	5.9124
T(4)	-2.978
T(7)	1.0007
T(26)	-0.091746
TK(21)	-0.1505
RT(2)	-1.176
RT(3)	0.12496
PP(15	-0.19097

Appendix B

Regression Equation Variable Counts

Each value is the number of times the variable appeared in 25 equations (all five stations and all five forecast lead-times are included).

	Leading up to 00UTC (afternoon)				Leading up to 12UTC (early morning)			
	Spring	Summer	Fall	Winter	Spring	Summer	Fall	Winter
GRNDT	1	5	1	0	1	1	0	0
PBLHT	3	3	4	3	1	0	6	0
REGIM	0	0	0	1	1	0	2	0
SHFLX	2	1	0	4	1	1	1	0
LHFLX	5	3	1	6	3	0	1	0
UST	0	0	2	1	0	1	1	0
SWDWN	1	1	1	6	0	0	0	0
LWDWN	0	1	0	0	1	0	0	2
SWOUT	0	2	2	2	0	0	0	0
LWOUT	2	0	1	1	2	1	2	1
SOIT1	3	1	3	3	2	1	0	0
SOIT2	2	1	2	0	1	0	0	1
SOIT3	0	0	2	3	0	0	0	0
SOIT4	3	1	6	1	0	0	1	0
SOIT5	2	1	1	2	0	0	0	0
SOIT6	0	2	3	0	0	0	0	1
T2	0	0	0	0	0	0	0	0
Q2	3	1	6	1	0	0	0	0
U10	1	0	3	0	0	0	0	0
V10	0	1	1	0	0	0	0	2
24PER	2	10	13	11	5	0	1	2

	Leading up to 00UTC (afternoon)				Leading up to 12UTC (early morning)			
	Spring	Summer	Fall	Winter	Spring	Summer	Fall	Winter
TK(1)	0	1	1	1	2	0	2	0
TK(2)	1	0	1	0	1	0	1	0
TK(3)	0	0	0	0	1	0	3	0
TK(4)	0	0	0	0	0	0	2	0
TK(5)	0	1	2	0	0	0	2	0
TK(6)	0	0	0	0	2	0	3	0
TK(7)	0	0	3	0	0	0	5	0
TK(8)	2	2	1	1	0	1	4	0
TK(9)	2	0	0	1	2	0	5	0
TK(10)	0	1	0	0	2	0	2	0
TK(11)	1	1	0	0	2	0	3	1
TK(12)	1	3	1	1	1	0	2	0
TK(13)	1	1	2	1	1	0	2	0
TK(14)	2	2	2	3	1	1	1	2
TK(15)	1	2	2	2	0	0	1	1
TK(16)	2	1	1	2	0	1	1	0
TK(17)	1	1	0	0	1	0	3	0
TK(18)	2	1	2	2	1	0	0	0
TK(19)	1	1	4	1	1	1	0	0
TK(20)	2	2	0	2	2	0	0	0
TK(21)	2	1	0	1	0	0	0	3
TK(22)	1	0	0	0	3	0	1	0
TK(23)	1	0	0	1	1	0	1	0
TK(24)	0	0	0	0	0	0	1	0
TK(25)	2	0	0	1	1	0	1	1
TK(26)	2	0	0	0	0	0	1	0
TK(27)	1	0	0	0	0	0	0	0
TK(28)	0	0	1	0	0	0	1	0
TK(29)	0	1	0	0	1	0	2	1
TK(30)	0	0	1	0	0	0	0	0
TK(31)	0	0	1	0	0	0	0	0

	Leading up to 00UTC (afternoon)				Leading up to 12UTC (early morning)			
	Spring	Summer	Fall	Winter	Spring	Summer	Fall	Winter
RT(1)	1	0	0	2	1	0	0	2
RT(2)	2	0	1	0	2	0	0	1
RT(3)	0	0	0	2	2	4	2	1
RT(4)	1	1	1	0	1	3	1	1
RT(5)	0	1	0	0	1	2	1	2
RT(6)	2	2	4	1	3	0	4	0
RT(7)	0	2	0	0	0	0	4	3
RT(8)	1	1	2	3	0	1	3	0
RT(9)	0	4	2	2	2	1	2	1
RT(10)	1	2	2	1	2	3	1	1
RT(11)	3	1	2	1	4	1	0	1
RT(12)	6	2	1	4	1	1	2	3
RT(13)	2	1	3	3	0	1	0	1
RT(14)	1	1	2	1	0	0	2	0
RT(15)	3	1	2	4	1	1	0	2
RT(16)	4	0	0	3	0	3	0	2
RT(17)	4	1	5	2	1	1	1	2
RT(18)	2	5	3	3	0	0	0	1
RT(19)	1	1	2	3	2	1	2	1
RT(20)	5	2	3	0	3	2	1	2
RT(21)	1	4	1	1	3	0	4	0
RT(22)	2	1	2	0	3	0	1	0
RT(23)	1	1	3	0	0	1	0	1
RT(24)	3	3	2	0	0	1	0	0
RT(25)	1	1	1	0	0	0	2	0
RT(26)	1	2	1	0	0	1	1	0
RT(27)	1	1	2	0	0	0	0	0
RT(28)	0	2	0	0	0	0	1	1
RT(29)	1	1	1	0	2	1	1	0
RT(30)	1	3	2	0	2	1	1	0
RT(31)	2	1	0	0	0	0	0	0

	Leading up to 00UTC (afternoon)				Leading up to 12UTC (early morning)			
	Spring	Summer	Fall	Winter	Spring	Summer	Fall	Winter
T(1)	0	0	0	0	0	0	0	1
T(2)	0	0	0	1	1	0	0	1
T(3)	0	0	0	2	0	0	0	1
T(4)	0	0	0	0	0	0	0	1
T(5)	3	1	0	1	0	0	0	0
T(6)	1	2	1	0	0	1	0	0
T(7)	1	5	3	1	1	0	0	2
T(8)	4	3	2	0	0	1	0	0
T(9)	0	3	2	1	0	0	0	0
T(10)	3	3	0	0	0	0	0	0
T(11)	2	3	0	4	0	1	0	0
T(12)	1	1	1	3	0	1	0	0
T(13)	5	0	0	6	0	0	0	0
T(14)	2	0	1	3	0	0	0	0
T(15)	1	1	0	0	0	0	0	0
T(16)	3	1	0	2	1	0	0	0
T(17)	2	0	0	2	0	0	0	1
T(18)	2	1	3	1	0	0	0	0
T(19)	1	3	1	0	0	0	0	0
T(20)	1	0	4	1	0	0	0	0
T(21)	1	0	2	0	1	0	0	0
T(22)	2	0	2	0	0	0	0	0
T(23)	1	2	1	0	0	0	0	0
T(24)	0	1	1	0	0	0	0	1
T(25)	0	0	2	0	1	0	0	1
T(26)	0	1	1	0	1	0	0	1
T(27)	0	1	2	0	1	0	1	4
T(28)	1	3	1	0	0	3	3	2
T(29)	1	1	2	0	0	1	0	0
T(30)	0	2	1	0	1	3	0	0
T(31)	1	2	0	0	1	1	1	0

	Leading up to 00UTC (afternoon)				Leading up to 12UTC (early morning)			
	Spring	Summer	Fall	Winter	Spring	Summer	Fall	Winter
Q(1)	1	0	1	2	0	0	2	0
Q(2)	0	1	0	0	0	0	0	0
Q(3)	0	0	0	1	0	0	1	0
Q(4)	1	1	0	1	0	1	0	0
Q(5)	0	0	1	0	0	0	0	0
Q(6)	0	0	0	0	1	0	0	0
Q(7)	0	1	2	1	0	0	0	0
Q(8)	1	0	1	0	0	1	1	0
Q(9)	2	1	1	0	0	1	0	0
Q(10)	0	3	0	0	0	1	1	0
Q(11)	0	1	1	0	2	0	2	0
Q(12)	0	1	1	1	2	1	1	1
Q(13)	0	2	1	1	1	0	1	0
Q(14)	1	0	0	0	2	0	3	0
Q(15)	0	0	1	1	2	0	1	1
Q(16)	2	0	2	0	0	0	1	1
Q(17)	2	0	2	2	1	0	1	1
Q(18)	2	0	1	2	1	0	1	1
Q(19)	1	0	5	4	1	0	0	0
Q(20)	1	2	6	2	1	0	0	0
Q(21)	1	1	2	4	0	0	1	1
Q(22)	0	1	2	1	2	1	1	0
Q(23)	0	1	2	0	0	1	1	1
Q(24)	1	2	2	1	0	3	0	0
Q(25)	0	2	2	0	1	3	2	0
Q(26)	0	0	2	0	0	1	0	0
Q(27)	0	0	0	1	0	1	1	0
Q(28)	1	4	0	2	1	0	3	1
Q(29)	1	1	1	2	0	0	4	1
Q(30)	1	2	2	2	0	1	1	0
Q(31)	0	3	0	3	0	0	0	1

	Leading up to 00UTC (afternoon)				Leading up to 12UTC (early morning)			
	Spring	Summer	Fall	Winter	Spring	Summer	Fall	Winter
PP(1)	0	0	0	0	1	2	1	0
PP(2)	0	0	0	0	0	0	0	0
PP(3)	0	0	0	0	0	0	0	0
PP(4)	0	0	0	0	0	0	0	0
PP(5)	0	0	0	0	0	0	0	0
PP(6)	0	0	0	0	0	0	0	0
PP(7)	0	0	0	0	0	0	0	0
PP(8)	0	0	0	0	0	0	0	0
PP(9)	0	0	0	0	0	0	2	0
PP(10)	0	0	0	0	0	0	1	0
PP(11)	0	0	0	0	0	0	1	0
PP(12)	0	0	0	0	0	0	0	0
PP(13)	0	0	0	0	0	2	0	0
PP(14)	0	0	0	0	1	0	0	0
PP(15)	0	0	0	0	0	0	0	1
PP(16)	0	0	2	0	0	0	0	0
PP(17)	0	1	3	0	0	0	1	0
PP(18)	0	0	1	0	0	1	0	0
PP(19)	0	0	1	0	0	0	0	0
PP(20)	0	0	2	0	0	0	0	0
PP(21)	1	0	2	0	0	0	0	0
PP(22)	4	1	0	0	0	0	0	0
PP(23)	0	0	1	0	0	0	0	0
PP(24)	0	0	0	0	0	0	0	0
PP(25)	0	0	0	0	0	0	0	0
PP(26)	0	1	0	0	0	0	0	0
PP(27)	0	0	0	0	0	0	0	0
PP(28)	0	0	0	0	0	0	0	0
PP(29)	0	1	0	0	0	0	0	0
PP(30)	0	1	0	0	0	0	0	0
PP(31)	1	0	0	0	0	0	0	0

	Leading up to 00UTC (afternoon)				Leading up to 12UTC (early morning)			
	Spring	Summer	Fall	Winter	Spring	Summer	Fall	Winter
U(1)	2	0	2	0	0	0	0	0
U(2)	0	0	0	1	0	0	0	0
U(3)	2	1	0	0	0	0	0	0
U(4)	0	0	1	1	1	0	0	0
U(5)	1	0	0	0	0	1	0	0
U(6)	0	0	0	0	1	1	0	1
U(7)	0	0	0	0	1	0	2	0
U(8)	0	0	1	0	0	0	0	0
U(9)	1	0	2	0	1	0	0	0
U(10)	0	0	0	0	0	1	0	0
U(11)	1	0	0	0	0	1	0	0
U(12)	1	1	0	0	0	0	1	0
U(13)	3	1	1	1	1	1	0	0
U(14)	0	1	1	0	2	1	0	0
U(15)	0	1	0	0	1	1	0	0
U(16)	0	2	1	1	3	0	1	2
U(17)	2	0	0	1	0	2	1	0
U(18)	0	0	1	1	0	0	0	2
U(19)	0	1	1	2	0	0	0	0
U(20)	2	1	0	2	1	1	1	0
U(21)	2	2	1	1	0	0	0	1
U(22)	0	0	1	2	1	0	0	0
U(23)	2	1	0	0	0	0	0	0
U(24)	0	1	0	0	1	0	0	0
U(25)	0	0	0	1	1	0	0	0
U(26)	1	0	0	1	0	1	0	0
U(27)	0	2	0	1	2	2	0	0
U(28)	1	0	1	1	1	0	0	0
U(29)	1	0	0	3	2	1	0	1
U(30)	3	0	2	1	0	1	1	0
U(31)	5	2	2	0	3	4	0	0

	Leading up to 00UTC (afternoon)				Leading up to 12UTC (early morning)			
	Spring	Summer	Fall	Winter	Spring	Summer	Fall	Winter
V(1)	0	3	0	1	1	2	2	0
V(2)	0	0	0	0	0	0	0	1
V(3)	0	0	1	1	0	0	0	0
V(4)	0	1	0	0	0	0	0	0
V(5)	0	0	1	0	0	0	1	0
V(6)	0	2	0	0	0	0	0	0
V(7)	0	1	0	0	0	0	0	1
V(8)	0	3	0	0	0	0	0	0
V(9)	0	0	1	0	0	0	1	0
V(10)	1	0	1	0	0	1	0	0
V(11)	0	1	1	0	1	0	0	0
V(12)	3	0	0	0	0	0	0	0
V(13)	0	0	0	0	1	0	0	0
V(14)	0	1	0	1	0	0	0	0
V(15)	1	2	0	0	1	0	0	0
V(16)	0	1	0	1	1	0	0	0
V(17)	0	1	2	0	1	1	0	2
V(18)	1	2	1	3	0	1	0	0
V(19)	1	1	1	0	0	1	0	1
V(20)	0	2	2	1	1	0	0	0
V(21)	0	1	0	1	1	3	1	0
V(22)	0	0	0	2	1	0	0	0
V(23)	0	1	1	0	0	0	0	1
V(24)	3	3	0	1	0	0	0	1
V(25)	1	0	0	1	1	0	0	0
V(26)	1	0	0	1	0	2	0	1
V(27)	0	1	1	1	0	2	0	0
V(28)	1	1	0	0	0	1	0	0
V(29)	0	1	0	0	3	1	3	2
V(30)	2	0	0	0	1	0	3	0
V(31)	2	5	1	0	1	1	0	0

	Leading up to 00UTC (afternoon)				Leading up to 12UTC (early morning)			
	Spring	Summer	Fall	Winter	Spring	Summer	Fall	Winter
W(1)	1	1	1	0	1	3	1	0
W(2)	0	0	0	0	0	0	0	0
W(3)	0	2	0	0	0	0	1	0
W(4)	1	0	0	0	1	1	0	0
W(5)	0	1	0	0	0	0	0	0
W(6)	0	0	0	0	0	0	0	0
W(7)	0	0	0	1	0	1	0	0
W(8)	0	1	0	0	0	0	0	0
W(9)	0	1	0	0	0	0	0	1
W(10)	5	3	0	0	0	0	0	0
W(11)	2	1	1	0	1	0	0	0
W(12)	1	0	1	0	1	0	0	0
W(13)	0	2	1	0	0	0	1	0
W(14)	2	0	0	0	0	0	1	0
W(15)	0	0	1	2	0	1	0	0
W(16)	0	0	1	1	0	1	0	1
W(17)	0	0	0	1	2	1	0	1
W(18)	0	1	1	1	0	1	0	1
W(19)	1	3	1	1	1	0	1	0
W(20)	0	1	0	3	1	1	0	0
W(21)	2	2	0	0	1	2	2	0
W(22)	0	1	0	1	0	0	1	0
W(23)	2	1	0	1	2	0	0	2
W(24)	0	0	1	1	0	0	1	0
W(25)	1	0	0	0	2	2	1	1
W(26)	0	0	1	1	0	0	0	0
W(27)	1	0	2	2	1	0	0	0
W(28)	1	1	2	2	1	0	1	0
W(29)	0	2	1	2	2	0	0	0
W(30)	2	1	1	1	2	0	0	1
W(31)	3	1	1	1	2	0	1	0
W(32)	1	2	2	1	1	1	2	0